"NEW PROCESSING APPROACHES FOR $Cu_2ZnSnSe_4$-BASED SOLAR CELLS"

Thesis submitted in partial fulfillment of the requirement for the PhD Degree issued by the Universitat Politècnica de Catalunya, in its Electronic Engineering Program.

Simón López Mariño

Thesis tutor: *Ramón Alcubilla González,*
Thesis advisors*: Edgardo Saucedo Silva, Marcel Placidi*

April 2016

TABLE OF CONTENTS

List of abbreviations

AFM	Atomic force microscopy
BIPV	Building integration photovoltaics
CBD	Chemical bath deposition
CIGS	$CuIn_{(1-x)}Ga_x(S_ySe_{1-y})_2$
CPV	Concentrator photovoltaics
CTE	Thermal expansion coefficient
CTS(e)	$Cu_2Sn(S_ySe_{1-y})_3$
CZTS(e)	$Cu_2ZnSn(S_ySe_{1-y})_4$
CZTSe	$Cu_2ZnSnSe_4$
DSSC	Dye-sensitized solar cells
EDX	Energy dispersed X-ray spectroscopy
E_g	Band gap energy
E_U	Urbach energy
FIB	Focused ion beam
FF	Fill factor
FWHM	Full with at half maximum
GB	Grain boundary
i-ZnO	Intrinsic ZnO
ITO	Indium Tin Oxide (In_2O_3:Sn)
J_{SC}	Short circuit current density
J-V	Current density-voltage
MJ	Multijunction
MoNa	Na doped Mo targets
η	Efficiency
OPV	Organic photovoltaics
PAS	Pre-absorber synthesis evaporation
PDT	Post deposition treatment (evaporation)
PI	Polyimide

PV	Photovoltaics
QD	Quantum dots
R2R	Roll-to-roll
SCR	Space charge region
SEM	Scanning Electron Microscopy
SLG	Soda Lime Glass
TCO	Transparent Conductive Oxide
TOF-SIMS	Time of flight secondary ion mass spectroscopy
V_{OC}	Open circuit voltage
XRF	X-ray fluorescence spectroscopy
XPS	X-ray photoelectron spectroscopy

ABSTRACT

The present thesis focuses on the promising semiconductor material kesterite ($Cu_2ZnSn(S,Se)_4$), known as CZTS(e), which is used in the second generation of solar cells, generally known as thin film photovoltaics (PV). This material relies on earth-abundant, low-cost and low toxic elements which certainly attract the interest of both research community and industry. Kesterite could replace its well known and already commercialised thin film counterpart, $CuIn_{(1-x)}Ga_x(S_ySe_{1-y})_2$ (CIGS), since it has similar structural and optoelectronic properties and also cell architecture, but does not rely on scarce elements such as In and Ga. In order to achieve a commercial stage, kesterite research needs to increase its still limited efficiency (12.6%), which is currently below the 15-18% required value. To achieve this goal, new tailored and customized processing solutions, dealing with major problems of this technology should be investigated and implemented. Moreover, increasing the potential market penetration of kesterite by diversifying its possible applications range can also be an appealing and interesting driver for the industry.

This work focuses on the pure Selenium kesterite compound, CZTSe, using a versatile and simple sequential two step process to synthesize this absorber. Sputtering and reactive thermal annealing are the techniques chosen to produce CZTSe based solar cells. In addition, two different substrates were used, soda lime glass (SLG) and flexible and light-weight stainless steel (SS) foils. The thesis scope is divided into two interrelated parts:

The first one deals with the proposal of novel and customized approaches to improve CZTSe-based devices performance, mainly using glass substrates. Three innovative processing solutions are already proven, published or under review in scientific journals and included in this work. Two of them deal with the critic Mo back contact region and the third one focuses on the absorber surface. As a result, two original ways to control the decomposition of the back contact interface and the excessive generation of $MoSe_2$ (overselenization) during the thermal treatment along with a chemical passivation route for the CZTSe surface are reported. Intermediate and thin i-ZnO layers and Mo multilayer configurations combined with nanometric MoO_2 layers are introduced at the back interface. Likewise, $KMnO_4/H_2SO_4$ + Na_2S aqueous solutions capable of removing ZnSe while passivating the absorber surface are successfully implemented. Direct evidence of their impact into devices performance is showed via optoelectronic devices characterization. Additionally, structural, morphological, electrical and compositional material characterizations are also included in this work.

The second part of this thesis focuses on the use of flexible and light-weight substrates alternative to conventional and rigid glass based ones. The use of these substrates add an extra value to the already mentioned advantages that kesterite accounts for. A biggest application niche, such as building integration photovoltaics (BIPV), portable consumer electronics, car chassis integration, space applications… etc., along with high throughput roll-to-roll (R2R) industrial manufacturing compatibility, could definitively ease kesterite commercialization.

SS foils have been used successfully in this work, producing the first CZTSe flexible thin-film device ever reported in the literature. Working with these substrates requires specific constraints to be considered, such as the undesired diffusion of impurities from the substrate towards the absorber during the annealing, and the need for an extrinsic alkali doping source due to the inherent lack of Na of these substrates.

This thesis includes a detailed optimization of Cr impurity diffusion barriers and Mo back contacts in order to minimize the detrimental effects of metallic substrate impurities in the devices performance.

Additionally, a comparison of different extrinsic alkali doping methods to effectively introduce Na and/or K in flexible and light-weight CZTSe solar cells is also reported. Na doped Mo targets (MoNa), SLG pieces introduced during the annealing, NaF and KF pre-absorber synthesis evaporation (PAS) and post deposition evaporation (PDT) were investigated. The Na role in CIGS has been extensively reported as necessary to improve devices performance. Nevertheless, the explanation for its benefits is still an open subject, and thereby its study in the kesterite field is a new and hot topic with only a few available publications. We report for the first time a detailed optimization for the use of MoNa layers combined with CZTS(e) technology. In regard to the K investigation, to the best of the author's knowledge, the work developed and published in this thesis is also the first contribution on the CZTS(e) field clearly proving beneficial effects of this alkaline element in CZTS(e) solar cell performance.

RESUMEN

Esta tesis se centra en el prometedor material semiconductor kesterita, ($Cu_2ZnSn(S,Se)_4$), conocido como CZTS(e), el cual se encuadra en la segunda generación de células solares, generalmente conocida como tecnologías fotovoltaicas de "capa fina". Este material está compuesto por elementos abundantes en la corteza terrestre, de bajo coste y baja toxicidad, por lo que atrae el interés tanto de la comunidad científica como de la industria. La kesterita podría llegar a reemplazar al semiconductor más conocido y ya comercializado $CuIn_{(1-x)}Ga_x(S_ySe_{1-y})_2$ (CIGS), ya que posee propiedades estructurales y optoelectrónicas similares, así como una arquitectura de dispositivo análoga, pero no depende de elementos más escasos en la corteza terrestre como son el In y el Ga. Para que la kesterita llegue a comercializarse, la investigación en este campo debe incrementar su todavía baja eficiencia (12.6%), y llegar al valor requerido en torno al 15-18%. Con este objetivo, procesos específicos y "customizados" para abordar problemas importantes de esta tecnología, han de ser investigados e implementados. Por otra parte, el hecho de incrementar el potencial de penetración de la kesterita en el mercado fotovoltaico diversificando su rango posible de aplicaciones comerciales, puede ser también un estímulo atractivo e interesante para la industria.

El presente trabajo se centra en la kesterita de selenio puro, CZTSe, usando un sencillo y versátil proceso secuencial de dos etapas para sintetizar este absorbedor. "Sputtering" y recocido térmico reactivo son las técnicas elegidas para producir células basadas en CZTSe. En lo que respecta al sustrato, se han usado dos tipos diferentes, vidrio convencional (soda lime glass) y hojas ligeras y flexibles de acero inoxidable. Por ello el marco en el que se divide la tesis está formado por dos partes interrelacionadas:

La primera consiste en proponer nuevas técnicas de proceso "customizadas" para mejorar la eficiencia de los dispositivos de CZTSe, principalmente usando sustratos tradicionales de vidrio. Tres soluciones de proceso innovadoras ya han sido demostradas y publicadas o "bajo revisión" en revistas científicas. Dos de ellas se centran en la región crítica del contacto trasero de Mo, y la tercera se centra en la superficie del absorbedor. En consecuencia, dos maneras originales de controlar la descomposición de la interficie de contacto trasero y la generación excesiva de $MoSe_2$ (sobreselenización) durante el recocido térmico, así como una ruta química para la pasivación de la superficie de CZTSe, son reportadas. Capas intermedias delgadas de i-ZnO y configuraciones multicapa de Mo combinadas con capas nanométricas de MoO_2, se han introducido en la interficie trasera. Así mismo, soluciones acuosas de $KMnO_4/H_2SO_4$ + Na_2S capaces de remover ZnSe y pasivar al mismo tiempo la superficie de CZTSe, se han implementado satisfactoriamente. Evidencia directa del impacto de estas innovaciones de proceso en la eficiencia de los dispositivos es mostrada a través de caracterización optoelectrónica de los mismos. Además, caracterizaciones de materiales de tipo estructural, morfológica, eléctrica y composicional, están incluidas también en esta tesis.

La segunda parte de esta tesis se centra en el uso de sustratos flexibles y ligeros, alternativos a los convencionales y rígidos basados en vidrio. El uso de este tipo de sustratos añade un valor extra a las

ventajas ya mencionadas con las que cuenta la kesterita. Un mayor nicho de aplicaciones, como la integración fotovoltaica arquitectónica en edificios, aplicaciones electrónicas portátiles, integración en chasis de vehículos, aplicaciones espaciales… etc., así como compatibilidad industrial con procesos de manufacturado de alto rendimiento tipo "roll-to-roll", podrían claramente facilitar la comercialización de la kesterita.

Hojas de acero inoxidable han sido utilizadas con éxito en esta tesis, produciendo el primer dispositivo flexible de CZTSe reportado en la literatura. Trabajar con estos sustratos requiere consideraciones tecnológicas adicionales, como pueden ser la difusión no deseada de impurezas del sustrato hacia el absorbedor durante el recocido, y la necesidad de una fuente extrínsica de dopaje alcalino, debido a la falta de Na inherente a los mismos.

Esta tesis incluye una optimización detallada de barreras de difusión de impurezas de Cr y de contactos de Mo, para evitar los efectos nocivos asociados a impurezas metálicas del sustrato en la eficiencia de los dispositivos.

Adicionalmente, una comparativa de diferentes métodos extrínsicos de dopaje alcalino para introducir de manera efectiva Na y/o K en células ligeras y flexibles de CZTSe es reportada también. Targets de Mo dopado con Na (MoNa), piezas de vidrio introducidas durante el recocido, evaporación pre-síntesis del absorbedor (PAS) de NaF y KF, así como evaporación post-depósito (PDT) de estos compuestos alcalinos han sido investigados. El papel del Na en el campo del CIGS ha sido reportado de manera extensa en la literatura. Sin embargo, la explicación de sus beneficios es todavía un debate abierto, y por lo tanto su estudio en el campo de la kesterita es un tema nuevo e interesante, con solamente unas pocas publicaciones disponibles. En este trabajo se reporta por primera vez una optimización detallada del uso de capas de MoNa combinadas con la tecnología de CZTS(e). En lo que respecta a la investigación con K, hasta donde el autor tiene conocimiento, el trabajo desarrollado y publicado, parte integrante de la misma, es también la primera contribución en el campo demostrando claramente los efectos beneficiosos de este elemento alcalino en la eficiencia de las células solares de CZTS(e).

PREFACE

The work presented in this thesis has been fully developed in the Catalonia Institute for Energy Research (IREC) within the Solar Energy Materials and Systems Group in Sant Adrià de Besòs (Barcelona), Spain, from 2012 to 2015. The main focus is implementing new processing approaches for CZTSe based solar cells, due to the high marketable potential of kesterite as low cost and earth-abundant photovoltaic material. The main objectives were tackling specific technological issues inherent to the technology working mainly on SLG substrates and developing a processing line for flexible and light-weight SS substrates as alternative to conventional rigid glass ones. As a result, different innovative processing steps have been developed and introduced in CZTSe technology and reported in four articles published in peer-reviewed journals. These articles constitute the main body of this thesis to allow for the Doctor in Philosophy Degree of the Universitat Politècnica de Catalunya (UPC) in Electronic Engineering, and they are listed below:

S. Lopez-Marino, M. Placidi, A. Perez-Tomas, J. Llobet, V. Izquierdo-Roca, X. Fontane, A. Fairbrother, M. Espindola-Rodriguez, D. Sylla, A. Perez-Rodriguez, E. Saucedo,*"Inhibiting the absorber/Mo-back contact decomposition reaction in $Cu_2ZnSnSe_4$ solar cells: the role of a ZnO intermediate nanolayer"*, Journal of Materials Chemistry A, 1, 2013, 19, 8338-8343.

S. López-Marino, Y. Sánchez, M. Placidi, A. Fairbrother, M. Espindola-Rodriguez, X. Fontané, V. Izquierdo-Roca, J. López-García, L. Calvo-Barrio, A. Pérez-Rodríguez, E. Saucedo, *"ZnSe Etching of Zn-Rich $Cu_2ZnSnSe_4$: An Oxidation Route for Improved Solar-Cell Efficiency"*, Chemistry – A European Journal, 2013, 19, 14814-14822.

S. López-Marino, M. Neuschitzer, Y. Sánchez, A. Fairbrother, M. Espindola-Rodriguez, J. López-García, M. Placidi, L. Calvo-Barrio, A. Pérez-Rodríguez, E. Saucedo, *"Earth-abundant absorber based solar cells onto low weight stainless steel substrate"*, Solar Energy Materials and Solar Cells, 2014, 130, 347-353.

S. López-Marino , Y. Sánchez , M. Espíndola-Rodríguez, X. Alcobé , H. Xie, M. Neuschitzer, I. Becerril , S. Giraldo , M. Dimitrievska , M. Placidi , L. Fourdinier, V. Izquierdo-Roca , A. Pérez-Rodríguez, Edgardo Saucedo, *"Alkali doping strategies for flexible and light-weight $Cu_2ZnSnSe_4$ solar cells"* , Journal of Materials Chemistry A, 2016, 4, 1895 – 1907.

Additionally, another processing innovation related to the back interface was under review at the time of the present thesis completion. This work is also listed below:

S. Lopez-Marino; M. Espindola-Rodriguez; Y. Sanchez; X. Alcobe; F. Oliva; H. Xie; M. Neuschitzer; S. Giraldo; M. Placidi; R. Caballero; V. Izquierdo-Roca; A. Perez-Rodriguez; E. Saucedo, *"The Importance*

of Back Contact Modification in High Efficiency $Cu_2ZnSnSe_4$ Solar Cells: the Role of a nanometric MoO_2 Layer", Nano Energy, 2015 (under review)

The content of the thesis is structured into five chapters, and it will be detailed next:

The first chapter is an introduction to PV, highlighting why this technology is relevant for the current global energy mix and which are its advantages. The fundamentals of photovoltaic energy and the physics of solar cells are also discussed. Furthermore, the main photovoltaic technologies are described, putting the stress on the second generation of thin-film PV, to which kesterite belongs. In particular, a state of the art of thin film chalcogenide technologies is included.

The second chapter is dedicated to the material object of study of this thesis, kesterite. The main structural, optical and electrical properties of this photovoltaic absorber are discussed. A description of the typical kesterite solar cell architecture is also included. The state of the art of the technology is deeply reviewed, emphasizing the main limitations that kesterite presents, which are currently hindering its progress. In addition, a brief review of flexible thin film chalcogenide devices, with particular emphasis on kesterite, is provided. Finally, the relevance of alkali doping for the chalcopyrite technology, and of course the kesterite one is discussed.

Chapter three and four explain the aim of this thesis and the objectives to be fulfilled. A description of the experimental and analytical methods used in this thesis is provided.

Chapter five is the main ax of the thesis since it embodies all the experimental results achieved in this work, which are divided in three subchapters, corresponding to three well distinguished paramount working areas.

The first sub-chapter is devoted to the back CZTSe/Mo interface, the main problems of this solar cell region are identified, and a state of the art with the main up-to-date solutions proposed in the literature is included. Different innovative processing solutions have been implemented in this thesis. The first one is related to the introduction of an intermediate nanometric i-ZnO layer between CZTSe and Mo to avoid CZTSe decomposition during the annealing at this back interface. The paper "Inhibiting the absorber/Mo-back contact decomposition reaction in $Cu_2ZnSnSe_4$ solar cells: the role of a ZnO intermediate nanolayer" summarizes the main results of this process innovation. It should be noted that a short abstract of each of the articles published which are part of this thesis is included in chapter five, but the actual articles can be found in the Appendices Section (A. S.). The second innovation is related to avoid the effects linked to the overselenization of the Mo back contact. Thus, different Mo multilayered configurations are examined, and a novel nanometric MoO_2 layer is introduced for the first time in the technology as part of the back contact. The implications of all of these back contact modifications in CZTSe solar cell performance are included in a manuscript with status "under review" in a high impact journal at the time

of this thesis submission. Therefore, this subsection will be fully developed in terms of results presentation, analysis and discussion.

The second subchapter deals with the absorber front interface, in particular with the consequences of removing the most common secondary phase of the CZTSe technology, i.e. ZnSe. Different oxidizing etchings are reviewed, and an aqueous $KMnO_4$ acidic solution is selected combined with a subsequent passivating etching relying in Na_2S aqueous solution. The bulk of this chapter is based on the paper "ZnSe Etching of Zn-Rich $Cu_2ZnSnSe_4$: An Oxidation Route for Improved Solar-Cell Efficiency".

The third and last subchapter is oriented to the development of flexible and light-weight CZTSe solar cells, using SS substrates and Cr diffusion barriers. Two different subsections can be identified. The first one summarizes the initial results giving rise to the first CZTSe device deposited on flexible SS foils. These preliminary findings are described in the paper "Earth-abundant absorber based solar cells onto low weight stainless steel substrate". The final subsection is a detailed comparison between different alkali doping methods to increase the performance of flexible CZTSe solar cells. Additionally, a complete Cr barrier and back contact optimization was performed, with the aim of improving the efficiency of the reference non-doped CZTSe solar cell. The paper "Alkali doping strategies for flexible and light-weight $Cu_2ZnSnSe_4$ solar cells" includes all the details for this last experimental results subsection.

The final chapter of this thesis includes a summary and conclusions of this work.

Finally, additional articles co-authored by Simón López and related to the thesis work are listed below:

H. Xie, S. Lopez-Marino, T. Olar, Y. Sánchez González, M. Neuschitzer, F. Oliva, S. Giraldo, V. Izquierdo-Roca, I. Lauermann, A. Pérez-Rodríguez, and E. Saucedo, On the Impact of Na Dynamics at the $Cu_2ZnSn(S,Se)_4$/CdS Interface During Post Low Temperature Treatment of Absorbers, ACS Applied Materials & Interfaces, 2016, DOI: 10.1021/acsami.5b12243.

Y. Sánchez, M. Espíndola-Rodríguez, H. Xie, S. López-Marino, M. Neuschitzer, S. Giraldo, M. Dimitrievska, M. Placidi, V. Izquierdo-Roca, F.A. Pulgarín-Agudelo, O. Vigil-Galán, and E. Saucedo, "Ultra-thin CdS for highly performing chalcogenides thin film based solar cells", Solar Energy Materials and Solar Cells, 2016, DOI: 10.1016/j.solmat.2015.12.037.

M. Espindola-Rodriguez, Y. Sanchez, S. Lopez-Marino, H. Xie, V. Izquierdo-Roca, D. Sylla, M. Neuschitzer, O. Vigil-Galan, E. Saucedo, and M. Placidi, "Efficient bifacial $Cu_2ZnSnSe_4$ solar cells", in Photovoltaic Specialist Conference (PVSC), 2015 IEEE 42nd, 2015.

S. Giraldo, M. Neuschitzer, S. Lopez-Marino, Y. Sanchez, H. Xie, M. Colina, M. Placidi, P. Pistor, V. Izquierdo-Roca, A. Perez-Rodriguez, and E. Saucedo, "Large performance improvement in $Cu_2ZnSnSe_4$

based solar cells by surface engineering with a nanometric Ge layer", in Photovoltaic Specialist Conference (PVSC), 2015 IEEE 42nd, 2015.

M. Placidi, M. Espindola-Rodriguez, S. Lopez-Marino, Y. Sanchez, M. Neuschitzer, V. Izquierdo Roca, X. Fontane, X. Alcobe, A. Perez-Rodriguez, and E. Saucedo, "$Cu_2ZnSnSe_4$ based solar cells prepared at high temperatures on Si/SiO_2 sodium-free substrate", in Photovoltaic Specialist Conference (PVSC), 2015 IEEE 42nd, 2015.

S. Giraldo, M. Neuschitzer, T. Thersleff, S. López-Marino, Y. Sánchez, H. Xie, M. Colina, M. Placidi, P. Pistor, V. Izquierdo-Roca, K. Leifer, A. Pérez-Rodríguez, E. Saucedo, "Large Efficiency Improvement in $Cu_2ZnSnSe_4$ Solar Cells by Introducing a Superficial Ge Nanolayer ", Advanced Energy Materials, 2015, 21, 1501070.

M. Neuschitzer, Y. Sanchez, T. Olar, T. Thersleff, S. Lopez-Marino, F. Oliva, M. Espindola-Rodriguez, H. Xie, M. Placidi, V. Izquierdo-Roca, I. Lauermann, K. Leifer, A. Pérez-Rodriguez, E. Saucedo, "Complex Surface Chemistry of Kesterites: Cu/Zn Reordering after Low Temperature Postdeposition Annealing and Its Role in High Performance Devices", Chemistry of Materials, 2015, 27, 5279-5287.

M. Placidi, M. Dimitrievska, V. Izquierdo-Roca, X. Fontané, A. Castellanos-Gomez, A. Pérez-Tomás, N. Mestres, M. Espindola-Rodriguez, S. López-Marino, M. Neuschitzer, V. Bermudez, A. Yaremko, A. Pérez-Rodríguez, "Multiwavelength excitation Raman scattering analysis of bulk and two-dimensional MoS_2: vibrational properties of atomically thin MoS_2 layers", 2D Materials, 2015, 2 , 035006.

J. Krustok, T. Raadik, M. Grossberg, S. Giraldo, M. Neuschitzer, S. López-Marino, E. Saucedo, "Temperature dependent electroreflectance study of $Cu_2ZnSnSe_4$ solar cells", Materials Science in Semiconductor Processing, 2015, 39, 251-254.

J. López-García, H Xie, V Izquierdo-Roca, D Sylla, X Fontané, M Blanes-Guardia, F Ramos, M Espindola-Rodriguez, S López-Marino, E Saucedo, A Pérez-Rodriguez, "Synthesis of $CuIn(S,Se)_2$ quaternary alloys by screen printing and selenization-sulfurization sequential steps: Development of composition graded absorbers for low cost photovoltaic devices", Materials Chemistry and Physics, 2015, 160, 237-243.

H. Xie, M. Dimitrievska, X. Fontané, Y. Sánchez, S. López-Marino, V. Izquierdo-Roca, V. Bermúdez, A. Pérez-Rodríguez, E. Saucedo, "Formation and impact of secondary phases in Cu-poor Zn-rich $Cu_2ZnSn(S_{1-y}Se_y)_4$ ($0 \leq y \leq 1$) based solar cells", Solar Energy Materials and Solar Cells, 2015, 140, 289-298.

M. Neuschitzer, Y. Sanchez, S. López-Marino, H. Xie, A. Fairbrother, M. Placidi, S. Haass, V. Izquierdo-Roca, A. Perez-Rodriguez, E. Saucedo, "Optimization of CdS buffer layer for

high-performance $Cu_2ZnSnSe_4$ solar cells and the effects of light soaking: elimination of crossover and red kink", Progress in Photovoltaics: Research and Applications, 2015, 23, 1660-1667.

M. Espindola-Rodriguez, J. López-García, D. Sylla, X. Fontané, Y. Sánchez, S. López-Marino, V. Izquierdo-Roca, W. Riedel, W. Ohm, S. Gledhill, O. Vigil-Galán, E. Saucedo, "Cu_2ZnSnS_4 absorber layers deposited by spray pyrolysis for advanced photovoltaic technology", Physica Status Solidi (a), 2014, 212, 126-134.

H. Xie, Y. Sánchez, S. López-Marino, M. Espíndola-Rodríguez, M. Neuschitzer, D. Sylla, A. Fairbrother, V. Izquierdo-Roca, A. Pérez-Rodríguez and E. Saucedo, "Impact of Sn(S,Se) Secondary Phases in $Cu_2ZnSn(S,Se)_4$ Solar Cells: a Chemical Route for Their Selective Removal and Absorber Surface Passivation", ACS Applied Materials & Interfaces, 2014, 6, 12744-12751.

M. Espindola-Rodriguez, D. Sylla, Y. Sanchez, S. López-Marino, X. Fontané, J. López-García, M. Placidi, A. Pérez-Rodríguez, O. Vigil-Galán, E. Saucedo, "Pneumatically sprayed Cu_2ZnSnS_4 films under Ar and Ar–H_2 atmosphere", Journal of Physics D: Applied Physics, 2014, 47, 245101.

A. Fairbrother, X. Fontané, V. Izquierdo-Roca, M. Placidi, D. Sylla, M. Espindola-Rodriguez, S. López-Mariño, F. A. Pulgarín, O. Vigil-Galán, A. Pérez-Rodríguez and E. Saucedo, "Secondary phase formation in Zn-rich $Cu_2ZnSnSe_4$-based solar cells annealed in low pressure and temperature conditions", Progress in Photovoltaics: Research and Applications, 2014, 22, 479-487.

F.A. Pulgarín-Agudelo, S López-Marino, A Fairbrother, M Placidi, V Izquierdo-Roca, PJ Sebastián, F Ramos, B Pina, A Pérez-Rodríguez, E Saucedo, "A thermal route to synthesize photovoltaic grade $CuInSe_2$ films from printed CuO/In_2O_3 nanoparticle-based inks under Se atmosphere", 2013, 5, 053140

A. Fairbrother, X. Fontané, V. Izquierdo-Roca, M. Espindola-Rodriguez, S. López-Marino, M. Placidi, J. López-García, A. Pérez-Rodríguez and E. Saucedo, ChemPhysChem, "Single-Step Sulfo-Selenization Method to Synthesize $Cu_2ZnSn(S_ySe_{1-y})_4$ Absorbers from Metallic Stack Precursors", 2013, 14, 1836-1843.

X. Fontane, V. Izquierdo-Roca, A. Fairbrother, M. Espindola-Rodriguez, S. Lopez-Marino, M. Placidi, T. Jawhari, E. Saucedo, A. Perez-Rodriguez, "Selective detection of secondary phases in $Cu_2ZnSn(S,Se)_4$ based absorbers by pre-resonant Raman spectroscopy", Photovoltaic Specialists Conference (PVSC), 2013 IEEE 39th, 2013, 2581-2584.

A. Fairbrother, X. Fontané, V. Izquierdo-Roca, M. Espindola-Rodriguez, S. López-Marino, M. Placidi, L. Calvo-Barrio, A. Pérez-Rodríguez, E. Saucedo, "On the formation mechanisms of Zn-rich Cu_2ZnSnS_4 films prepared by sulfurization of metallic stacks", Solar Energy Materials and Solar Cells, 2013, 112, 97-105.

PREFACIO

El trabajo presentado en esta tesis se ha desarrollado completamente en el Institut de Recerca en Energia de Catalunya (IREC), dentro del grupo de Materiales y Sistemas para la Energía Solar en Sant Adrià de Besòs (Barcelona) en el periodo de marzo de 2012 a diciembre de 2015. El foco principal es la implementación de nuevas técnicas de procesado para células solares basadas en CZTSe, debido al gran potencial comercial de la kesterita como material fotovoltaico de bajo coste y abundante en la corteza terrestre. Los principales objetivos se centran en abordar problemas tecnológicos específicos e inherentes a esta tecnología, trabajando para ello con sustratos de vidrio convencionales y al mismo tiempo desarrollando una línea de proceso para sustratos flexibles y ligeros de acero inoxidable como alternativa a los rígidos y más comunes de vidrio. Como resultado, varias técnicas de procesado diferentes e innovadoras han sido desarrolladas e introducidas en la tecnología de CZTSe y reportadas en cuatro artículos evaluados y revisados de manera independiente en revistas científicas. Estos artículos constituyen el cuerpo principal de esta tesis para poder optar al título de Doctor en Ingeniería Electrónica de la Universitat Politècnica de Catalunya (UPC), y se detallan a continuación:

S. Lopez-Marino, M. Placidi, A. Perez-Tomas, J. Llobet, V. Izquierdo-Roca, X. Fontane, A. Fairbrother, M. Espindola-Rodriguez, D. Sylla, A. Perez-Rodriguez, E. Saucedo, *"Inhibiting the absorber/Mo-back contact decomposition reaction in $Cu_2ZnSnSe_4$ solar cells: the role of a ZnO intermediate nanolayer"*, Journal of Materials Chemistry A, 1, 2013, 19, 8338-8343.

S. López-Marino, Y. Sánchez, M. Placidi, A. Fairbrother, M. Espindola-Rodriguez, X. Fontané, V. Izquierdo-Roca, J. López-García, L. Calvo-Barrio, A. Pérez-Rodríguez, E. Saucedo, *"ZnSe Etching of Zn-Rich $Cu_2ZnSnSe_4$: An Oxidation Route for Improved Solar-Cell Efficiency"*, Chemistry – A European Journal, 2013, 19, 14814-14822.

S. López-Marino, M. Neuschitzer, Y. Sánchez, A. Fairbrother, M. Espindola-Rodriguez, J. López-García, M. Placidi, L. Calvo-Barrio, A. Pérez-Rodríguez, E. Saucedo, *"Earth-abundant absorber based solar cells onto low weight stainless steel substrate"*, Solar Energy Materials and Solar Cells, 2014, 130, 347-353.

S. López-Marino , Y. Sánchez , M. Espíndola-Rodríguez, X. Alcobé , H. Xie, M. Neuschitzer, I. Becerril , S. Giraldo , M. Dimitrievska , M. Placidi , L. Fourdinier, V. Izquierdo-Roca , A. Pérez-Rodríguez, Edgardo Saucedo, *"Alkali doping strategies for flexible and light-weight $Cu_2ZnSnSe_4$ solar cells"* , Journal of Materials Chemistry A, 2016, 4, 1895 – 1907.

Adicionalmente, otra innovación relacionada con el procesado de la interficie trasera de células solares CZTSe se encontraba "bajo revisión" en una revista científica durante la redacción de esta tesis. Este trabajo es el siguiente:

S. Lopez-Marino; M. Espindola-Rodriguez; Y. Sanchez; X. Alcobe; F. Oliva; H. Xie; M. Neuschitzer; S. Giraldo; M. Placidi; R. Caballero; V. Izquierdo-Roca; A. Perez-Rodriguez; E. Saucedo, *"The Importance of Back Contact Modification in High Efficiency $Cu_2ZnSnSe_4$ Solar Cells: the Role of a nanometric MoO_2 Layer"*, Nano Energy, 2015 (under review)

El contenido de esta tesis está estructurado en cinco capítulos, y se detallará a continuación:

El primer capítulo es una introducción a la fotovoltaica, destacando porqué esta tecnología es relevante para el mix energético global actual, y cuáles son sus ventajas. Los fundamentos de la energía fotovoltaica y las bases de la física aplicadas a células solares son también discutidos. Además, las principales tecnologías fotovoltaicas son revisadas, poniendo al acento sobre la segunda generación basada en tecnologías fotovoltaicas de capa fina, dentro de las cuales se sitúa la kesterita. De manera más detallada, se incluye también una revisión del estado actual de las tecnologías de capa fina basadas en calcogenuros y sus últimos avances.

El segundo capítulo está dedicado por completo al objeto de estudio de esta tesis, la kesterita. Las principales propiedades estructurales, ópticas y eléctricas de este absorbedor fotovoltaico son discutidas. Una descripción de la arquitectura típica de las células solares de kesterita es también detallada. Los últimos avances de esta tecnología son analizados en profundidad, poniendo el énfasis en las principales limitaciones que la kesterita presenta, las cuales están ralentizando actualmente su potencial desarrollo a nivel industrial. De manera adicional, una revisión breve de las tecnologías flexibles de capa fina basadas en calcogenuros, con el acento particular en la kesterita, está incluida en este capítulo. Finalmente, la relevancia del dopaje alcalino para la tecnología basada en calcopiritas, y por supuesto para la kesterita, es revisada.

Los capítulos tercero y cuarto explican el propósito de esta tesis y los objetivos a cumplir. Una descripción de los métodos experimentales y de caracterización usados en esta tesis está incluida también.

El capítulo cinco es el eje principal de esta tesis ya que aglutina todos los resultados experimentales alcanzados en la misma. Este capítulo está dividido en tres subcapítulos correspondientes a tres areas de trabajo principales y muy diferenciadas.

El primer subcapítulo está dedicado a la interficie CZTSe/Mo, en él los principales problemas de esta región son identificados, y una revisión con los últimos avances en la literatura científica en cuanto a técnicas de procesado para la misma es desgranada. Varias soluciones innovadoras para procesar esta interficie han sido implementadas en esta tesis. La primera está relacionada con la introducción de una capa intermedia y nanométrica de ZnO intrínseco entre el absorbedor de CZTSe y el contacto de Mo, para evitar la descomposición de la kesterita en la región trasera durante el recocido térmico. El artículo "Inhibiting the absorber/Mo-back contact decomposition reaction in $Cu_2ZnSnSe_4$ solar cells: the role of a ZnO intermediate nanolayer" incluye los principales resultados de esta innovación en el procesado de la

kesterita. Se ha de tener en cuenta que de cada uno de los artículos publicados que son parte primordial de esta tesis se incluye un breve resumen en el capítulo cinco, pero los artículos en su formato de revista científica pueden ser consultados en la parte correspondiente a Apéndices. La segunda solución está relacionada con evitar los efectos indeseables ligados a la sobreselenización del contacto trasero de Mo. Por consiguiente, diferentes configuraciones multicapa de Mo son examinadas, y una innovación basada en la utilización de una capa nanométrica de MoO_2 es introducida por primera vez en el campo científico de la kesterita como parte del contacto trasero. Las implicaciones de todas estas modificaciones del contacto trasero en la eficiencia de los dispositivos de CZTSe, están incluidas en un manuscrito con estatus "bajo revisión" en una revista científica de alto impacto durante la redacción de esta tesis. Por ello, la sección correspondiente a esta parte se ha desarrollado completamente y de manera convencional en lo que respecta a presentación de resultados y su análisis y discusión.

El segundo subcapítulo trata sobre la interficie frontal del absorbedor, en concreto sobre las consecuencias de eliminar una de las fases secundarias más comunes de la tecnología de CZTSe, el ZnSe. Diferentes ataques químicos oxidativos son analizados, y de entre ellos una solución acuosa ácida de $KMnO_4$ es seleccionada en combinación con un tratamiento químico pasivante basado en una disolución acuosa de Na_2S. La parte más relevante de este apartado, la que concierne al análisis y discusión de los resultados, está basada en el artículo "ZnSe Etching of Zn-Rich $Cu_2ZnSnSe_4$: An Oxidation Route for Improved Solar-Cell Efficiency".

El tercer y último subcapítulo está orientado hacia el desarrollo de células solares ligeras y flexibles de CZTSe, usando sutratos de acero inoxidable y barreras de difusión química de Cr. Dos secciones distintas forman parte del mismo. La primera sintetiza los resultados iniciales que han dado lugar al primer dispositivo de CZTSe depósitado en sustratos de acero inoxidable. Estos resultados preliminares están descritos en el artículo "Earth-abundant absorber based solar cells onto low weight stainless steel substrate". La otra sección incluye una comparación detallada entre distintos métodos de dopaje alcalino para incrementar la eficiencia de células solares flexibles de CZTSe. Adicionalmente, una optimización muy completa del contacto trasero y de la barrera de Cr fue llevada a cabo, con el fin de mejorar la eficiencia de las células de referencia no dopadas. El artículo "Alkali doping strategies for flexible and light-weight $Cu_2ZnSnSe_4$ solar cells" incluye todos los detalles para esta última sección de la parte dedicada a los resultados.

El capítulo final de esta tesis es un resumen con las principales conclusiones de la misma.

Por último, artículos adicionales relacionados con el trabajo experimental de esta tesis en los que Simón López ha participado como coautor se listan a continuación:

H. Xie, S. Lopez-Marino, T. Olar, Y. Sánchez González, M. Neuschitzer, F. Oliva, S. Giraldo, V. Izquierdo-Roca, I. Lauermann, A. Pérez-Rodríguez, and E. Saucedo, On the Impact of Na Dynamics at

the $Cu_2ZnSn(S,Se)_4$/CdS Interface During Post Low Temperature Treatment of Absorbers, ACS Applied Materials & Interfaces, 2016, DOI: 10.1021/acsami.5b12243.

Y. Sánchez, M. Espíndola-Rodríguez, H. Xie, S. López-Marino, M. Neuschitzer, S. Giraldo, M. Dimitrievska, M. Placidi, V. Izquierdo-Roca, F.A. Pulgarín-Agudelo, O. Vigil-Galán, and E. Saucedo, "Ultra-thin CdS for highly performing chalcogenides thin film based solar cells", Solar Energy Materials and Solar Cells, 2016, DOI: 10.1016/j.solmat.2015.12.037.

M. Espindola-Rodriguez, Y. Sanchez, S. Lopez-Marino, H. Xie, V. Izquierdo-Roca, D. Sylla, M. Neuschitzer, O. Vigil-Galan, E. Saucedo, and M. Placidi, "Efficient bifacial $Cu_2ZnSnSe_4$ solar cells", in Photovoltaic Specialist Conference (PVSC), 2015 IEEE 42nd, 2015.

S. Giraldo, M. Neuschitzer, S. Lopez-Marino, Y. Sanchez, H. Xie, M. Colina, M. Placidi, P. Pistor, V. Izquierdo-Roca, A. Perez-Rodriguez, and E. Saucedo, "Large performance improvement in $Cu_2ZnSnSe_4$ based solar cells by surface engineering with a nanometric Ge layer", in Photovoltaic Specialist Conference (PVSC), 2015 IEEE 42nd, 2015.

M. Placidi, M. Espindola-Rodriguez, S. Lopez-Marino, Y. Sanchez, M. Neuschitzer, V. Izquierdo Roca, X. Fontane, X. Alcobe, A. Perez-Rodriguez, and E. Saucedo, "$Cu_2ZnSnSe_4$ based solar cells prepared at high temperatures on Si/SiO_2 sodium-free substrate", in Photovoltaic Specialist Conference (PVSC), 2015 IEEE 42nd, 2015.

S. Giraldo, M. Neuschitzer, T. Thersleff, S. López-Marino, Y. Sánchez, H. Xie, M. Colina, M. Placidi, P. Pistor, V. Izquierdo-Roca, K. Leifer, A. Pérez-Rodríguez, E. Saucedo, "Large Efficiency Improvement in $Cu_2ZnSnSe_4$ Solar Cells by Introducing a Superficial Ge Nanolayer ", Advanced Energy Materials, 2015, 21, 1501070.

M. Neuschitzer, Y. Sanchez, T. Olar, T. Thersleff, S. Lopez-Marino, F. Oliva, M. Espindola-Rodriguez, H. Xie, M. Placidi, V. Izquierdo-Roca, I. Lauermann, K. Leifer, A. Pérez-Rodriguez, E. Saucedo, "Complex Surface Chemistry of Kesterites: Cu/Zn Reordering after Low Temperature Postdeposition Annealing and Its Role in High Performance Devices", Chemistry of Materials, 2015, 27, 5279-5287.

M. Placidi, M. Dimitrievska, V. Izquierdo-Roca, X. Fontané, A. Castellanos-Gomez, A. Pérez-Tomás, N. Mestres, M. Espindola-Rodriguez, S. López-Marino, M. Neuschitzer, V. Bermudez, A. Yaremko, A. Pérez-Rodríguez, "Multiwavelength excitation Raman scattering analysis of bulk and two-dimensional MoS_2: vibrational properties of atomically thin MoS_2 layers", 2D Materials, 2015, 2 , 035006.

J. Krustok, T. Raadik, M. Grossberg, S. Giraldo, M. Neuschitzer, S. López-Marino, E. Saucedo, "Temperature dependent electroreflectance study of $Cu_2ZnSnSe_4$ solar cells", Materials Science in Semiconductor Processing, 2015, 39, 251-254.

J. López-García, H Xie, V Izquierdo-Roca, D Sylla, X Fontané, M Blanes-Guardia, F Ramos, M Espindola-Rodriguez, S López-Marino, E Saucedo, A Pérez-Rodriguez, "Synthesis of $CuIn(S,Se)_2$ quaternary alloys by screen printing and selenization-sulfurization sequential steps: Development of composition graded absorbers for low cost photovoltaic devices", Materials Chemistry and Physics, 2015, 160, 237-243.

H. Xie, M. Dimitrievska, X. Fontané, Y. Sánchez, S. López-Marino, V. Izquierdo-Roca, V. Bermúdez, A. Pérez-Rodríguez, E. Saucedo, "Formation and impact of secondary phases in Cu-poor Zn-rich $Cu_2ZnSn(S_{1-y}Se_y)_4$ ($0 \leq y \leq 1$) based solar cells", Solar Energy Materials and Solar Cells, 2015, 140, 289-298.

M. Neuschitzer, Y. Sanchez, S. López-Marino, H. Xie, A. Fairbrother, M. Placidi, S. Haass, V. Izquierdo-Roca, A. Perez-Rodriguez, E. Saucedo, "Optimization of CdS buffer layer for high-performance $Cu_2ZnSnSe_4$ solar cells and the effects of light soaking: elimination of crossover and red kink", Progress in Photovoltaics: Research and Applications, 2015, 23, 1660-1667.

M. Espindola-Rodriguez, J. López-García, D. Sylla, X. Fontané, Y. Sánchez, S. López-Marino, V. Izquierdo-Roca, W. Riedel, W. Ohm, S. Gledhill, O. Vigil-Galán, E. Saucedo, "Cu_2ZnSnS_4 absorber layers deposited by spray pyrolysis for advanced photovoltaic technology", Physica Status Solidi (a), 2014, 212, 126-134.

H. Xie, Y. Sánchez, S. López-Marino, M. Espíndola-Rodríguez, M. Neuschitzer, D. Sylla, A. Fairbrother, V. Izquierdo-Roca, A. Pérez-Rodríguez and E. Saucedo, "Impact of Sn(S,Se) Secondary Phases in $Cu_2ZnSn(S,Se)_4$ Solar Cells: a Chemical Route for Their Selective Removal and Absorber Surface Passivation", ACS Applied Materials & Interfaces, 2014, 6, 12744-12751.

M. Espindola-Rodriguez, D. Sylla, Y. Sanchez, S. López-Marino, X. Fontané, J. López-García, M. Placidi, A. Pérez-Rodríguez, O. Vigil-Galán, E. Saucedo, "Pneumatically sprayed Cu_2ZnSnS_4 films under Ar and Ar–H_2 atmosphere", Journal of Physics D: Applied Physics, 2014, 47, 245101.

A. Fairbrother, X. Fontané, V. Izquierdo-Roca, M. Placidi, D. Sylla, M. Espindola-Rodriguez, S. López-Mariño, F. A. Pulgarín, O. Vigil-Galán, A. Pérez-Rodríguez and E. Saucedo, "Secondary phase formation in Zn-rich $Cu_2ZnSnSe_4$-based solar cells annealed in low pressure and temperature conditions", Progress in Photovoltaics: Research and Applications, 2014, 22, 479-487.

F.A. Pulgarín-Agudelo, S López-Marino, A Fairbrother, M Placidi, V Izquierdo-Roca, PJ Sebastián, F Ramos, B Pina, A Pérez-Rodríguez, E Saucedo, "A thermal route to synthesize photovoltaic grade $CuInSe_2$ films from printed CuO/In_2O_3 nanoparticle-based inks under Se atmosphere", 2013, 5, 053140.

A. Fairbrother, X. Fontané, V. Izquierdo-Roca, M. Espindola-Rodriguez, S. López-Marino, M. Placidi, J. López-García, A. Pérez-Rodríguez and E. Saucedo, ChemPhysChem, "Single-Step Sulfo-Selenization Method to Synthesize $Cu_2ZnSn(S_ySe_{1-y})_4$ Absorbers from Metallic Stack Precursors", 2013, 14, 1836-1843.

X. Fontane, V. Izquierdo-Roca, A. Fairbrother, M. Espindola-Rodriguez, S. Lopez-Marino, M. Placidi, T. Jawhari, E. Saucedo, A. Perez-Rodriguez, "Selective detection of secondary phases in $Cu_2ZnSn(S,Se)_4$ based absorbers by pre-resonant Raman spectroscopy", Photovoltaic Specialists Conference (PVSC), 2013 IEEE 39th, 2013, 2581-2584.

A. Fairbrother, X. Fontané, V. Izquierdo-Roca, M. Espindola-Rodriguez, S. López-Marino, M. Placidi, L. Calvo-Barrio, A. Pérez-Rodríguez, E. Saucedo, "On the formation mechanisms of Zn-rich Cu_2ZnSnS_4 films prepared by sulfurization of metallic stacks", Solar Energy Materials and Solar Cells, 2013, 112, 97-105.

1. INTRODUCTION

1.1. Why PV?

Solar irradiation can be considered as an unlimited resource, highly available and more than enough to satisfy the world energy demand. The total solar energy that reaches the Earth surface could meet existing global energy needs 10,000 times over. In order to understand the dimensions of this natural resource a comparison with other energy sources is presented in Figure 1. It is important to stand out that fossil fuels are expressed with regard to their total reserves, while renewable energy sources (RES) to their yearly potential [1].

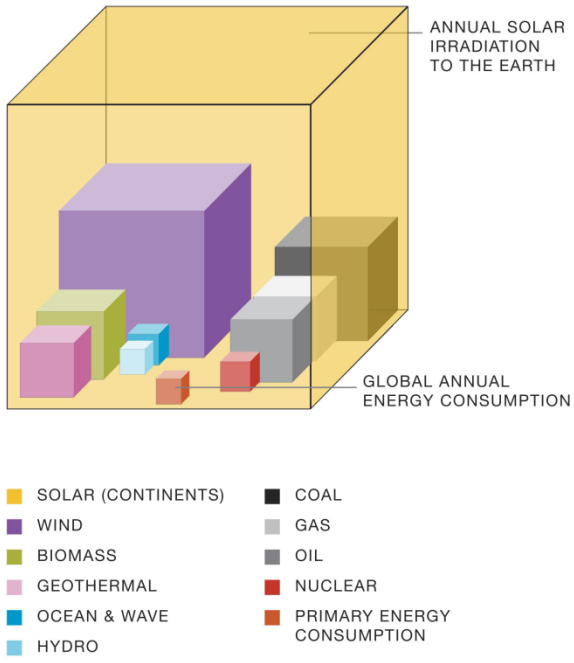

Figure 1: Solar Irradiation versus established global energy resources [1].

Therefore, PV exploits the most abundant, inexhaustible and clean of all the renewable energy resources till date [2].

PV is a fairly simple and elegant way to generate environmentally friendly, renewable electricity. The technological advantages rely on several features such as: low maintenance requirement, silent operation, proximity to electricity demand, production profile concentrated during peak hours, integration in buildings, and high modularity, adapting to a wide range of applications. Among the latter: water pumping, communications, solar home systems, satellites and space vehicles, reverse osmosis plants, megawatt scale power plants…etc [1-3].

PV has an enormous potential for cost reduction, in less than 10 years a price decrease of around 75% for PV systems for different market segments has become real. System prices below 1€/W_p (for utility scale

PV above 1 MW) are now common in several EU countries [4]. Recently PV System prices have experienced a slower decline or even small increase indicating that the speed of future cost reduction may decrease after a few years of market stagnation [5].

The EPIA already forecasted in 2011 PV could provide up to 12% of the EU electricity demand by 2020 under a paradigm shift scenario, i.e. helping technological and market deployment with a regulatory framework, and 9% of the world's electricity needs in 2030 [1]. Due to the strong price decline in PV electricity generation cost over the past few years, that target seems now perfectly reachable and even exceeded with a prediction of a 15% EU electricity demand covered by PV under a positive scenario [4].

PV is a lucrative but sustainable business. EPIA estimated within the paradigm shift scenario, a global annual revenue of over €200 billion for an annual market size of around 135 GW. Furthermore, PV contributes to a local socioeconomic development, since at least 50-55% of the total value of a PV system is created close to the end market [1]. Regarding the employment potential, EPIA under the assumption of 30 jobs per MW installed, forecasted 3.8 million jobs worldwide by 2020 (paradigm shift scenario) [6]. PV was the largest renewable energy employer in 2014 with 2.5 million jobs [7]. Nevertheless, strong market adjustments were produced in the past years due to instability in the modules market prices generated by overcapacities. As a result, current trends show a displacement of the job market from Europe towards USA and countries of the Asia-Pacific region [5, 7].

PV has achieved important milestones in the last years, almost unimaginable just little time before, proving its consolidation and progress within the world's energy landscape. In 2014 the world cumulative installed capacity achieved 178 GW with 40 GW newly installed. In the case of Europe, the installed capacity is decreasing for three years in a row. Nevertheless, the 2020 PV targets defined in 2009 have been reached in 2014 with close to 90 GW of PV capacity, being still the main world actor in terms of installed PV. At the same time, for the fifth year in a row, PV was one of three most installed sources of electricity in Europe together with wind and gas [4]. Regarding to its integration in the electricity grid, Italy, Germany and Greece already cover 7% of their electricity demand by PV, and in some regions like Extremadura in Spain up to 30% of the yearly electricity demand was provided by PV [4, 8].

1.2. How PV works? PV basics

PV is the direct conversion of sunlight into electricity. The photovoltaic effect is defined as the emergence of a voltage between two electrodes in or attached to a liquid or solid system in response to light irradiation. It was first observed in the 19th century by Becquerel, but it was not until the 1950s that solar cells found practical use as electricity generators. Solar photovoltaic cells were invented at Bell Labs in the United States in 1954, they were based in Si, as a growing electronics industry boosted this semiconductor development. The first solar cells were used in space satellites for electricity generation

since the late 1950s. The satellite Vanguard I launched in 1958 carried a few Si solar cells (see Figure 2). Efficiencies were low, between 7-8% [3, 9, 10]

Figure 2: Source: NSSDC-NASA COSPAR ID: 1958-002B. Satellite Vanguard I with six square (roughly 5 cm on a side) solar cells mounted on its body.

A photovoltaic cell is a diode with a great surface exposed to the sun, connected to an external circuit to extract the electricity generated. A semiconductor diode is made of two regions: an n-type semiconductor and a p-type semiconductor. The n-type implies that the semiconductor crystal is doped with impurities that increase the number of negative charged carriers (electrons), and the p-type is doped to increase the number of positive charged carriers (holes). The boundary of these two regions is called p-n junction. A built-in potential is created in the junction, as a consequence of the diffusion of the main charged carriers from each side of the junction to the opposite. This phenomenon leads to the development of an electric field that opposes the diffusion of the main charged carriers.

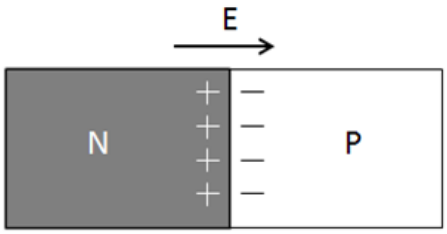

Figure 3: p-n junction with in-built electric field.

If a photon with energy equal or higher than the Energy band gap (E_g) of the absorber strikes a PV cell, then some electrons are able to raise their energy level and to get free. Therefore electron-hole pairs are generated. These electron-hole pairs can act as charge carriers providing they are in, or close to the p-n junction. They can be accelerated by the electric field and thereby getting separated by the p-n junction.

As a result, an electric current can be created, producing work over an external load connected to the PV cell trough a circuit when an external positive voltage is applied [11].

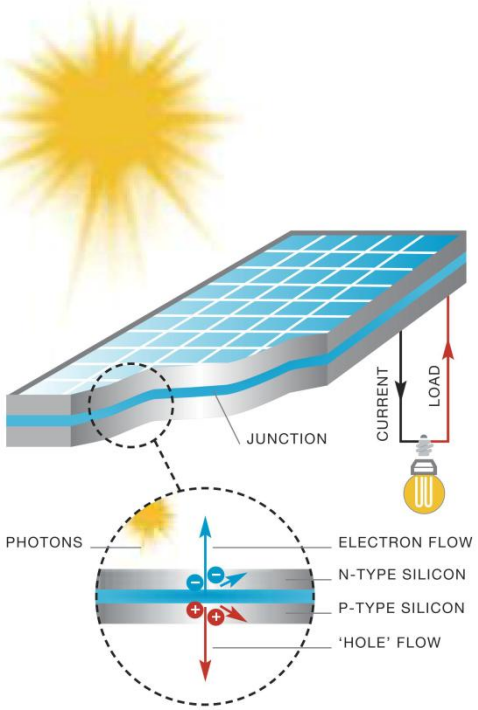

Figure 4: Example of the photovoltaic effect [1].

PV systems embody two main elements:

- Modules (also referred to as panels): They consist on solar cells interconnected to provide a nominal power, which varies from 50 Wp up to 350 Wp, depending on the technology and module size.
- Balance-of-System (BoS): comprises electronic components, cabling, support structures and, if applicable, electricity storage, optics and sun trackers.

As it was already mentioned, PV systems are highly modular, i.e. they can be linked together (arrays) to provide power from a few watts (lighting applications in stand-alone systems) to tens of megawatts (Utility scale power plants) covering a full range of applications and uses [1, 3].

J-V characteristics of a solar cell.

The solar cell operation is based on a diode. Therefore, the current-voltage (J-V) dependency under dark conditions can be obtained through the ideal Shockley diode equation [12, 13]:

$$J(V) = J_0 \left[exp\left(\frac{q}{k_B T} V\right) - 1 \right] \qquad (1)$$

Where J(V) is the current density (mA/cm^2 is a usual unit), J_0 is the diode saturation current density, q is the electron charge, k_B is the Boltzmann constant and T the temperature. An exponentional behavior of the current J with the applied voltage V is produced and it can be seen in figure 5:

When the diode is illuminated with sun light and additional photocurrent density (J_{ph}) term needs to be added to equation 1. This term represents the constant generation of charge carriers due to the illumination.

$$J(V) = J_0 \left[exp\left(\frac{q}{k_B T} V\right) - 1 \right] - J_{Ph} \qquad (2)$$

This equation is the base for the electrical characterization of a solar cell, and its graphic behavior can be seen in figure 5.

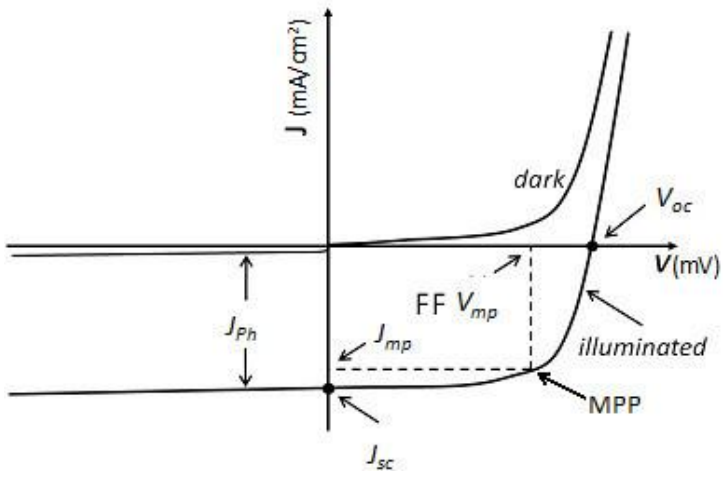

Figure 5: J-V characteristics of an ideal diode solar cell when non-illuminated (dark) and illuminated. Modified from [14].

As it can be seen in figure 5 the maximum current density value that can be reached in the region of electricity generation can be obtained for V = 0, i.e. in short circuit conditions. The value is referred to as short circuit current (J_{sc}). If the circuit is not closed, J(V)= 0, a voltage is created under illumination. This maximum voltage that can be achieved in the region of power generation is called open circuit voltage (V_{oc}).

To determine the highest power that can be extracted from the solar cell these values cannot be used since they belong to unreal operation conditions. The maximum power point will be defined instead by a point on the illuminated curve which maximizes the product J by V. This point is known as maximum power point (MPP), and will be determined by J_{mp} and V_{mp} as it can be easily seen in figure 6. The ratio between the maximal power point ($J_{mp} \cdot V_{mp}$) and the maximum theoretical power ($J_{sc} \cdot V_{oc}$) is called Fill Factor (FF). The FF is a way to quantified the ”squareness” of the J-V curve and it is aimed to be as big as possible. Graphically it is the area within the J-V curve defined by the MPP.

$$FF = \frac{J_{mp} \cdot V_{mp}}{J_{sc} \cdot V_{oc}} \quad (3)$$

The efficiency of a solar cell (η) can be defined as the ratio between the maximum generated power (P_{max}) and the incoming solar spectrum power density (P_{solar}).

$$\eta = \frac{P_{max}}{P_{solar}} = \frac{FF \cdot J_{sc} \cdot V_{oc}}{P_{solar}} \quad (4)$$

The typical value for P_{solar} is approximated by the solar spectrum AM1.5G, which is around 100 $mWcm^{-2}$.

J_{sc}, V_{oc}, η and FF are important parameters to characterize a solar cell. Nevertheless, a real solar cell cannot just be described by equation (2). A real solar cell has resistances and they should be taken into account. The series resistance of a solar cell, R_s, embodies resistance of the bulk of the semiconductor material, resistance between metal and semiconductor and resistance of the metal contacts themselves. Another resistance term, the shunt resistance, R_{sh}, accounts for possible shunts across the p-n junction. The equivalent circuit of a solar cell taking these terms into account is shown in figure 6:

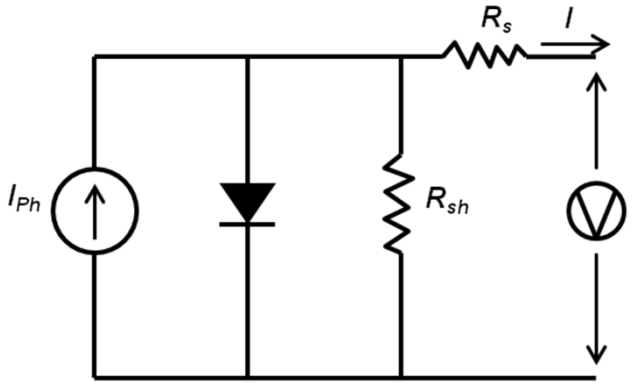

Figure 6: Equivalent circuit model for conventional solar cells.

The equation (2) for an ideal solar cell can be modified including the resistance terms, R_s and R_{sh}, and then be expressed as follows:

$$J(V) = J_0 \left[exp\left(\frac{q(V - JR_s)}{k_B T}\right) - 1 \right] + \frac{V - JR_s}{R_p} - J_{Ph} \quad (5)$$

It is important to note that eq (5) derived from the ideal Shockley diode equation hardly applies for thin-film solar cells. The reason is that recombination losses in the electronic transport, mostly non-radiative recombination losses, are not taking into account. Therefore, it is necessary to introduce in equation (5) the diode ideality factor A, which in equation (1) is assumed to be equal to 1. It has to be noted that A typically has a value between 1 and 2 [12].

$$J(V) = J_0 \left[exp\left(\frac{q(V - JR_s)}{A k_B T}\right) - 1 \right] + \frac{V - JR_s}{R_p} - J_{Ph}$$

Non-radiative recombination losses or Shockley-Read-Hall recombination are generated by states in the band gap created by defects. This will cause that the Voc of the solar cell will be lower than its radiative limit, as it is commonly observed in real world solar cells [15].

Any of several different recombination paths could dominate the device behavior at V_{OC}, including recombination currents in the space-charge or neutral regions of the absorber layer or at any of the critical interfaces, including the absorber/emitter interface or back contact. These specific equations are summarized in ref. [16, 17]. A visual scheme of the band diagram for a CZTS(e) solar cell is shown in Figure 7 in which the main recombination paths mentioned before are indicated with letters from A to D.

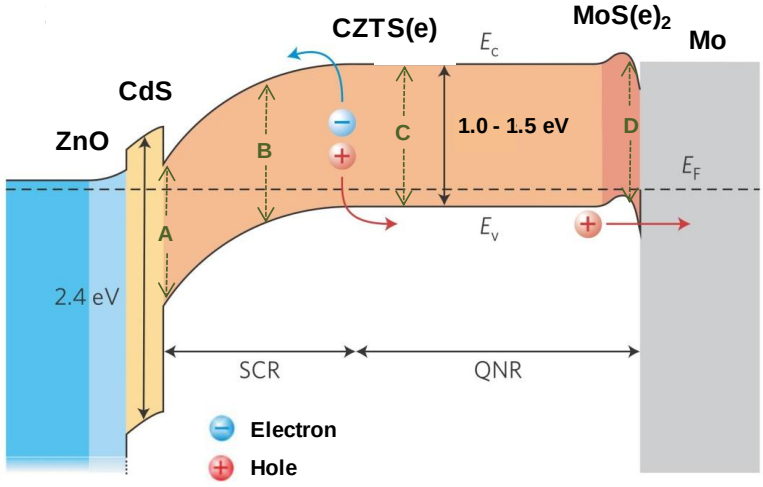

Figure 7: Schematic band diagram of a CZTS(e) solar cell modified from [18]. A-D denote four different recombination pathways. A-recombination at the CdS/CZTS(e) interface, B- in the space charge region (SCR), C- in the neutral region and D- at the back contact.

The experimental determination of A, J_0 and activation energy of the dominant recombination pathway from V_{OC} extrapolation to 0 K are good indicators to assess the dominant recombination pathway and its impact in recombination losses [17, 19, 20].

1.3. Main PV technologies

R&D and industrialisation have led to a portfolio of available PV technology options at different levels of maturity. PV technologies are usually classified as first, second and third generation. First generation covers crystalline Si (c-Si) based devices. Second generation includes thin film technologies, while third generation includes emerging and novel technologies [1, 3].

First Generation

Within the first generation, c-Si cells are usually made from wafers cut from Si ingots or blocks. Typical wafer thicknesses are currently below 200 µm. Depending on the way the wafers are produced different types of cells can be distinguished [1, 3, 21].

- Mono-crystalline Si (mc-Si): This technology implies a high amount of embodied energy, mainly in the fabrication of the Si ingots. Therefore, the energy payback time is considerably high compared with other technologies (1.5-3.3 years depending on irradiation). Today mc-Si accounts for the second highest share of the module market (around 36%). Module efficiencies range between 16 and 24% [5, 21].
- Polycrystalline Si (pc-Si): The embodied energy is reduced with this technology; energy payback time between 1.1-2.1 years. The Si quality in terms of electrical and optical properties is also inferior to the mc-Si counterpart. As a consequence, modules efficiencies are also lower (14-18%), but what is crucial, production costs, are too. It represents the biggest market share with a figure of 56% [5, 21].
- Ribbon and sheet defined film growth: Thin ribbons and sheets are directly fabricated from the Si melt. Their market presence is residual and market trends foreseen a moderate increase for next years.

Alternative cell configurations like the Heterojunction with Intrinsic Thin Layer (HIT), developed by Sanyo electronics have also led to outstanding commercialized efficiencies around 21% and record cell ones of 25.6% [22, 23]. It consists of a thin, single-crystal wafer sandwiched between ultra-thin amorphous silicon (a-Si) layers. Figure 8 shows the basic structure of a HIT solar cell.

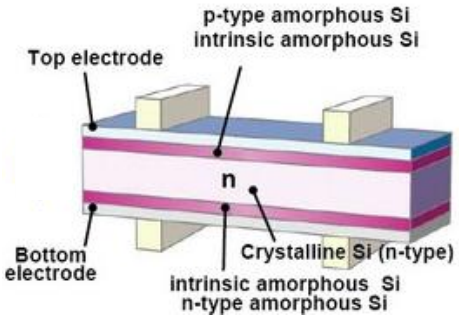

Figure 8: Source Sanyo Corporation, 2012. HIT solar cell structure.

Nowadays, processes to avoid large use of materials inherent to thick Si wafers led to thin transfer Si modules with 21% efficiency and 35 um thick Si wafers [24]. The porous Si (PSI) layer transfer process, developed by the research institute ISFH in Germany made possible to reuse a conventional c-Si wafer up to 13 times [25].

Second generation

The second generation of PV arose as a response to the high prices coupled with Si solar cells. Factors like strong price fluctuation in Si feedstock, which is in part related to the Si main use within the Si electronics industry, have strongly encouraged the development of thin films.

Thin film modules are constructed by depositing extremely thin layers of photoactive material on to a low-cost backing such as glass, stainless steel or plastic. Therefore they can be flexible, increasing their applications niche. Moreover, their low energy pay back times (< 1 year in southern Europe), good high temperature and/or low light level performance and integrated manufacturing make them highly appealing for the industry [1, 21, 26, 27]

Thin-film materials for solar cells have a direct band gap which allows for effective photons absorption. These materials have very high absorption coefficients, and thereby the use of thicknesses of less than 1 micrometer to absorb most of the incident light becomes possible. Through this technology, the resulting cells are usually less than 5 μm in total thickness, so that material usage is very low (about a factor of 30-100 less than in crystalline wafer based materials) [3].

At present time, thin films have an enormous potential to reduce the price to power ratio ($/W) of PV modules due to, among other factors, high efficiency, less usage of semiconductor materials, possibility of utilizing large area inexpensive substrates to fabricate solar cells and monolithically series connected cells produced with this technology suitable for high throughput [28]. It has to be noted that cell efficiencies have already exceed pc-Si in the case of CdTe and CIGS [29, 30].

Regarding industrial expansion, currently the top priorities for the research community are to increase the substrate areas and deposition speeds while keeping material uniformity, cheap and durable packaging, thin polymer substrates...etc. The ultimate goal will be to reduce manufacturing costs per watt and to increase cell and modules efficiencies [1, 26, 27]

Thin films currently account for about 10% of the market. Despite previous market forecasts anticipated a steady growth for the future, new market analyses foresee an stabilization of their market share for the next five years. This is mainly due to the current low-cost for c-Si based modules (60% reduction in the past three years) [5, 27, 31].

Four types of thin film modules are commercially available, Amorphous Silicon (a-Si), Cadmium Telluride (CdTe), Copper, indium, gallium, (di)selenide/(di)sulphide (CIGS) and copper, indium, (di)selenide/(di)sulphide (CIS). These technologies will be further addressed in section 1.4.

Third generation

The third generation appears with the aim to boost the efficiency of previous PV concepts. The top 31% efficiency level for 1 sun single junction devices, known as the Shockley Queisser limit, is challenged by the technologies and concepts behind this generation. Efficiencies ranging between 30% and 60% are targeted.

Within the third generation that is beginning to emerge in the market, it is possible to distinguish between concentrator photovoltaics (CPV), emerging technologies, and novel technologies [1].

Concentrator photovoltaics (CPV) are usually used with c-Si and GaAs wafer based technologies, since they rely on expensive substrates and growth processes. In order to reduce that cost, concentration of incident light using lenses and/or mirrors was investigated and developed. At the same time, in order to absorb more efficiently the solar spectrum, different junctions made of different energy band gap semiconductors can be assembled together. These devices are known as multi-junction (MJ) solar cells. Combining MJ solar cells and concentration systems efficiencies over 30% can be reached, exceeding the 31% Shockley-Queisser limit inherent to single junction PV technology [3, 32]. It is important to highlight that CPV needs to operate under direct sunlight conditions to be highly efficient. Therefore, expensive sun tracking systems operate along with CPV. Currently the world record efficiency belongs to a III-V four junction GaInP/GaAs, GaInAsP/GaIn solar cell, reaching 46% under 508 suns [33]. CPV modules offer now efficiencies up to 36% [5].

In the group of emergent technologies, the label emergent implies that at least one proof of concept for these technologies exists or they can be considered as long term replacement for already consolidated technologies, such as c-Si and thin films [34].

Within this group the main technologies, which have already entered the market are organic PV (OPV), advanced inorganic thin films and thermo-photovoltaic (TPV). OPV suppliers already announced plans to increase production lines to more than 1 GW in 2012. It is possible to distinguish between fully OPV, and hybrid organic-inorganic devices, mainly represented by Dye-sensitized solar cells (DSSC) until perovskite based solar cells rapidly emerged in the past few years [1].

The main advantage of using OPV, DSSC and perovskites is their compatibility with high throughput R2R industrial processes and low manufacturing costs or high potential for it. The major issue of technologies relying in organic layers is to address the low stability and short lifetime due to degradation upon exposure to UV light and oxygen. At the moment commercialized OPV devices for powering consumer goods, such as mobiles battery chargers, last around 3 years. Currently small area cells are in the range of 11-12% for both OPV and DSSC [24]. Perovskites are hybrid inorganic-organic lead or tin halide based photoactive materials derived from DSCC. Currently, the most efficient configuration is a

thin-film solar cell architecture with certified performances already at 20.1% [24]. Nevertheless, as it was already mentioned significant degradation upon light and moisture takes place in a few hours.

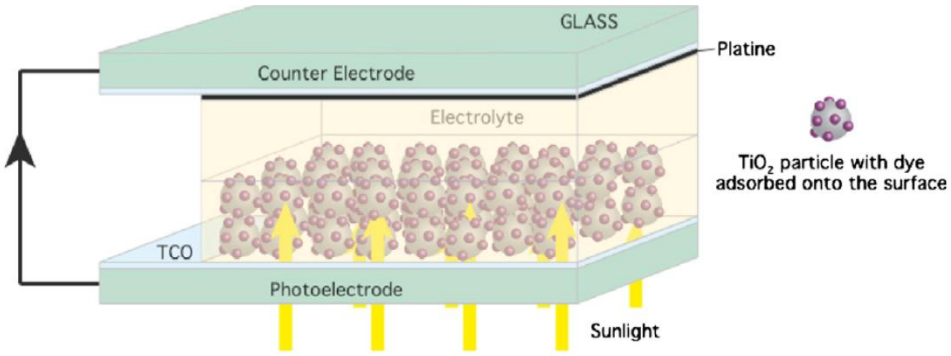

Figure 9: Schematic representation of the dye-sensitised solar cell, taken from [35].

In the category of advanced inorganic thin films it is important to stand out thin film crystalline Silicon. Crystalline Silicon on glass (CSG) is a relatively new thin film c-Si device. An antireflection coating, along with a 1-2 μm thick pc-Si grown by PECVD is deposited onto a textured glass. High manufacturing yields are possible because no TCO is necessary. Minimodules with 10.5% efficiency have been produced [24, 36].

Thermophotovoltaics is a technology based on low band gap solar cells which can be used in combined heat and power (CHP) systems. A thermal emitter produces radiation in the near infrared of infrared range, which can be absorbed by a PV diode, and then generating electricity. III-V semiconductors are commonly used in the solar cells. This concept could be applied in the future to concentrating solar technologies [34]

Regarding novel technologies, the term "novel" applies to developments and ideas that can potentially lead to innovative and disruptive technologies [34]. At the moment how to translate their theoretically demonstrated potential to carry efficiency up to 66% in proved highly performing devices, remains a challenge.

The use of nanomaterials and nanotechnology is the basis of these concepts. Nanomaterials allow for band gap tunability and multiple exiton generation. Controlling the size and dimensionality of semiconductors offers the possibility to tune their optoelectronic properties. This is due to quantum confinement effects [37, 38].

All of these features along with the possibility of solution processing, have boost research in nanotechnology, especially in solar cells. Two main objectives are targeted by these technologies: tailoring the properties of the active layer to match effectively the solar spectrum, and modifying solar

spectrum to maximize its absorption in the active layer. The first implies the introduction of nanostructures in the active layer, while the latter implies acting at the periphery of the active layer [3].

Structures like quantum wells (QW), quantum wires and quantum dots (QD) can be introduced in the active layer.

QD have been added to OPV solar cells or DSSC in order to increase the spectral response to longer wavelengths of these devices, and to increase light absorption. The concept has been demonstrated, but no higher efficiencies than conventional OPV have been obtained yet [37].

QD have been used as well to create intermediate band (IB) solar cells. A better utilization of the full solar spectrum could be achieved with one or more narrow IBs properly located in the band gap of a wide gap semiconductor. IBs can act as stepping stones to allow low energy photons to transfer electrons from the conduction band to the valence band [39]. InAs QD have been intensively investigated within this area [3].

In order to modify the solar spectrum, concepts to avoid high energy photons thermalization and non-absorption of low energy ones, such us up and down conversion, are currently investigated. The operating principle is shown in Figure 10. Two types of wave-converting materials have gathered attention: lanthanides and organic materials [3, 40]. Additionally, surface plasmonic effects or plasmonics can be used to shift the wavelengths of the solar spectrum to frequencies which allows for maximal photon collection. Light concentration and/or scattering can arise trough the interaction between metallic NPs and light creating advantageous optical properties [3]. This effect has been demonstrated in materials like Si [41] and OPVs [42].

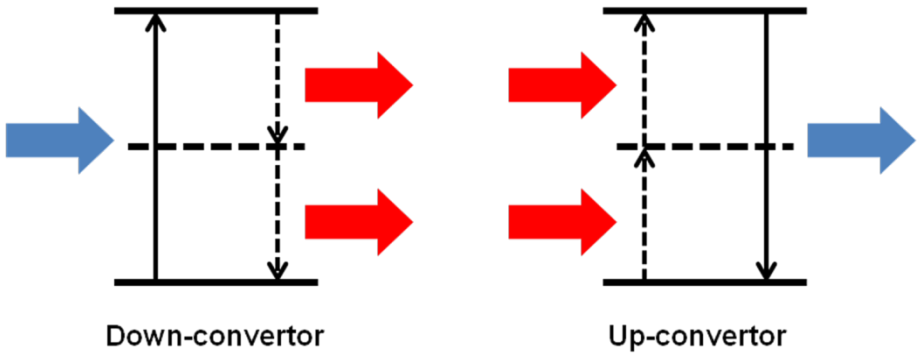

Figure 10: Down conversion: a high-energy photon is converted to two low-energy photons; Up conversion: 2 low energy photons are converted to a high energy photon.

1.4. Thin-film Solar cells

- Amorphous Silicon (a-Si):

The amorphous Si is a mixture of Si and Hydrogen (5-20 at. %H). It has a direct optical band gap of 1.7 eV, and a high absorption coefficient, which limits the thickness of the active region to about 1 µm thick, thereby reducing costs. Amorphous Si has an inherent problem related to stability under light illumination (Staebler-Wronski effect). To address this issue tandem cells and triple junction cells have been developed. Different alloys of a-Si with C and Ge make possible these configurations [43]

Currently module efficiencies are around 7% for a-Si modules [5, 44].

Another technology known as micromorph solar cells, based on a two phases material (microcrystalline Silicon, µcSi): crystalline Si immersed in an amorphous Si matrix, also addresses degradation under intense light conditions. Hybrid a-Si/ µcSi multi-junction configurations already allows for 12% module efficiencies [24, 43].

- Cadmium Telluride (CdTe):

CdTe cells have been produced since the 60's based in the heterojunction: CdTe/CdS as the active region. CdTe has a direct energy band gap, close to the optimum for PV energy conversion 1.5 eV, as well as a high optical absorption coefficient (>10^5 cm^{-1}), allowing for a reduced material usage to absorb the incoming light. The most common structure for this device is shown in figure 11, and it has the following layer series: Glass-TCO-CdS-CdTe-Back contact. This configuration is referred to as "superstrate configuration" [45].

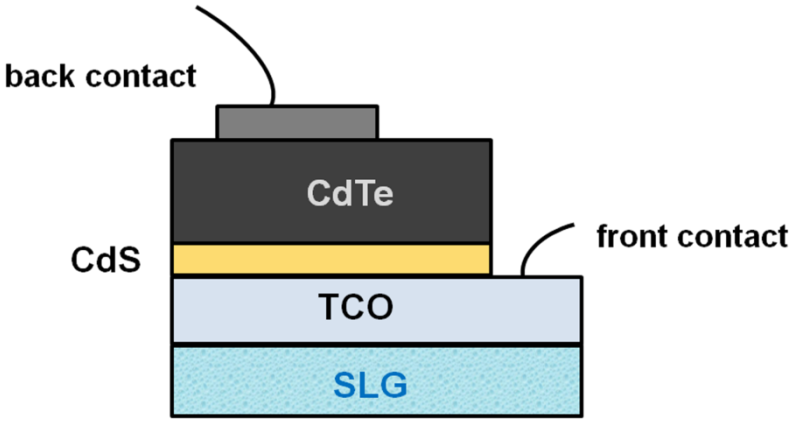

Figure 11: Cross sectional view for the superstrate configuration for CdTe.

Today CdTe solar cells are the most economical thin film technology. First Solar is the main CdTe manufacturer, achieving 5 GW cumulative production capacity already at the end of 2011, and being the

first world's larger thin-film solar module manufacturer and the fifth solar cell producer in the world [5, 46]. First Solar claims to have the lowest energy payback time among commercial technologies (<8 months), and the lowest cost per module (0.4 $/W). Commercial modules efficiencies are about 14% [21, 47, 48]. Currently 21.5% efficient CdTe solar cells have been produced at the lab scale [24, 29].

- Copper, indium, gallium, (di)selenide/(di)sulphide (CIGS) and copper, indium, (di)selenide/(di)sulphide (CIS).

Cu ternary semiconductors started to be used in the early 70's. The most promising heterostructure was CdS/$CuInSe_2$, reaching efficiencies at 12% for single crystals and at 6% for thin films [49]. Nevertheless, the incorporation of Ga was soon realized to widen the energy band gap to about 1.2 eV, and improve the quality of the material making possible to achieve higher efficiencies. CIGS, can absorb most of the incident light within a few microns of material due to a direct energy band gap and high optical absorption coefficient [43].

CIGS modules fabrication follows the substrate configuration, from back to front. As there is no need for a transparent supporting material, more choices are liable regarding the substrates. Flexible substrates like metal foils and polymers can be used [28]. The world manufacturer leader is Solar Frontier with at least 1 GW production capacity [5].

The typical layered cell structure Ni-Al/TCO/ZnO/CdS/CIGS/Mo/Soda-lime glass for a CIGS device is shown in figure 12:

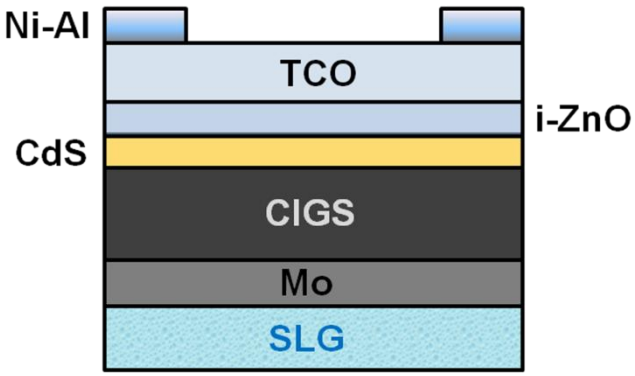

Figure 12: Cross sectional view of a CIGS thin film solar cell on SLG substrate.

CIGS offer the highest efficiencies of all thin film technologies. Efficiencies of 21.7% have been achieved in the laboratory using vacuum techniques [30]. Nevertheless, a quite complex multi-compound structure has made manufacturing techniques more complicated and less standardized than for other cells. Subsequently, production costs increase. Current module efficiencies are about 14% [5]

Despite all the progress achieved by CdTe and CIGS based solar cells, some concerns regarding their future permanency in the market are nowadays posed. The first one is related to the toxicity issues arisen from the use of Cd in the modules. Japan has forbidden their commercialization and sells in the country. Nevertheless, there are some studies that ensure the stability, easy recycling of CdTe modules and thereby their compatibility with health and environmental standards [50, 51]. The second one is the big concern related to the scarcity of Te, Ga and In. The European commission and the US Department of Energy (DOE) have deemed Te, Ga and In as critical or near critical in terms of supply risk [52, 53] .

The high and/or volatile price (specially of In, mainly used in the LCD industry) of these elements could compromise the modules competitiveness in the PV market. Furthermore, future energy needs in the Terawatt level could never be reached due to these raw materials limited availability. A cap of 20 GW per year is predicted for both technologies already for 2020 [54]. As a result of these issues, development of earth-abundant and environmentally benign chalcogenides, based on Cu, Zn and Sn, has captured the attention of the thin film PV research community. CZTS(e) based absorbers are the most promising candidates to compete directly with CdTe and CIGS technologies.

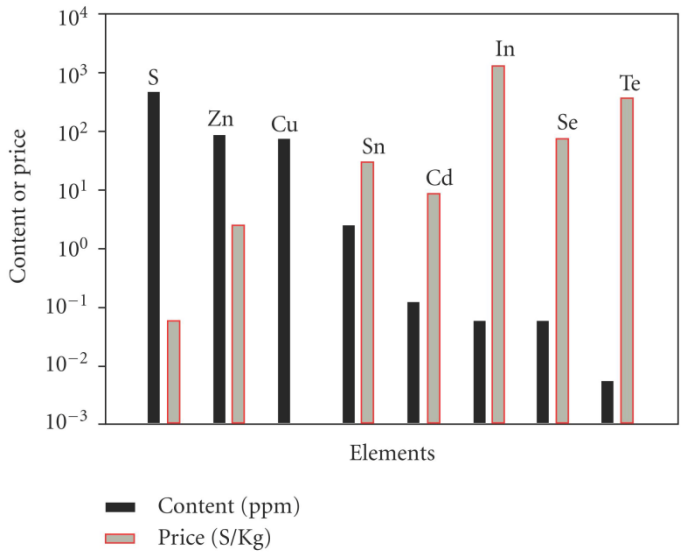

Figure 13: Content and world trading price of the elements used in light absorbers CdTe, $Cu_2ZnSn(S,Se)_4$, and $CuInSe_2$ for thin film solar cells. Figure from [55].

It should be noted that kesterite solar cells share device architecture with CIGS technology, therefore a rapid progress was possible in the past few years. Nevertheless, efficiency improvements remain at the 12% level since 2013, pointing out to the need for customized processing developments to address specific technological issues inherent to kesterite and different from CIGS based devices [56]. These aspects will be analyzed in the next chapter.

2. KESTERITE

2.1. Material properties

Structural properties

Kesterite is a I_2–II–IV–VI_4 quaternary compound and a mineral which can be found in nature, always with Fe in its composition: $Cu_2(Zn,Fe)SnS_4$ [57]. The kesterite crystalline structure can be derived from the zinc-blende or sphalerite cubic one using cross substitutions and respecting the octet rule [58]. As it can be seen in Figure 14 by starting from zinc blende and substuting Zn(II) by Cu(I) and In(III) and/or Ga(III) it is possible to obtain the tetragonal chalcopyrite structure of $Cu(In,Ga)Se_2$ or $CuInSe_2$. Likewise, the kesterite structure can de derived from the chalcopyrite one, replacing half of the In and/or Ga with Zn and another half with Sn. The fact that CZTS(e) and CIGS have similar structural features gives rise to similar optical and electronic features as it will be shown later.

In the literature two principal crystallographic structures known as stannite type (ST) (group $I\bar{4}2m$) and Kesterite type (KS) (space type $I\bar{4}$) have been identified for CZTS(e) [57]. Nevertheless, *ab initio* calculations showed that the kesterite phase formation is slightly less energetic than the stannite phase, i.e. being more stable [59, 60]. The cation position is different in both structures, in the KS the Cu-Zn and Cu-Sn atoms alternate on z = 0 and 1/2 and on z =1/4 and 3/4 positions, respectively, whereas in ST Zn-Sn and Cu atoms alternate on equivalent positions. Another difference is the anion position, in kesterite-type structure the anion occupies a (x, y, z) position, and in the ST type structure the anion lies on a (x, x, z) position [57, 61]. Due to the similarities between the KS and the ST phase, XRD diffraction makes difficult their discrimination, and Neutron diffraction is used as suitable characterization technique to distinguish them [62, 63]. Raman spectroscopy is also a powerful technique to assess structural features [64], but its key role for the kesterite technology lies in the field of secondary phases discrimination, which will be discussed further on. In addition, thin films or powder with disordered kesterite structure and nanoparticles with wurtzite crystalline structure have also been reported [62, 63, 65-67]. Disorder in the Cu-Zn lattice planes can occur when fast cooling of the synthesized absorbers takes place [62, 68, 69].

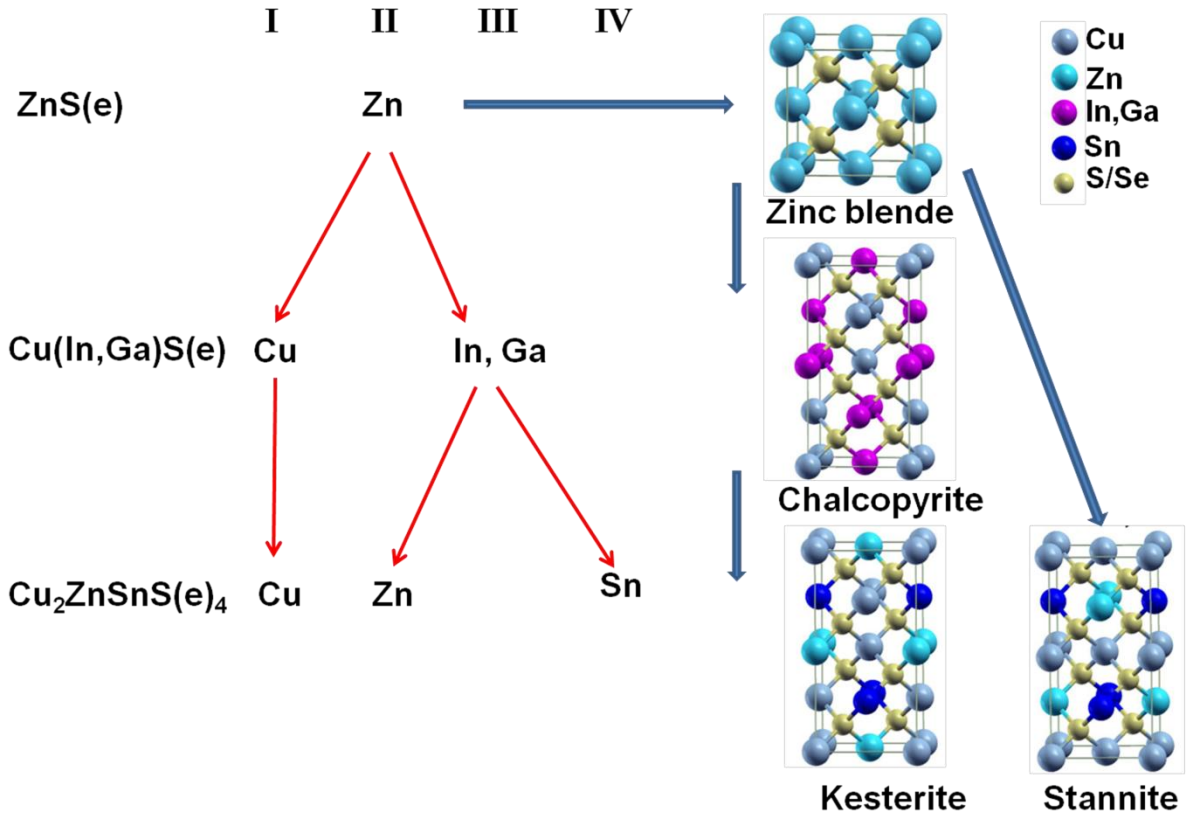

Figure 14: Crystal structure of Zinc blende, chalcopyrite, kesterite and stannite derived from [61].

Optoelectronic properties

Regarding its optoelectronic features, the kesterite compound exhibits p-type conductivity derived from its intrinsic point defects and it has a direct tunable band gap depending on the anion composition, i.e. S/(S+Se) ratio. Values around 1.5 eV for the pure Sulphide [70-72] and 1 eV for the pure Selenide [73, 74] have been reported, being a nearly ideal candidate for solar spectrum matching. The band gap of CZTS(e) can also be tuned by adding other elements without changing the crystalline structure, such as for instance Ge (IV), with theoretical band gap between 1.0-1,5 eV for CZTGSe when varying the Ge/(Ge+Sn) ratio from 0 to 1 [75]. Likewise, Cd (II) cation substitutions can tune the band gap for $Cu_2Zn_{1-x}Cd_xSnS_4$ from 1.1 to 1.5 eV for different x values (different trends have been reported), but in contrast with Ge, the kesterite structure will change to stannite structure for the pure Cd compound (x=1) [76-78]. Furthermore, kesterite has a large absorption coefficient > 10^4 cm^{-1} [70, 79]. Single junction CZTS(e) devices have the potential for 30-34% efficiency [80].

The hole mobilities are reported between 0.1 and 40 cm^2 V^{-1} s^{-1}, with the highest value for the pure Se compound [81-83]. The carrier density has been reported with values spanning from 10^{15} to 10^{18} cm^{-3} [56, 81, 84, 85]. An increase of carrier concentration was correlated with higher S content [84]. The resistivity has been reported from 10^{-3} to 600 Ω cm [83]. The large differences in the values reported are linked to a

wide variety of deposition techniques coupled to a fairly complex multinary compound with multiple secondary phases and electrically active point defects.

Defects

The defects with the lowest energy formation in the kesterite system are Cu_{Zn} and V_{Cu}, both acceptor-type and thereby generally assumed as responsible for the p-type conductivity [86, 87]. However, the position of the Cu_{Zn} defect with respect to the Valence Band Maximum (VBM) is slightly less shallower than the V_{Cu}, being 0.1 eV for the former and 0.02 eV for the latter [86].

Formation of donor defects, on the contrary are energetically more unfavored. Nevertheless, neutral defect complexes such as (Cu_{Zn} + Zn_{Cu}) and (V_{Cu} + Zn_{Cu}) are also relatively easily formed, especially in common Cu poor Zn rich growth conditions [87]. It should be noted that Cu poor Zn rich conditions are systematically reported as necessary to obtain high efficient devices [88], as it will be discussed later on. In consequence, the formation of deep donor defects acting as recombination centers in the band gap could be suppressed by more electronically benign non charged defect complexes [86, 87]. Thus, kesterite has been judged as possessing an electronically benign character [87].

2.2. Kesterite solar cells. State of the art

The photovoltaic effect in CZTS(e) compounds was proved by the first time in 1988 by Ito and Nakazawa. A heterodiode made by a thin film transparent conductive Cadmium Tin Oxide (CTO) and CZTS thin film on stainless steel, produced an open circuit voltage of 165 mV [70].

Katagiri et al. reported in 1996 a sequentially evaporated CZTS film using electron beam evaporation. Device configuration was very close to the standard used today. The sequence of layers was glass/Mo/CZTS/CdS/ZnO:Al. The efficiency reported was 0.66% and the open circuit voltage 400 mV [89]. Since then, a lot of progress has been done in kesterite devices, reaching 9.2% efficiency for a CZTS absorber, 11.6% for CZTSe and 12.6% for a CZTSSe based solar cell [56, 85, 90].

The conventional device structure reproduces the CIGS based devices one as it was previously stated, and thereby it consists on SLG substrates or steel or polymer foils coated with Mo from magnetron sputtering (500-1000 nm), the $CZT(S,Se)_4$ absorber (1-2 μm), CdS buffer layer from chemical bath deposition (CBD) (30-60 nm) and i-ZnO/TCO (50-100 nm/250-500 nm) from magnetron sputtering, acting as transparent window and contact layers. The TCOs more frequently used are AZO (ZnO:Al) and ITO (In_2O_3:Sn). Metal contacts of Ni/Al can be deposited by thermal or e-beam evaporation and MgF_2 antireflective coating also from e-beam evaporation can further complete the devices. This device architecture is shown next:

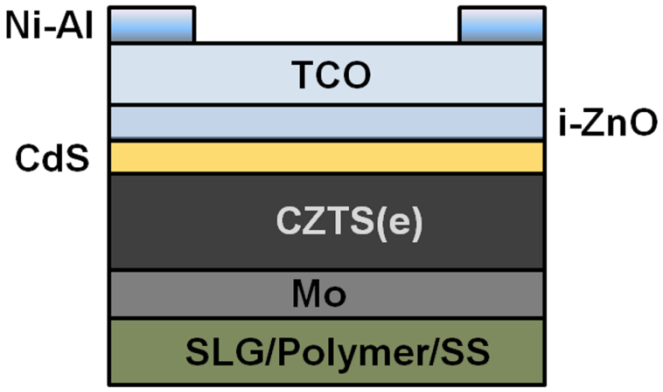

Figure 15: Scheme of conventional CZTS(e) solar cell configuration.

The techniques to produce kesterite are divided in two big categories, non-vacuum based methods and vacuum based ones. In contrast with CIGS, the highest efficiencies are obtained with cost effective non-vacuum techniques, although vacuum based ones are currently at fairly similar efficiency values [56, 85].

Among the non-vacuum or solution based deposition methods must be highlighted electrodeposition, spray and spin coating techniques. Electrodeposition led to 8.2% CZTSe solar cell obtained by sequential Cu-Sn-Zn electroplating and subsequent 550 ºC reactive annealing [91]. The spray technique recently led to a remarkable 10.8% CZTSSe solar cell using water-ethanol solution to disperse Cu-Zn-Sn-S colloids in a globe box, and subsequent annealings in N_2 and Se atmospheres [92]. Regarding spin coating, the largest efficiencies have been obtained for CZTSSe absorbers with this simple method. 11.8% efficient cells were produced using DMSO as solvent along with metal salts and thiourea as Cu-Zn-Sn and S sources respectively, followed by annealing in Se atmosphere [93]. The current world record, 12.6%, already set in 2013 by the New York based research center of IBM was also produced with a similar approach, although relying in highly toxic and explosive hydrazine solvent [56].

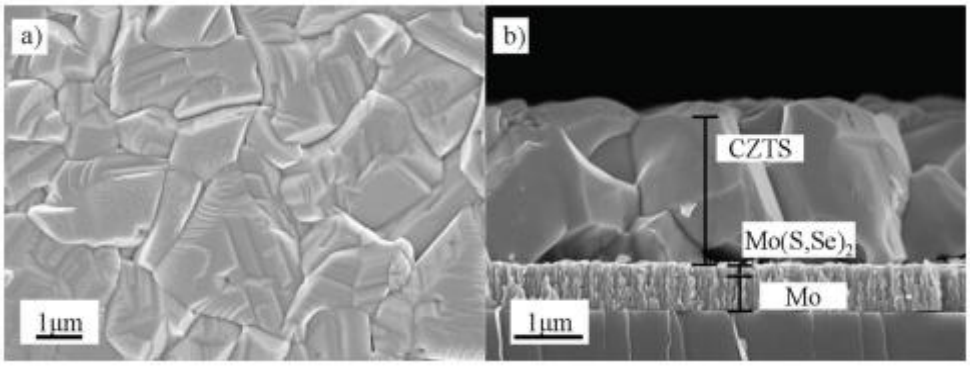

Figure 16: A) Top SEM view of a 12.6% world record CZTSSe solar cell. B) Cross sectional SEM view of a 2 μm sized CZTSSe absorber from the same solar cell. Both images are from ref [56].

Regarding vacuum methods the most relevant are sputtering and co-evaporation. Co-evaporation at 150 ºC followed by reactive Se annealing at 590 ºC allowed for 11.6% CZTSe solar cells obtained by IBM [85]. In the case of sputtering combined with reactive annealing as successive processing steps, 9.2% CZTS minimodules of 14 cm^2 aperture area were produced by Solar Frontier [90]. Additionally an impressive 11% for a similar submodule but based on CZTSSe absorbers was also fabricated by Solar Frontier after absorber band gap grading via Sulphur modification and reduction of back ZnS segregation [94].

It has to be noted that in the last years many new companies focusing on kesterite have emerged, as well as CIGS companies using their knowhow to push kesterite technology forward. As it was already mentioned, the Japanese CIGS company Showa Shell has produced the highest efficiency CZTSSe submodules with 11% efficiency using a sputtering process [94]. A smaller CIGS US based company, AQT, using co-sputtering achieved a 9.3% CZTSSe solar cell [84]. Other non European companies with efficiencies exceeding 8% are Dupont (8.5%, spin coating) [95], and Toyota (9.1%, sputtering) [24, 96]. In the case of Europe, an innovative Estonian-Austrian company named Crystalsol is developing a new solar cell design. The absorber is composed by 40 um sized single crystalline CZTSSe monograins, individually covered by a thin CdS layer and glued together with epoxy to a polymer film. A certified 8.4% solar cell was obtained with this technology [97]. Finally, the German CIGS company Avancis has produced 6.6% CZTSSe devices using proprietary rapid thermal and sputtering processes for already commercialized CIGS modules [98].

Table 1: State of the art of CZTS(e) solar cells with efficiencies ≥ 8%, reporting absorber type, deposition technique, annealing condition and institution.

Material	Deposition technique	Annealing condition	η (%)	Institution	Ref
CZTS	Sputtering	H_2S-Ar	9.2	Solar Frontier	[90]
	Co-evaporation	S-RTP	8.4	IBM	[99]
	Electrodeposition	S	8.0	RCSEC-Japan	[100]
CZTSe	Co-evaporation	Se	11.6	IBM	[85]
	Sputtering	Se+Sn	10.6	IREC	[101]
	Electrodeposition	Se+Sn	8.2	Nexcis-IREC	[91]
CZTSSe	Spin coating (hydrazine)	S-RTP	12.6	IBM	[56]
	Spin coating (DMSO)	Se	11.8	WA University	[93]
	Sputtering	Sulphurization after Selenization	11.0	Solar Frontier	[94]
	Spray (water-ethanol)	N_2-Se	10.8	IMRA	[92]
	Monograin powder	Quartz ampoules	8.4	Crystalsol	[97]

It can be concluded that kesterite has captured a lot of attention in the past few years. So far best devices are compositionally either Se rich or Se pure, pointing out towards intrinsic problems when having more Sulphur in its composition [102, 103]. Since 2009 the top leading deposition techniques were the solution based ones, IBM pushed forward the technology when achieving efficiencies around 10% already in that year [104]. Nevertheless, in recent years several deposition methods have exceed that value being closer to the current efficiency record value of 12.6% also set by IBM in 2013 [56, 85, 94, 105]. The present work focuses on high vacuum industrially scalable sputtering + reactive annealing methods using conventional SLG substrates and more novel flexible and light-weight SS ones. The core of this thesis is to address relevant limitations that are inherent to the kesterite technology and different from the more mature and established CIGS based one. Additionally, a deep study on the implementation of CZTSSe on flexible and light-weight steel substrates is included, which could definitively increase the ambitioned PV market penetration due to more diversified market niches.

The main peculiarities and limitations of kesterite technology are discussed in the next section.

2.3. Main technology problems. Challenges to address

As it was previously mentioned the aim of this thesis is developing and investigating new customized processing approaches for the improvement of CZTSe based thin film solar cells. Several innovative processing approaches to address some of the major issues of this technology are already published and included in this thesis.

Despite its rapid progress in recent years CZTS(e) barely has half of the efficiency of the more mature and already commercialized CIGS chalcogenide absorber, having achieved only 12.6% efficient solar cells compared with the 21.7% CIGS record values [30, 56]. The targeted 18-20% efficiency value necessary for market production is thereby very far at the moment [20, 106, 107]. The truth is that although kesterite shares a lot of similarities in terms of optical and electrical properties with its already commercialized CIGS chalcogenide counterpart, many singular features make kesterite a much more challenging material [103, 108, 109]. Currently, a remarkable V_{OC} deficit when compared with the CIGS chalcopyrite cousin is the issue most frequently reported as the major problem to overcome to definitively boost kesterite based devices efficiency [106, 110, 111]. The sources of this V_{OC} deficit have been mainly linked to potential fluctuations in the CZTS(e) structure reducing the fundamental gap of the material and/or band gap fluctuations [111-113]. The presence of high concentration of defects in the bulk and at the interfaces of CZTS(e), compositional non uniformities within the absorber and the inevitable co-existence of multiple secondary phases along with the kesterite absorber, are often mentioned in the literature as plausible causes [103, 106, 113].

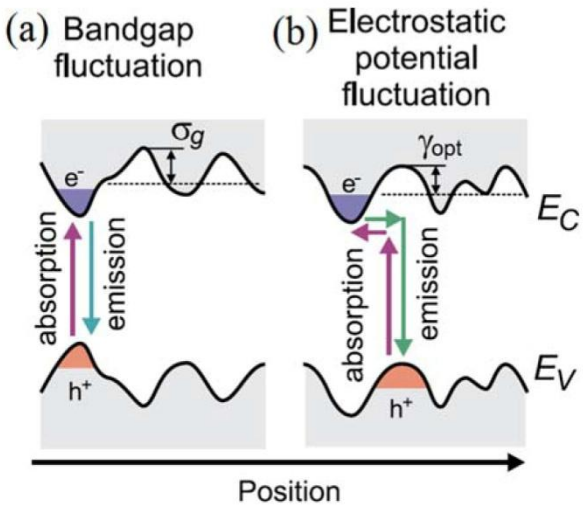

Figure 17: Band gap variations as a result of band gap fluctuations (a) and electrostatic potential fluctuations (b) from ref [111].

It seems clear that to improve CZTS(e) devices changes in the processing conditions to maximize V_{OC} must be performed, with the bulk and interfaces of the material as paramount working areas. Whereas

chemical etchings have proved to be an important tool to modify the properties of the p-n junction, and therefore to improve V_{OC} among other parameters, changing the back contact interface led as well to significant improvements [114-120]. This is the reason one of the main parts of this doctoral thesis is dedicated to the back and front interfaces of CZTSe devices.

Since the origin of the large V_{OC} deficit might be related with the intrinsic differences that kesterite has when compared with its chalcopyrite cousin CIGS, these differences are presented below.

One of the most relevant differences is the much narrower thermodynamic region for the single phase quaternary compound that has been determined for CZTS(e) at the common growth temperatures of 550 ºC [121, 122]. Moreover, chemical potential-based stability diagrams also reveal a very limited stable CZTSe formation region, which is further reduced for Cu poor conditions [102]. As a consequence, important drawbacks related to the coexistence of secondary phases along with the main CZTS(e) phase can be expected. It is important to note that so far, the best performing devices rely on absorbers that are Cu-poor and Zn-rich in their final composition, as it was already confirmed in 2009 by Katagiri [88]. These off-stoichiometric conditions will inevitably lead to the formation of secondary phases, and most likely ZnSe [109, 123]. Figure 18a shows the CZTSe experimentally determined pseudoternary diagram from binary Cu_2Se, ZnSe and $SnSe_2$ evidencing its narrow single phase region indicated by a red circle. The green circle corresponds to the most common Cu-Zn-Sn compositional working area, which predominantly gives rise to ZnS(e) secondary phases. Furthermore the stable chemical potential region of the CZTSe constituents is shown for Cu-rich and Cu-poor conditions in Figure 18b and c respectively.

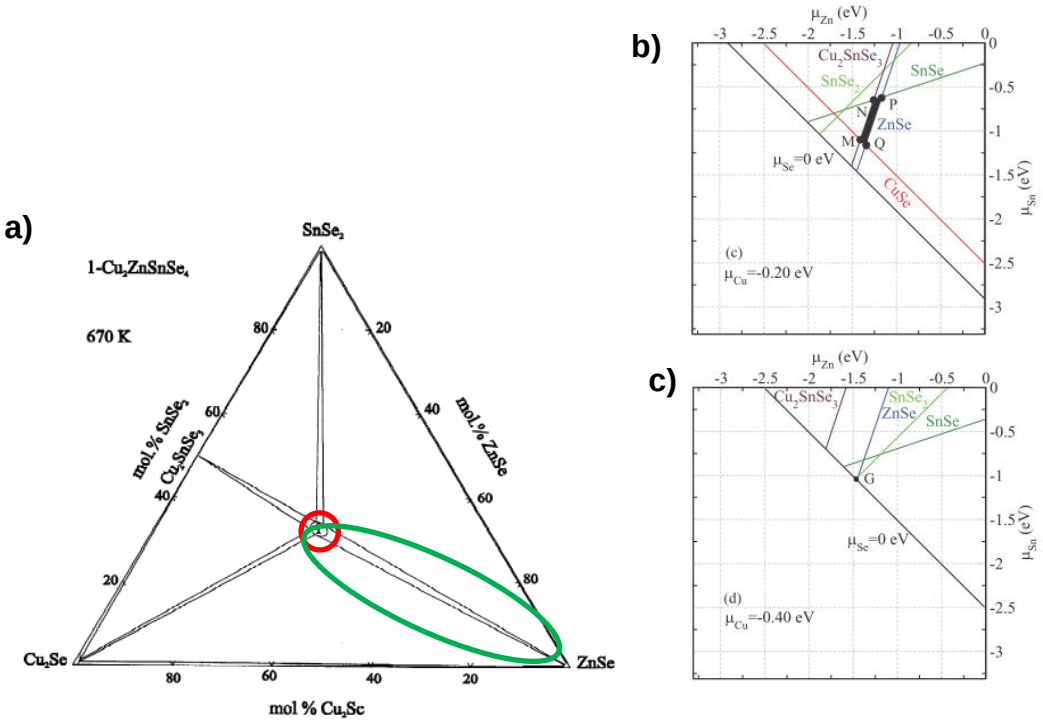

Figure 18: a) Pseudoternary phase diagram for CZTSe at 550 ºC adapted from [121]. The red circle indicates the single phase CZTSe region, and the green one the Cu poor Zn rich region which allows for high efficiency kesterite devices; calculated chemical potential CZTSe stable region for μZn and μSn planes with Cu rich conditions (b) and Cu poor conditions (c) from [102]. Black area indicates the stable region.

The influence of ZnS(e) in CZTS(e) solar cells performance has been studied in several works and it will be discussed later in section 5.2. Within the course of this thesis an innovative oxidizing and passivating chemical etching to remove ZnSe from Zn-rich CZTSe absorbers has been developed and published in an article attached in the Appendices section (A.S.) A3

In addition to the limited compositional synthesis window for kesterite compared with CIGS it has to be added a higher thermal instability due to the higher volatility of its constituents, mainly Sn and Zn [123, 124]. Kesterite can decompose already at 400 ºC and therefore careful control of the partial pressure of main gaseous species involved in the kesterite equilibrium formation should be considered. Thus, Se(g) and SnSe(g) partial pressures should be high enough to avoid kesterite to decompose into its binary and ternary compounds as it can be observed in reaction (1) [123-126].

$$2Cu_2SnS(e)_{3(s)} + 2ZnS(e)_{2(s)} \leftrightarrow 2Cu_2ZnSnS(e)_{4(s)} \leftrightarrow 2Cu_2S(e)_{(s)} + 2ZnS(e)_{(s)} + 2SnS(e)_{(g)} + 1/2S(e)_{2(g)} \quad (1)$$

Scragg et al. have also pointed out another singularity that is clearly in contrast with CIGS [127]. The widely accepted stability and inert character of the Mo back contact for CIGS solar cells can no longer be applied for kesterite based solar cells. A degradation of the Mo/CZTS interface upon thermal annealing

inducing the formation of the related CZTS binaries and MoS_2 was demonstrated. Furthermore, existence of this reaction for the Selenide compound has also been proposed (see equation 2), but no experimental data was published for this system until a novel approach included in this thesis to limit the degradation at the back contact interface was developed by our research group. Based on thermodynamic calculations the free energy of the decomposition reaction was determined resulting in -100 kJ for the pure selenide compound, and -150 kJ for the sulphide one. Additionally, the work of Scragg et al. was done using a sulphur-free atmosphere in the annealing processes. This contrasts with the thermal treatments usually performed for the synthesis of device grade absorbers, which are done in S(e) or $H_2S(e)$ containing atmospheres, in some cases also with Sn or SnS(e) to prevent Sn loss during the annealing [105, 125, 128]. As a result, there was a strong motivation for the study of the potential occurrence of this decomposition reaction in the case of the selenide system when using standard thermal processes. Under Se atmosphere annealings reaction (3) and (4) are likely to occur as reported in a publication part of this thesis in ref [115], which can be found in the A.S. A1.

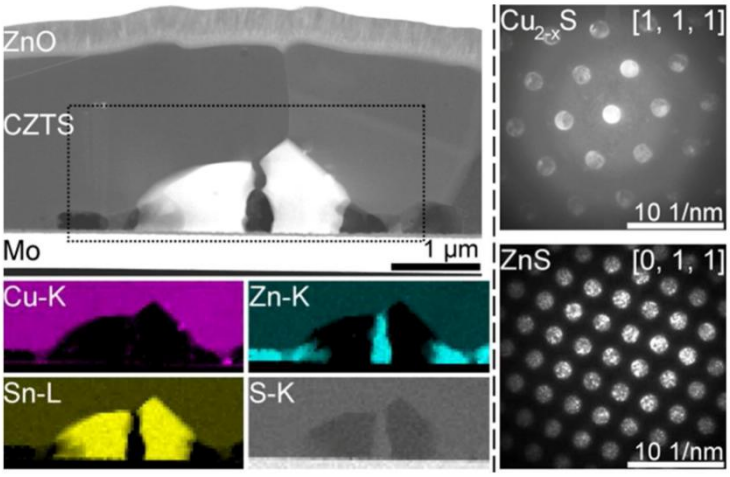

Figure 19: TEM image of a CZTS film, indicating the area mapped by EDS. Secondary phases, Sn-S and Zn-S are detected at the CZTS/Mo back interface due to decomposition during annealing. Image obtained from [127].

$$2Cu_2ZnSnS(e)_{4(s)} + Mo_{(s)} \rightarrow 2Cu_2S(e)_{(s)} + 2ZnS(e)_{(s)} + 2SnS(e)_{(s)} + MoSe_{2(s)} \quad (2)$$

$$xCu_2S(e)_{(s)} + (1-(x/2))Se_{2(g)} \rightarrow 2Cu_xSe_{(s)} \quad (3)$$

$$2SnS(e)_{(s)} + Se_{2(g)} \rightarrow 2SnS(e)_{2(g)} \quad (4)$$

The present PhD Thesis proposes two customized solutions to avoid or minimize undesired effects at the back CZTSe/Mo interface. The goal is to reduce the presence of voids and the poor morphology resulting from loss of gaseous species and to limit and control the formation of $MoSe_2$. In consequence, during the course of this thesis an intrinsic ZnO layer and multilayered Mo back contacts combined with thin

intermediate MoO_2 layers have been implemented as processing strategies to minimize back interface issues.

To sum up, it is evident that using similar technological CIGS processing steps to produce CZTS(e) devices has contributed to accelerate their development in the last years. Nevertheless, clear evidences of new challenges to address in kesterite based solar cells are well identified now. As a result, it is of utmost importance to develop new customized processes to tailor kesterite main drawbacks and to boost its progress in the PV competitive market, such as the ones included in this Thesis.

2.3.1. CZTS(e)/Mo interface engineering. State of the art

Introducing changes to the conventional Mo back contact is necessary to minimize the decomposition reaction between CZTS(e) and Mo reported in the literature (see eq (2)) [127]. This undesired reaction is connected with the presence of secondary phases, usually binaries of Cu, Zn and Sn, and also voids due to the volatility of some of the decomposition reaction products [115, 127]. It is important to note, that even the best devices reported in the literature exhibit holes at the back contact interface, causing a poor morphology that can affect the optoelectronic properties of the devices [56, 128]. Additionally, a thicker $MoSe_2$ layer can be formed by the uncontrolled reaction between the chalcogen, Mo and CZTSe known as overselenization, and thereby affecting as well the solar cells performance [119]. Nevertheless, despite it is commonly agreed that $MoSe_2$ can be detrimental for solar cells when present in large amount, it seems also clear that is necessary to allow for a good ohmic contact at the back region [129-131].

So far, several layers have been introduced in addition to the Mo back contact with the aim of coping with its instability during the thermal annealing treatments. A TiN layer has proved to be an effective way to control the overselenization of the back contact, i.e. the $MoSe_2$ thickness. A thickness as low as 20 nm improved the V_{OC} more than 100 mV and the efficiency from 2.95% to 8.9 [119]. Moreover, an energy barrier at the back contact of 135 meV reported in the literature, was significantly reduced by the introduction of a TiN layer of 100 nm, reducing the series resistance, R_S, and increasing the efficiency [118]. During this PhD thesis, the introduction of a 10 nm i-ZnO layer between the Mo and the CZTSe absorber was suggested to reduce the detrimental degradation of the back solar cell interface. The results showed a morphology improvement of the back contact interface by reducing voids and minimizing the decomposition reaction, generating less secondary phases at this region identified with Raman spectroscopy. As a result, an important improvement in J_{SC} and FF increased the efficiency from 2% to 6% [115]. Similar results were reported for the pure sulfide, CZTS, using 10 nm of ZnO, 30 nm of TiB_4 and 20 nm of Ag [132-134].

Despite improving the performance of our devices by the introduction of the i-ZnO nanometric layer, a very thick $MoSe_2$ layer was usually formed and still very often with a significant presence of holes. It has to be noted that the annealing treatment when developing the ZnO intermediate layer process was further

optimized, being higher in temperature (525 ºC versus 550 ºC), increasing the chances for thicker $MoSe_2$ and/or voids at the back contact region. In consequence, the developing of a process to control the $MoSe_2$ formation was crucial to push further the efficiencies and the reproducibility of our CZTSe devices. We studied several Mo configurations such as monolayers, bi-layers and tri-layers in terms of $MoSe_2$ formation and device performance, among other features. These results are included in both section 5.1.2 and A.S. A2. They are part of one manuscript with status under review at the time of this thesis submission.

Traditionally, it was commonly agreed in CIGS solar cells and later for kesterite technology, that a bi-layer structure is necessary to achieve good adhesion properties (bottom layer) and good electrical features (upper layer) simultaneously [135-137]. In our particular case when using low pressure conditions and high power density for the Mo deposition, our films showed good electrical features, sheet resistance ~ 0.2-0.3 Ω/sq for 800 nm of Mo layer, but no poor adhesion properties in contrast with the literature [136, 137]. However, a severe problem of overeselenization as it can be seen in Figure 20 usually occurred. Therefore, we decided to invert the typical stack order of bi-layers configuration in terms of pressure that is commonly reported in the literature: bottom/high pressure and top/low pressure, in order to deal with this problem. The main reason to do so, is that an increase in the sputtering pressure can lead to a higher incorporation of O_2 from the background sputtering environment reducing the formation of $MoSe_2$ [138]. This can be due to a more porous structure with more inter-granular space where impurities can be adsorbed and/or diffuse [135, 139].

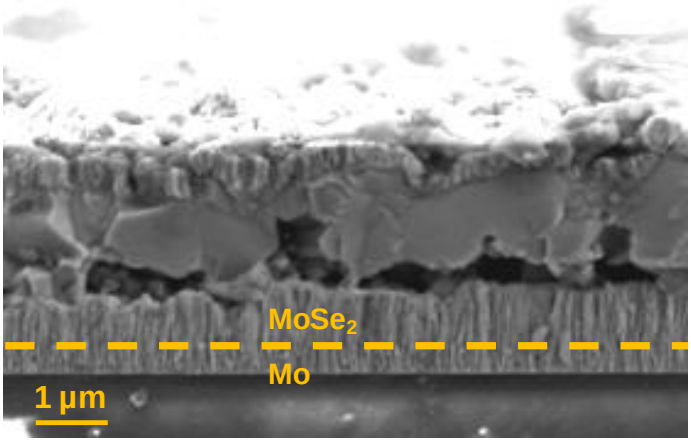

Figure 20. SEM cross sectional image of a full CZTSe solar cell based on a Mo monolayer sputtered at low pressure (previous baseline). Note the overselenized Mo back contact with a large $MoSe_2$ layer formation (~800 nm).

Another interesting aspect to be considered is the oxygen content in the Mo back contact. It has been reported for both CIGS and CZTS(e) its beneficial effect for solar cell performance when present in a certain amount [140, 141]. In the case of CZTS, an increase in O content in the Mo back contact, via annealing in N_2 atmosphere at 550 ºC for 10 min, coupled with an increase in Na content, led to a

reduction of the MoS_2 layer after the thermal annealing, reducing considerably the R_S [141]. A similar effect, reducing $MoSe_2$ thickness, has been reported to be beneficial for CZTSSe solar cells, where 1% of O_2 was incorporated to the Mo during the sputtering process [138]. Thus, it can be inferred that the study of Mo oxidation processes and/or its oxides, MoO_2 and MoO_3 are highly relevant for the thin film solar cell community.

So far, the effect of a MoO_2 layer with varying thickness was only reported for CISe absorbers by Duchatelet et al., by oxidizing Mo coated SLG substrates in a tubular furnace for specific time. In this way, the formation of $MoSe_2$ was suppressed with minimum impact in the sheet resistance of the back contact [142]. Nevertheless, the use of this thermal growth method is limited in terms of layer homogeneity and thickness control. Furthermore, to obtain a controlled stoichiometry 1:2 in the Mo:O ratio can be also fairly complex. In consequence, we investigated for the first time the introduction of a controlled and thin MoO_2 layer thermally evaporated from the pure oxide powder in several Mo configurations in CZTSe solar cells. The layer results in an effective way to prevent the overselenization of the back contact even using as low thickness as 10 nm. As a result, we obtain a large improvement in solar cell performance, mainly related to a dramatic increase in V_{OC} and FF, but also shunt resistance, R_{SH}, linked with a remarkable change in CZTSe grain size. Furthermore, relevant structural changes in both $MoSe_2$ and CZTSe layers due to the presence of the MoO_2 were also observed. The results of the MoO_2 study are included as well in both section 5.1.2 and A.S. A2.

2.3.2. CZTS(e) secondary phases removal by chemical etchings

In this section the main chemical processes applied to kesterite technology are reviewed, with special emphasis in the oxidizing/passivating chemical etching developed in this thesis to remove ZnSe and different oxides from the CZTSe absorber surface.

ZnSe is a wide band gap (2.71 eV) n-type semiconductor [143]. The influence of ZnS(e) in CZTS(e) solar cells has been studied in several works. In the case of CZTS, the presence of ZnS was detected at the back of devices with 8.4% efficiency [99], and yet considered just like a "dark space", i.e. reducing the effective volume of the absorber, and not harming significantly the device performance further. In contrast, the presence of ZnS at the back in CZTSSe devices was determined to cause a series resistance (R_S) increase [94]. Likewise, ZnS detection (location not specified) in other devices was correlated with a decrease of 25% in the efficiency [144]. Furthermore, a clear evidence of its detrimental role when present at the surface of CZTS absorbers was also pointed out [114]. In this case after a selective chemical etch in HCl the devices showed a 50% improvement in the efficiency, tied to an increase in J_{SC}, V_{OC} and FF.

In regards to ZnSe, direct evidence of J_{SC} reduction due to the presence of a ZnSe phase at the front of the absorber was also reported [145]. Moreover, an extended analysis of the role of this phase related to its

position in the absorber (surface and back regions) was also investigated [146, 147]. The results showed how ZnSe at the back region is much less harmful for the device performance than when it is located at the surface region of the absorber. Large degradation of V_{OC}, J_{SC} and FF was reported. It was pointed out that large grains of ZnSe at the surface region impede the formation of good ohmic contact with the CdS buffer layer.

It can be inferred then that detection of these secondary phases is a paramount issue to develop effective removal processes. It is well-known that CZTS(e) and ZnS(e) have similar X-ray diffraction patterns, making secondary phase identification difficult [148]. In consequence, Raman spectroscopy has emerged as a powerful complementary tool, among other techniques [64, 116, 144, 149-151]. Using a UV excitation source (325 nm) and a blue excitation one (457.9 nm), quasi-resonant Raman excitation conditions can be achieved for ZnS [114, 150] and ZnSe [116, 149] respectively. This allows efficient detection of even very low quantities of these secondary phases, because of the strong enhancement of the efficiency of the main Raman peaks characteristic of these phases resulting from the quasi-resonant excitation conditions.

It is clear that effective removal of secondary phases is necessary to push CZTS(e)-based devices forward in the efficiency-oriented marketability race. So far, a few effective etchings have been reported for CZTS(e) absorbers besides the well established KCN one adopted from CIGS technology to remove $Cu_xS(e)_y$ secondary phases [152-155]. In the case of CZTS thin films, only etching in deionized water (DIW) [156] and in HCl [114] have proved to be significantly effective regarding the efficiency of the devices. As for the solid solution CZTSSe, a chemical etching based on aqueous $(NH_4)_2S$ solutions allowed for an effective removal of $Sn_xS(e)_y$ secondary phases and passivation of the surface due to surface oxides removal. In this work, the passivation mechanism takes place via formation of S bonds from $(NH_4)_2S$ solution while removing Oxygen bonds at the absorber surface [120]. Another passivation etching was reported as well for CZTSSe using 30s 0.5 M HCl solution and subsequent dip in 0.5 M 67 ^{o}C Thiourea solution for 1 h, although in this case no surface Sulphur bonding was reported. An impressive increase from 6.3% to 10.3% was obtained [157].

Regarding CZTSe polycrystalline films, only a reference using both Br in methanol (Br_2-MeOH) and HCl, along with a further etching in 5% KCN is reported in the literature [117]. The use of Br_2-MeOH is coupled with a decrease of Cu and Sn at the surface, related to the selective etching of a Cu-Sn-Se (CTSe) secondary phase, and HCl to a reduction of Zn, related to etching of the ZnSe secondary phase. However the relative improvement in efficiency is moderate, with just 0.5% gained after the KCN etch and the main improvement related to the V_{OC}. In contrast, the use of 1% Br_2-MeOH in CZTSSe and CZTS kesterite monograin (40 μm) solar cells was linked to a Sn surface enrichment, and formation of Sn-O and/or Sn-Br species, which can be dissolved after KCN etching, giving the best results for this type of cell architecture [158, 159].

Before the development of the oxidizing etching included in this work, there was no clear evidence of an effective etching to remove ZnSe in Se-pure or Se-rich thin-film kesterite-based devices which had a significant impact on the device efficiency. It has to be noted that at the present time, these devices hold the highest efficiencies of kesterites, and thereby removing ZnSe is highly interesting for the CZTS(e) research community [85, 141].

In this thesis an oxidizing route relying in inexpensive and relatively non toxic oxidizers (compared with KCN and Br_2), like $KMnO_4$ and H_2O_2 in a mineral acid, H_2SO_4, along with a subsequent etching in an aqueous Na_2S solution is proposed for an effective removal of ZnSe from the absorber surface. Furthermore, a passivation of the surface states in CZTSe absorbers was also observed. An absolute efficiency increase of 40% was achieved [116].

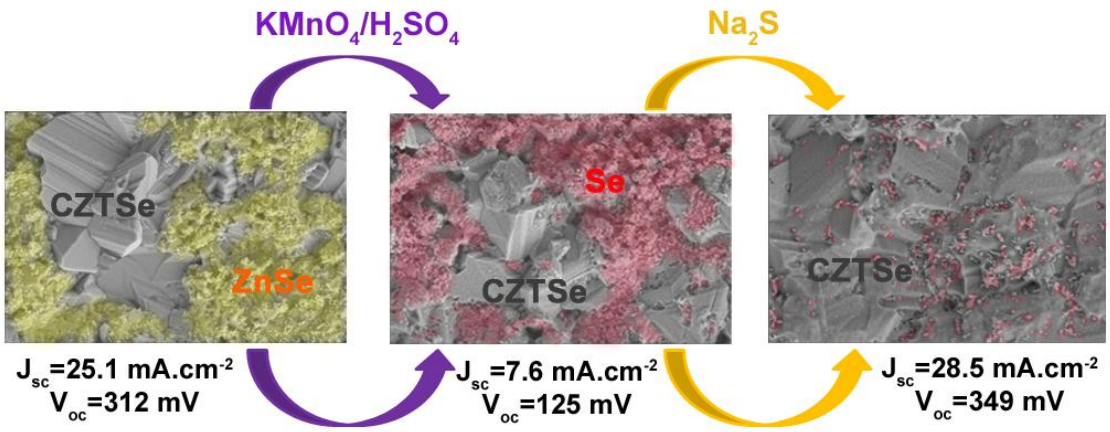

Figure 21: SEM top view of as-annealed, $KMnO_4$ in H_2SO_4 etched and Na_2S etched CZTSe samples. The ZnSe phase is completely removed from the surface after an oxidizing etch. Improvements in J_{SC} and V_{OC} are achieved after the same. Image modified from [116].

2.4. Flexible and light weight CZTSe solar cells

In this section an overview of flexible and light-weight thin film chalcogenide solar cells is presented. More stress on kesterite devices is placed, which are still in an initial development stage when using flexible substrates.

CIGS has currently the highest efficiency among all thin film solar cells with a 21.7% efficient glass based cell [30]. Thin-film PV offers the advantages of low manufacturing costs but the majority of the modules production is based on glass. The fact of using light-weight and flexible substrates could further reduce the manufacturing costs due to their compatibility with high throughput roll-to-roll industrial processes and monolithic integration of solar cells on modules [160]. Furthermore, the range of applications will be considerably broadened: BIPV, portable electronics, chasis of vehicles, space applications…etc. Until very recently, the efficiencies of flexible thin film devices were behind their

glass-based counterparts, but the Swiss research institute EMPA managed to equal the performance of the best polycrystalline Si solar cell with a certified 20.4% CIGS based solar cell on polyimide (PI) [161]. Regarding commercial products, the now Chinese and US based Miasolé CIGS company has reached the world record for a flexible module with an efficiency of 15.7% [162]. Nevertheless, many challenges have to be addressed when considering this type of substrates choice.

The first one deals with the mechanical, chemical and thermal compatibility with all the solar cell processing steps (vacuum, high temperatures over 500 ºC, chemical attacks from etchings and chemical bath deposition (CBD) of buffers …). Additionally, the surface roughness of the substrate should be kept as low as possible to avoid shunt paths on the devices. The second one is the absence of Na, which benefits will be discussed later in section 5.3, thereby requesting a mandatory extrinsic Na supply. Finally, for some of the substrates it is necessary the incorporation of a chemical barrier to avoid the diffusion of metal impurities from the substrate (mainly Fe, Cr and Ni coming from the SS and Al from the Aluminium substrates) to the absorber during its growth process. It has to be noted that additionally, some adhesion promoting layers, such as Ti can be added, and good encapsulation layers to prevent damage from UV and moisture are mandatory when producing finished modules [160, 163].

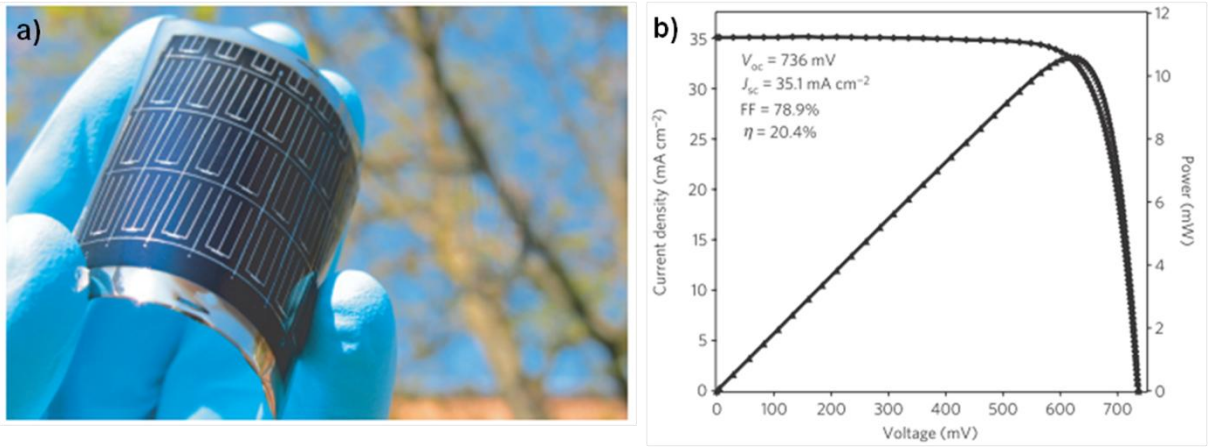

Figure 22: a) Image of a flexible CIGS minimodule on PI; b) I-V curve of the world record thin film flexible CIGS solar cell on PI substrate. Images taken from ref [18, 161].

The substrates that are commonly used can be divided in metals, polymers and ceramics. Among the metals the most relevant ones are Ti, Al and SS (ferritic, austenitic or mild steel). Ti foils have been used with a record efficiency of 17.9% [164], Al foils with 17.1% [165, 166], and SS foils with 17.7% [167]. Regarding the plastics, PI substrates currently hold the world record, achieved using a surface modification process for the CIGS absorber. A 20.4% efficient cell was obtained via co-evaporation at low temperature (< 500 ºC) [161]. In the case of ceramics, ZrO_2 sheets have similar efficiencies, 17.7%, to the ones reported for Ti and SS [168]. It is important to mention that PI substrates only allow for

maximum substrate temperatures of 500 ºC to avoid decomposition. This is clearly in contrast with the other substrates, which allow for T ≥ 600 ºC.

Regarding the impurity barrier layers, usually metallic nitrides or oxide compounds are used such as Al_2O_3 [169], SiO_x [170, 171], ZnO [172], TiN [163] and Si_3N_4 [139]. Cr has also been reported as a successful chemical barrier [173]. It has to be noted that Al_2O_3, SiO_x and ZnO, besides avoiding the diffusion of undesired elements to the absorber, can act as dielectric barriers which allow for the monolithic connection of solar cells in the final module.

For this thesis the choice of substrate has been SS since as it was already mentioned it has a good thermal stability over 500 ºC in contrast with PI substrates, it has a good matching thermal expansion coefficient with CZTSe (similar to the one reported for CIGS), and it is cheaper when compared to Ti and ZrO_2 sheets for instance. Al substrates could be a cheaper option but their CTE is much higher than the CZTSe and the SS ones, especially when compared to the ferritic SS. A table with the CTE values for different materials is shown next.

Table 2: Thermal expansion coefficients (CTE) for different substrates, barrier and solar cell layers. Values taken from [160, 174].

Material	*CTE [10^{-6} K^{-1}]*	*Material*	*CTE [10^{-6} K^{-1}]*
Substrates		**Barrier layers**	
SLG	9	SiO_x	1-9
Ferritic Steel	10-11	Al_2O_3	6-8
Austenitic Steel	10-17	Cr	4.9-8.2
Ti	8.6	ZnO	4.75/2.9
Al	23.1	**Solar cell layers**	
Polyimide	12-24	Mo	4.8-5.9
ZrO_2	5.7	CIGS (CZTS(e))	8-11

Regarding the diffusion barrier Cr was chosen since it has a better CTE match to Mo than Al_2O_3 and SiO_x, and is much cheaper than TiN or Si_3N_4.

The use of flexible substrates combined with thin film CZTS(e) absorbers is barely reported in the literature, only a few devices are reported in the same. CZTS cells via solution based methods were produced on PI (0.49%) [175], Al foils (1.94%) [176] and Mo foils (2.41%) [177]. Regarding vacuum based methods, sputtering deposition was used to produced CZTS solar cells on flexible glass substrates (3.09%) [178] and stainless steel (SS) substrates (4.2%) [179]. During the course of this thesis a 3.5% CZTSe efficient device using austenitic SS (SS304) was produced via sequential sputtering of metallic elements + reactive annealing on SS foils (3.5%) using a Cr diffusion barrier [180]. This was the first flexible thin film CZTSe device reported in the literature. Nevertheless, this device was produced with no extrinsic Na supply which is crucial to allow for high efficient devices [85], as it will be explained in the next section.

Currently, ferritic SS substrates (SS 430) which have lower CTE than austenitic SS substrates, and thereby better thermal expansion match to CZTSe, along with Mo and Cr layers, are used by our research group. These type of substrates are commonly used in the CIGS field. By studying different alkali doping strategies, such as MoNa targets, SLG pieces added during the annealing, NaF and KF pre-absorber synthesis evaporation (PAS) and post deposition evaporation (PDT), we manage to tackle the optimum alkali content and the most suitable process to introduce that alkali into our CZTSe absorbers. Furthermore, we performed a detailed Cr barrier and back contact optimization in order to minimize impurities diffusion from the substrate and to avoid device performance reduction. As a result, we have produced record 5.6% and 6.1% efficient flexible CZTSe solar cells using KF and MoNa with a surface Ge doping respectively. These results will be discussed in detail in chapter 5, section 5.3.2.

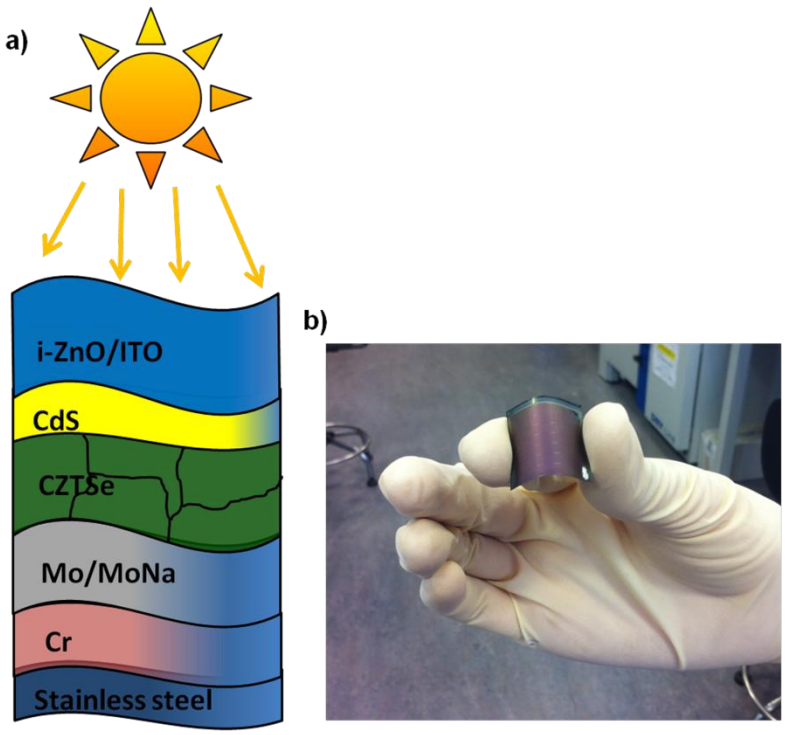

Figure 23: a) Visual scheme of the flexible CZTSe devices configuration used in this thesis. b) 2.5x2.5 cm^2 flexible CZTSe solar cells on SS developed in IREC.

2.5 Alkali doping

In this section the relevance of alkali doping in thin film chalcogenide technologies is discussed, highlighting the main advances of this relevant topic in CZTS(e) field. Whereas Na has been proved to be paramount for CIGS technology, at the moment only a few literature contributions can be found in the CZTS(e) domain. The use of K as dopant is currently a hot and strategic topic in CIGS, which had not been reported in the literature for CZTS(e) technology until part of the results of this thesis were published.

It is widely accepted for CIGS that a certain amount of Na is necessary to produce high performing devices [161, 181, 182]. The improvement on solar cell parameters is related to an increase in V_{OC} and FF, whereas J_{SC} is barely affected or slightly reduced [183-185]. Moreover, an increase in p-type conductivity [186-188], reduced donor density N_D [188], and thereby increased net hole concentration, enhanced grain growth and polycrystalline (112) texturing [189, 190] and reduced inter-diffusion of In and Ga [191] with direct impact on band gap grading, are commonly reported. Nevertheless, contradictory reports in terms of grain growth and preferential orientation can also be found in the literature, clearly making alkali doping a subject still open to debate [182].

Among the main explanations for the Na beneficial effects is the passivation of defects at the grain boundaries (GB) via Na catalytic effect for the oxygenation of Se vacancies, V_{Se}, which act as donors.

This effect will increase the p-type doping, eliminate recombination centers and improve inter-grain transport [192, 193]. This might be one of the reasons that explain a benign behavior of GBs in CIGS [194]. It has to be noted that the beneficial effect of Na has been proved to be independent of the polycrystalline nature of the CIGS. Na led to an increase in hole density and drastic reduction of compensating donor densities in epitaxial CIGS films, thereby in the absence of GBs [188].

Na naturally out-diffuses from the SLG substrates to the absorber upon heating during the absorber synthesis [195]. Nevertheless, it is much more convenient to effectively control its diffusion and final amount in the absorber via extrinsic supply from a Na precursor [189]. The optimum amount of Na in CIGS is considered to be 0.1-0.5 at%, which is commonly the amount supplied naturally upon SLG heating [196-198]. Usually NaF is used as the source of Na, and can be evaporated on the back contact prior to the absorber synthesis, during the absorber synthesis or incorporated via a post-deposition step [191]. So far the highest efficiencies in the CIGS field have been obtained using a post-deposition treatment [161]. Additionally, Na can be supplied from Na doped Molybdenum targets, Mo:Na, which is highly convenient for the industry since it will be already integrated in the back contact deposition step, increasing production throughput and reducing costs [139, 163]. The study of other alkali dopants such as Li, Cs and K was also reported in the literature [186, 189], but with no better results in device performance when compared to Na doping. Nevertheless, recently a combined post deposition treatment of NaF with KF has led to the latest CIGS efficiency advances, including the world record efficiency for a thin-film flexible device, 20.4% [161, 199]. As a result, the research activity in K has now become a hot and strategic topic in CIGS field [199-202].

Regarding the influence of Na on CZTS(e) only a few publications are available. The reported effects are analogue to the ones observed for CIGS. Similar grain growth enhancement and (112) texturing have been observed [203-207]. An increase in device efficiency, coupled to a higher V_{OC} and FF was also reported [207-211]. This performance improvement was coupled with an increase in hole density and mobility, shallower acceptor level and reduction of certain deep trap centers. Moreover, a reduction in J_{SC} has been coupled to a decrease in the SCR and a slight decrease in minority carrier lifetime was noticed as well [208]. For a non vacuum process, based on knife coating of a Na containing nanocrystals (NCs) ink, an increase in minority carrier lifetime was observed when comparing the Na containing CZTSSe absorber to a non Na containing one [212]. Finally, a positive effect for minority carriers transport has been proved for CZTSSe absorbers at the GBs, due to a higher positive potential attracting electrons and repelling holes [213]. This effect could be related to an observed correlation between Na content and passivation of non-radiative recombination centers at the GBs [214, 215].

As it was already mentioned the use of K is still in a preliminary stage in the kesterite field with no literature reports yet. In the case of other alkali dopants, Li has been recently identified in CZTSSe devices by Xin et al. as responsible for an efficiency increase, due to V_{OC}, FF and J_{SC} improvement,

achieving 11.8%, which is the highest efficiency for a non-hydrazine solution processed kesterite device [93]. A conductivity increase of one order of magnitude and an inversion of the electric field polarity at the GBs, driving away minority carrier electrons were confirmed. The latter would be in contrast with the first electric model proposed for GBs in CZTS(e), more in agreement with CIGS, i.e. GBs positively charged and thereby repelling holes and attracting minority carrier electrons, i.e. favoring electronic transport [213, 216, 217]. In any case, a similar GBs behavior to the one proposed by Xin et al. has also been identified by Sardashti et al. observed for CZTSSe absorbers following and oxidation, oxygen removal and subsequent air post-annealing route [218], such as the one we have used in this work to produce our CZTSe solar cells, as reported by Neuschitzer et al [219].

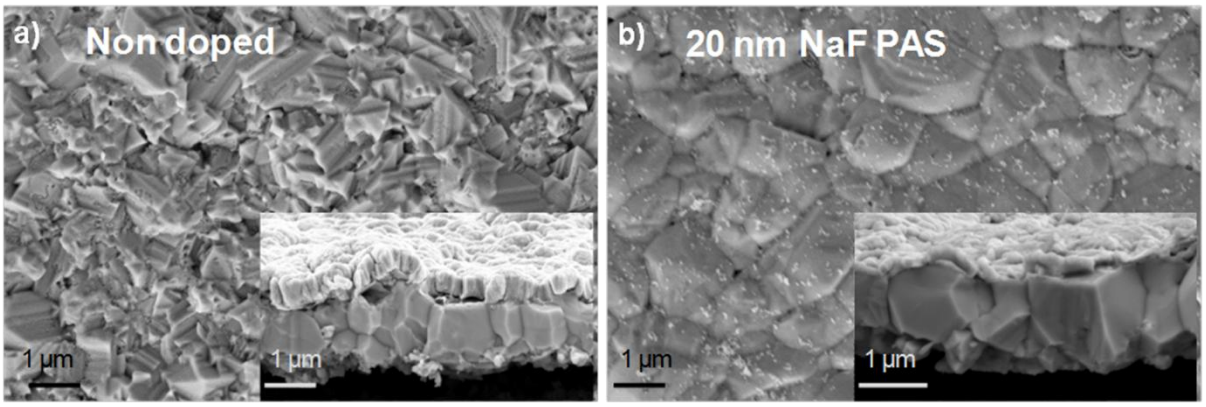

Figure 24: SEM top view images of CZTSe absorbers grown on flexible and light-weight SS substrates (Inset belongs to full CZTSe devices based on these absorbers); a) non alkali doped CZTSe absorber and b) CZTSe absorber doped with 20 nm of NaF deposited with a pre-absorber synthesis method (PAS). Note the surface morphology improvement when using Na during the absorber growth.

It can be concluded that studying the effects of alkali in CZTS(e) is still a hot and relevant topic. Thus, a significant part of the present thesis was devoted to the investigation of the Na and/or K impact on CZTSe solar cells performance on alkali free SS substrates. The fact of working with flexible and light substrates further increased the novelty and interest of the work done.

3. AIM AND OBJECTIVES

The aim of this thesis is to identify specific limitations that kesterite technology presents to customize new processing approaches which directly address the detrimental effects of these limitations in CZTSe based solar cells. These new processing approaches were mainly implemented in glass-based CZTSe solar cells but this thesis has an additional goal. This goal consists in diversifying the market niche of kesterite solar cells implementing its development in flexible and light-weight stainless steel substrates. By doing so, the future targeted commercialization could be eased in the quite competitive and complex current PV market.

The main objectives of the present PhD thesis are:

a) Reviewing the main PV technologies to stand out the advantages of new chalcogenides thin films relying in earth-abundant elements such as CZTS(e) photovoltaic absorbers. Analyzing as well some of the main problems of these materials to identify and to implement new processing solutions to tackle them.
b) Synthesis of CZTSe absorbers from a sequential two step process: sputtering of Cu-Zn-Sn metallic stack followed by reactive annealing under vacuum in Ar with Se and Sn powders.
c) Developing processing steps to avoid detrimental effects at the CZTSe/Mo interface, such as poor morphology and voids and excessive $MoSe_2$ formation.
d) Developing a chemical etch to remove common secondary phases at the CZTSe surface, using cheap and relatively non toxic chemicals.
e) Implementing the use of flexible and light-weight substrates in CZTSe solar cells processing, in contrast to conventional and rigid SLG.
f) Studying the influence of Cr diffusion barrier and back contact modification in flexible CZTSe devices on SS.
g) Studying the impact of alkali dopants, Na and/or K, into flexible CZTSe devices performance on alkali free SS substrates.
h) Conducting structural, morphological, electrical and compositional characterization of CZTSe bulk, surfaces and interfaces within the solar cell architecture along with an optoelectrical characterization of the CZTSe devices developed in this thesis.

4. METHODOLOGY

To fulfill the objectives previously listed, an extensive research based on experimental work to develop CZTSe solar cells trough multiple processing steps was carried out. This experimental work was completed with a wide range of data analysis based on material and devices characterization. The experimental processing steps and characterization techniques will be addressed later on.

The majority of the work developed in this thesis was carried out at the laboratory of the Solar Energy Materials and Systems Group of the research institute IREC. All the solar cells included in this work were produced in the IREC facilities. Only part of the materials characterization was done outside the institute, for instance at the Centres Cientifics i Tecnogics de la Universitat de Barcelona (CCiTUB).

4.1. Two step process

As it was already mentioned the solar cells were prepared following the typical structure used in CIGS, illustrated in Figure 15. The absorber synthesis process is a two-step process, which consists on a first step where the material or the metallic precursors are synthesized/deposited at low temperature. Subsequently, a thermal treatment under an inert gas and inside a graphite box is carried out in the presence of Sn and Se powders to minimize the CZTS(e) decomposition due to the loss of volatile species [125]. This treatment leads to the formation of a material with suitable crystalline properties for PV applications. It should be noted that so far the best CZTS(e) devices have been produced using two step processes [56, 85, 90].

4.2. Experimental

The processing steps to complete a full solar cell are summarized next:

Substrate preparation: The SLG and SS substrates were cleaned with a basic soap and rinsed with deionized water. Immediately after, they were submitted to an ultrasonic bath cleaning process in the following solvent sequence: acetone, isopropanol and deionized water. The time of the ultrasonic treatment for each solvent was 10 min at a temperature of 55 ºC. Finally, the substrates were dried with a nitrogen flux. In the case of the SS substrates they were flattened on a SLG substrate with kapton tape to ease their vacuum and chemical processing. An additional cleaning step using RF (100 W, $2x10^{-2}$ mbar Ar pressure and 5 min) plasma after the solution based cleaning, was applied to both substrates. Prior to Mo deposition a diffusion Cr barrier layer with thickness range 200-1000 nm was DC-sputtered (120 W, $4.5x10^{-3}$ mbar Ar pressure) on the SS after the RF plasma etching.

10x10 cm^2 Mo coated soda-lime glass or stainless steel substrates (~800 nm) were prepared by DC-magnetron sputtering using 99.99% purity targets (Ac450, Alliance Concepts) with different sputtering conditions as part of this thesis. Power densities ranging from 2.8-4.2 W/cm^2 and Ar pressures from

$1.15x10^{-3}$ mbar to $5x10^{-3}$ mbar were applied and these variations are discussed in detail in chapter 5, in sections 5.1.2 and 5.3.2. As a result, sheet resistances in the 0.2-0.7 Ω/□ range were measured. Additionally, 10-30 nm of i-ZnO were deposited onto some Mo substrates by DC-pulsed magnetron sputtering deposition (CT100, Alliance Concepts, 1.5 W/cm^2, $1x10^{-3}$ mbar, 19.9 sccm Ar and 0.1 sccm O_2, room temperature, 90 s (10 nm) or 180 s (20 nm)), using 99.99% purity targets.

Metallic layers deposition by DC-magnetron sputtering: as precursors for absorber films, Cu/Sn/Cu/Zn metallic stacks are deposited by DC-magnetron sputtering (AC450 Alliance Concepts) using 99.99% purity targets. A Cu/Sn/Cu/Zn stack order is selected for the following reasons: i- a very thin Cu layer (<10 nm) is deposited onto the substrates because it enhances the morphology of the Sn layer that is deposited in the next step (roughness), ii- Sn is the second layer in order to prevent or reduce the evaporation of volatile Sn-Se species during the annealing process; iii- Cu is deposited in the middle of the stack because of its high diffusion coefficient and because it readily alloys with Sn to form bronzes and with Zn to form brasses; and finally iv- Zn is deposited on the top of the stack to promote the accumulation of Zn-excess towards the surface. The conditions for the deposition of each metal are: Sn (0.64 W/cm^2, $3.5x10^{-3}$ mbar), Cu (1.27 W/cm^2, $3.5x10^{-3}$ mbar) and Zn (1.27 W/cm^2, $3.5x10^{-3}$ mbar). In all cases the substrate is rotated at 10 rpm and unheated, i.e. deposition is made at room temperature, though some heating may occur as a result of the deposition process. The thickness of the stacks is determined by X-ray fluorescence spectroscopy (XRF) (Fisherscope XVD) previously calibrated with inductively coupled plasma optical emission spectroscopy (ICP-OES) measurements. The overall composition of the stacks calculated from the XRF measurements usually lies on the range: Cu/(Zn+Sn) = 0.75-0.85 and Zn/Sn = 1.15–1.30.

Figure 25: AC 450 Alliance concept DC sputtering system. Three cathodes are on top of the circular deposition chamber.

Reactive annealing: the metallic precursor samples (5x5 cm^2 in area) are reactively annealed in a three zone tubular furnace capable of working in vacuum (10^{-4} mbar) and inert gas atmosphere (Ar). For this step a graphite box (81.9 cm^3 in volume) is used under a selenium + tin atmosphere at different temperatures, ranging from 450 -550 ºC ± 2 ºC during 45 min under Ar atmospheres varying from 1.5 mbar to 1 bar. Crucibles, with either 50-100 mg of selenium powder (Alfa-Aesar, 99.995%) and 5 mg of tin powder (Alfa-Aesar, 99.999%) are inside the box. The heating ramp is usually set at 20 ºC/min, and the natural cooling down to room temperature typically takes two hours.

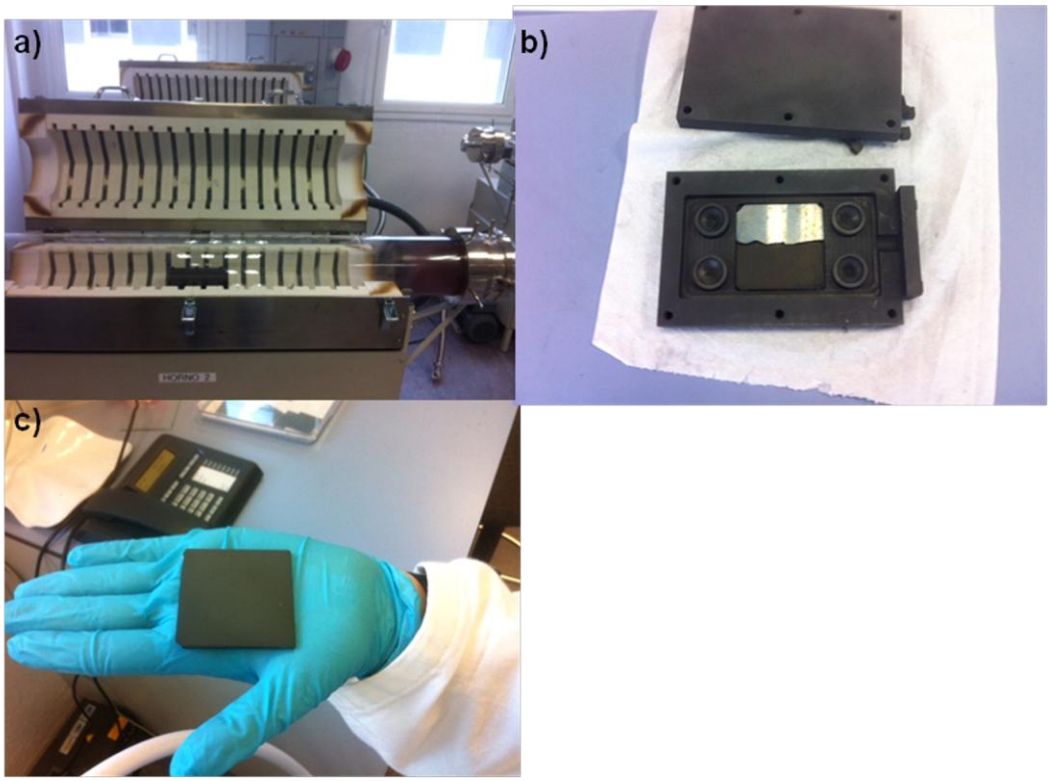

Figure 26: a) Three zone quartz tubular furnace capable to work at 10^{-4} mbar vacuum regime, b) Graphite box for 5x5 cm^2 samples and four crucibles for Sn and S(e) powder and c) 5x5 cm^2 CZTSe absorber annealed at 550 ºC.

Device fabrication: After annealing the absorbers are etched in H_2SO_4 (1 M) acidic aqueous solutions mixed with an oxidizing $KMnO_4$ (0.01M) aqueous solution. A subsequent etch in an aqueous Na_2S (1 M) or $(NH_4)_2S$ solution is necessary to remove elemental Se from the surface. Devices are fabricated by depositing CdS (60 nm) by CBD onto the kesterite layers, followed by the DC-pulsed sputtering deposition of i-ZnO (50 nm) and ZnO:Al (450 nm, R□ = 19Ω/□) (CT100, Alliance Concepts) or In_2O_3:Sn_2O_3 (90%-10%) (300 nm, R□ = 60Ω/□). For the optoelectronic characterization 3x3 mm^2 cells are scribed using a micro diamond scriber MR200 OEG, thus avoiding the necessity of metallic grid deposition onto the TCO surface. It has to be noted that Ni/Al metallic grids (or Ag metallic grid) are currently under implementation in our research group, along with the use of an antireflective coating of MgF_2.

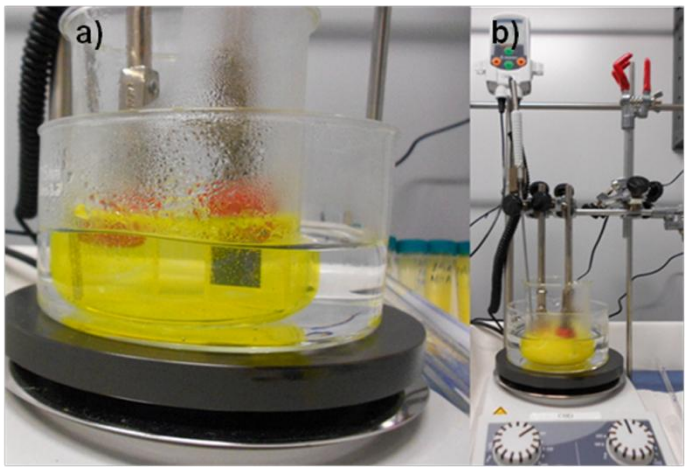

Figure 27: a) Precipitation reaction of the CdS with the characteristic orange colored solution. b) Experimental setup for the CBD of CdS. The process requires steady stirring and temperature control.

Figure 28: CT100 Alliance concepts for DC-pulsed magnetron sputtering of the window layers.

4.3. Material and device characterization

Morphological and compositional characterization:

- Scanning Electron Microscopy (SEM) was applied to analyze both absorber/back contact surface morphology and the cross sectional view of whole solar cells/back contacts. A ZEISS Serie Auriga microscope and 5-10 kV accelerating voltage was used. Compositional EDX anlysis were performed with an Oxford Instrument X-Max 20 mm^2 detector at 10-20 kV coupled to the Zeiss equipment.

- X-Ray fluorescence spectroscopy (XRF) allowed determining metallic and absorber layers composition and thicknesses. A Fischerscope XVD system was used. System

calibration with inductively coupled plasma optical-emission spectroscopy (ICP-OES, Perkin–Elmer Optima 3200 RL) was taking into account in the measurements performed.

- Atomic force microscopy (AFM): was used to determine the substrates and absorbers roughness and their morphological topography. A Park Systems XE-100 in tapping and contact modes was used.

- Auger spectroscopy (AES): was used to obtain the in-depth compositional profiles of all the constituent elements of the solar cells: Mo, Zn. Cu, Sn, Se, Fe, Cr, Cd and S are the most relevant to this thesis. The measurements were performed using a Phi 670 scanning Auger nanoprobe.

- X-ray Photoelectron Spectroscopy (XPS): was used to analyze the chemical nature of the surface of the absorbers. A PHI 5500 Multitechnique System (from Physical Electronics) with a monochromatic X-ray source (Aluminium Kα line of 1486.6 eV energy and 350 W), placed perpendicular to the analyzer axis and calibrated using the $3d_{5/2}$ line of Ag with a full-width at half-maximum (FWHM) of 0.8 eV was used to perform the measurements. The analyzed area was a circle of 0.8 mm diameter, and the selected resolution for survey spectra was 187.5 eV of pass energy and 0.8 eV/step, while for the spectra of the different elements was 23.5 eV of pass energy and 0.1 eV/step. All measurements were made in an ultra high vacuum (UHV) chamber pressure at about $5x10^{-9}$ mbar. To avoid any possible inferred modification of the surface, measurements were performed without the usual Ar^+ sputtering of the samples. Therefore, some content of carbon (adventitious C) and oxygen related to the atmospheric contamination was present on the surface. Moreover, in order to correct the binding energy axis for all the samples the single peak that appears in the $Cu2p_{3/2}$ region was fixed at 932.0 eV. This showed to give the same results as if the C1s peak from adsorbed carbon is fixed at 284.8 eV.

- Time of flight secondary ion mass spectroscopy (TOF-SIMS): was used to obtain the in-depth elemental compositional profiles of CZTSe absorbers along with Na and K alkali dopants and Fe and Cr metallic impurities from SS substrates. A TOF-SIMS IV instrument from ION-TOF was used, employing for sputtering a secondary O_2^+ ion gun operating at 2 keV, current of 421 nA and raster size of 350×350 μm^2 was used. An area of 200×200 μm^2 was analyzed using a 25 KeV pulsed Bi_3^+ primary analysis Ion Gun.

Structural characterization

- X-ray Diffraction (XRD): was performed using a PANalytical X'Pert PRO MPD Alpha1 powder diffractometer in Bragg-Brentano θ/2θ geometry, 2θ from 4° to 145° with step size of 0.017° and measuring time of 200 s per step, using Cu $K_{\alpha 1}$ radiation (λ = 1.5406 Å) selected by a Johansson type Ge (111) primary monochromator and a X'Celerator detector. Additionally a Bruker D8 Advance equipment was also used in a similar configuration.

- Raman spectroscopy: a LabRAM HR800-UV Horiba-Jobin Yvon spectrometer coupled with an Olympus metallographic microscope was used. Backscattering measurements were made using a 532 nm excitation wavelength with the laser spot focused on the surface of samples. The power was kept below 0.45 mW at a magnification of 100X (spot diameter approx. 0.8 μm). Measurements were performed focusing the laser spot on the surface of the substrate after mechanical removal of the absorber layer. Mapping measurements were made scanning a 10x10 μm^2 area with 1 μm steps, using a motorized x-y table coupled to the Raman setup. Raman measurements were also performed using both 457.9 nm and 514.5 nm excitation wavelengths (blue and green respectively) with a T64000 Horiba-Jobin Yvon spectrometer in backscattering configuration. In both cases excitation power density on the sample surface was kept below 100 kW/cm^2, in order to avoid the presence of thermal effects in the spectra.

Figure 29: LabRam HR800-UV Horiba-Jobin Yvon suitable for Raman mapping measurements.

Figure 30: T64000 Horiba-Jobin Yvon. Pre-resonant conditions for ZnSe detection are achieved with a blue excitation laser wavelength.

Optoelectronic characterization of CZTS(e) devices

- J-V characterization under illumination and in dark: to measure the optoelectronic properties a Sun 3000 class AAA solar simulator from Abet Technology (uniform illumination area of 15x15 cm^2) was used. Measurements were carried out after the calibration of the system with a reference Si solar cell under AM 1.5 illumination and fixing the temperature of the samples to 298 K.

- External Quantum Efficiency (EQE) of the cells was measured with a Bentham PVE300 system in the 300-1600 nm wavelength range, and calibrated by using Si and Ge photodiodes.

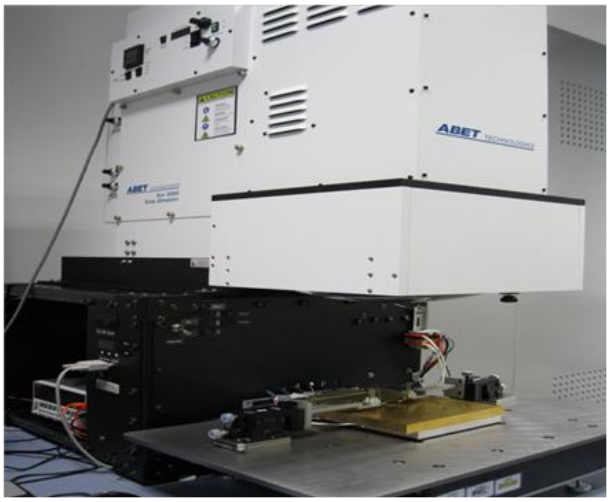

Figure 31: Solar simulator class AAA from ABET technologies. Temperature can be keeped at 25 ºC for standard measurements.

Capacitance-Voltage (C-V) measurements were performed in the dark at room temperature with a frequency of 100 kHz and a modulation voltage of 50 mV using an impedance analyzer from Novocontrol Technologies. From C-V measurements charge carrier concentration profiles were calculated assuming a relative dielectric permittivity of $\varepsilon = 8.5$ for CZTSe [220, 221].

5. RESULTS

This chapter summarizes all the processing innovations and optimizations carried out for CZTSe devices developed in this thesis. The main working areas were three: CZTSe/Mo back interface, CZTSe absorber surface and CZTSe developed on flexible and light-weight SS substrates. Likewise, the back solar cell region and the flexible CZTSe devices working areas are subdivided in two sections every one. "Minimizing decomposition at CZTSe/Mo interface" and "Mo multilayer configurations: Role of MoO_x thin layers" the former, and "Proof of concept: First CZTSe flexible solar cell" and "Alkali doping strategies for flexible and light-weight CZTSe solar cells" the latter.

Four peer-reviewed and published articles are included in each section or subsection, with the exception of subsection 5.1.2, which results belong to a manuscript with status "under review" at the thesis completion time, to be published in a high impact journal. As previously mentioned, each section or subsection includes a short summary of the main experimental results achieved during this thesis, with the exception of subsection 5.1.2. This part of the thesis is developed in a "classic" way with regard to results analysis and discussion. It has to be noted that all the articles can be found in their journal format in the Appendices section (A.S.). In addition, supplementary information for the results of subsection 5.1.2 can be also found in A.S. A2.

5.1. Tackling the CZTSe/Mo critical interface in CZTSe solar cells

It was already stated in section 2.3.1 that one of the main technological issues that could be hindering the kesterite technology from further progress is the back CZTSe/Mo interface. Thus, one of the major efforts of this thesis was developing new approaches to minimize or to avoid degradation effects at this solar cell region, arising from the annealing step when CZTSe absorbers are synthesized or re-crystallized in contact with common Mo back contacts. Two new concepts were studied and implemented in CZTSe solar cells. The first one is the use of nanometric intermediate i-ZnO layers between the Cu-Zn-Sn metallic precursors and the Mo before the annealing step. The second one is the use of multilayer Mo configurations to avoid overselenization of the back contact and effectively control the amount of $MoSe_2$ generated underneath the CZTSe absorber during the thermal treatment. Furthermore, MoO_2 layers were incorporated in these Mo configurations generating additional benefits in the absorber sintering and devices optoelectronic properties. These new processing ideas are developed in the next sub sections.

5.1.1. Minimizing decomposition at CZTSe/Mo interface

With the aim of minimizing detrimental effects linked to the reported decomposition reaction between Mo and CZTS(e) during the annealing [127], such as poor morphology due to significant presence of voids, secondary phases…etc, the role of an intermediate i-ZnO layer was investigated. This layer is already present in the CZTS(e) solar processing as part of the transparent conductive layers. It is

commonly deposited after the CdS in order to prevent from shunt paths due to inhomogeneous absorber coverage by the buffer layer. Thus, the use of this ZnO layer is convenient and appealing under an industrial point of view.

The ZnO layer was DC-sputtered after the Mo deposition and prior to the Cu-Sn-Cu-Zn metallic stack precursor that it is used in this thesis [115]. The main idea was avoiding direct contact between the Mo and the CZTSe absorber during the annealing. Thus, ZnO layers of 10 and 20 nm were compared with a reference sample processed without this layer. The results showed an improved CZTSe/$MoSe_2$ interface morphology for the samples processed with the ZnO layer corroborated by SEM analysis of Focused ion beam (FIB) prepared lamellas of full CZTSe solar cells. An important reduction of voids was easily noticeable. Regarding the solar cells, a significant increase in the performance of the devices was obtained, from 2.5% to 6% when using a 10 nm ZnO intermediate layer.

Deeper analysis of the back contact interface after a lift off process with Raman spectroscopy, revealed the presence of Cu and Zn binary phases coming from the CZTSe decomposition reaction. In contrast only a ZnSe phase and significantly reduced when compared with the non containing ZnO processed sample was detected for the 10 nm ZnO based case. As a result, the decomposition reaction for the pure selenide compound was first demonstrated in this work and in real annealing conditions, i.e. in the presence of Se+Sn atmosphere. This is in contrast with the work previously reported by Scragg et al. where the degradation reaction was proved only for the pure sulphide compound and with no S(e), neither Sn in the reactive atmosphere [127].

These findings are included in the first article submitted for the Doctor of Philosophy in Electronic Engineering of the Universitat Politècnica de Catalunya, published in *Journal of Materials Chemistry A*, entitled “Inhibiting the absorber/Mo-back contact decomposition reaction in $Cu_2ZnSnSe_4$ solar cells: the role of a ZnO intermediate nanolayer” (DOI: 10.1039/C3TA11419H). This article can be found in the Appendix A1 section.

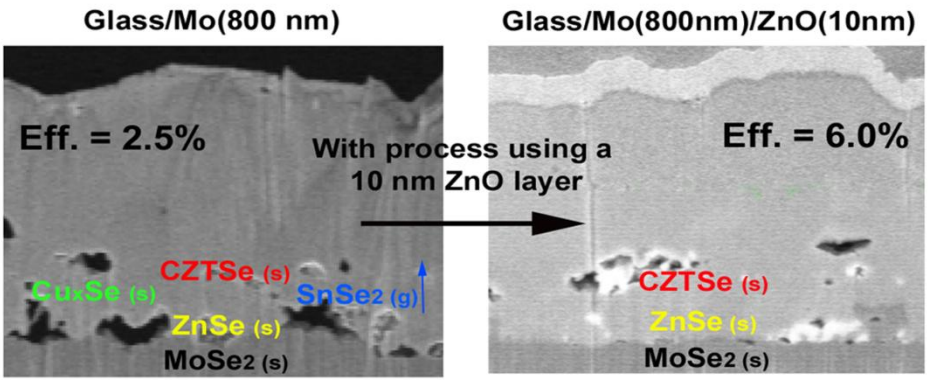

Figure 32: Graphical abstract for the article "Inhibiting the absorber/Mo-back contact decomposition reaction in $Cu_2ZnSnSe_4$ solar cells: the role of a ZnO intermediate nanolayer". An improvement in the CZTSe/$MoSe_2$ morphology combined with a reduction of secondary phases presence when using 10 nm intermedaite i-ZnO layer led to a device performance increase from 2.5% to 6%.

It has to be noted that after our development of the nanometric i-ZnO as a functional part of the back contact, a similar work was published for the pure sulphide kesterite compound [134]. Furthermore, a relevant PV research institute such as the Belgium based IMEC has also introduced our ZnO intermediate back concept in their high efficiency devices processing [128].

5.1.2. Mo multilayer configurations. Role of MoO_x thin layers

Despite the use of i-ZnO layer was a beneficial processing improvement in terms of CZTSe/Mo interface morphology and CZTSe devices efficiency, a significantly thick $MoSe_2$ layer was usually still present in our devices. It is well known that a thick $MoS(e)_2$ layer can increase R_S and therefore reduce J_{SC}, FF and ultimately decrease devices efficiency [119, 222]. In consequence, further attention was required for the CZTSe solar cells back interface, and Mo multilayered configurations were developed with the aim of minimizing the negative effects of overselenization of the back contact. Mo monolayers (previous baseline) were compared with bi-layers and tri-layers. Additionally, a nanometric intermediate MoO_2 layer was also introduced in all the Mo configurations studied and used for the first time in CZTS(e) technology.

As it was mentioned before, several Mo configurations (monolayer, bi-layer and tri-layer) were produced based on different DC magnetron sputtering deposition conditions. To configure the back contact layouts up to 3 different conditions were used, and we named them after Mo_A, $Mo_{A'}$ and Mo_B. A layer of MoO_2 was introduced in some cases as part of the Mo back contact configurations, either on top of the mono- and bi-layers and usually combined with a Mo_A cap layer with thickness ranging from 20 to 70 nm. The Mo sputtering conditions used in this work are shown in Table 2, and a comprehensive summary with all the information regarding layer type, thickness and sheet resistance of the final configurations is also listed in Table 3.

Table 2. Sputtering deposition conditions for the Mo layers involved in the back contact configurations subject of this study.

Layer	Power (W/cm^2)	Pressure (mbar)	Temperature (ºC)
Mo_A	4.2	$1.3x10^{-3}$	RT[a)]
$Mo_{A'}$	4,2	$3x10^{-3}$	RT
Mo_B	2,8	$5x10^{-3}$	RT

[a)]Room Temperature

Table 3. Summary of the different back contact configurations (sample name, layer configuration, layer thickness and sheet resistance).

Sample name	Layer configuration	Thickness (nm)	Sheet resistance (ohm/sq)
Mo_1	Mo_A	800	0.22
Mo_1-10MoO_2	Mo_A+MoO_2+Mo_A	800+10+30	0.22
Mo_1-20MoO_2	Mo_A+MoO_2+Mo_A	800+20+30	0.22
Mo_2	$Mo_{A'}$+Mo_B	150+500	1.00
Mo_2-10MoO_2	$Mo_{A'}$+Mo_B+MoO_2+Mo_A	150+500+10+30	1.06
Mo_2-20MoO_2	$Mo_{A'}$+Mo_B+MoO_2+Mo_A	150+500+20+30	1.06
Mo_3	Mo_A+Mo_B	150+500	0.8
Mo_3-10MoO_2	Mo_A+Mo_B+MoO_2+Mo_A	150+500+10+30	0.79
Mo_3-20MoO_2	Mo_A+Mo_B+MoO_2+Mo_A	150+500+20+30	0.77
Mo_4	Mo_A+Mo_B+Mo_A	250+500+(20,30,50,70)	0.58-0.60
Mo_4-20MoO_2	Mo_A+Mo_B+MoO_2+Mo_A	250+500+20+(20,30,50,70)	0.60-0.61

The experiments performed in this work are divided into two different parts. The first part is devoted to the comparison between Mo monolayers and bi-layers. The impact of the introduction of a thin MoO_2 layer (10 and 20 nm) along with a sacrificial Mo_A cap layer (30 nm) in these configurations on back contact selenization and CZTSe solar cells optoelectrical properties is investigated.

The second part focuses on the impact of a Mo_A cap layer thickness (from 20 to 70 nm), as part of a tri-layer configuration, with and without an intermediate 20 nm MoO_2 layer on the optoelectronic parameters of CZTSe solar cells. A graphical summary with the back contact layouts for the different experimental parts is included in Figure 33

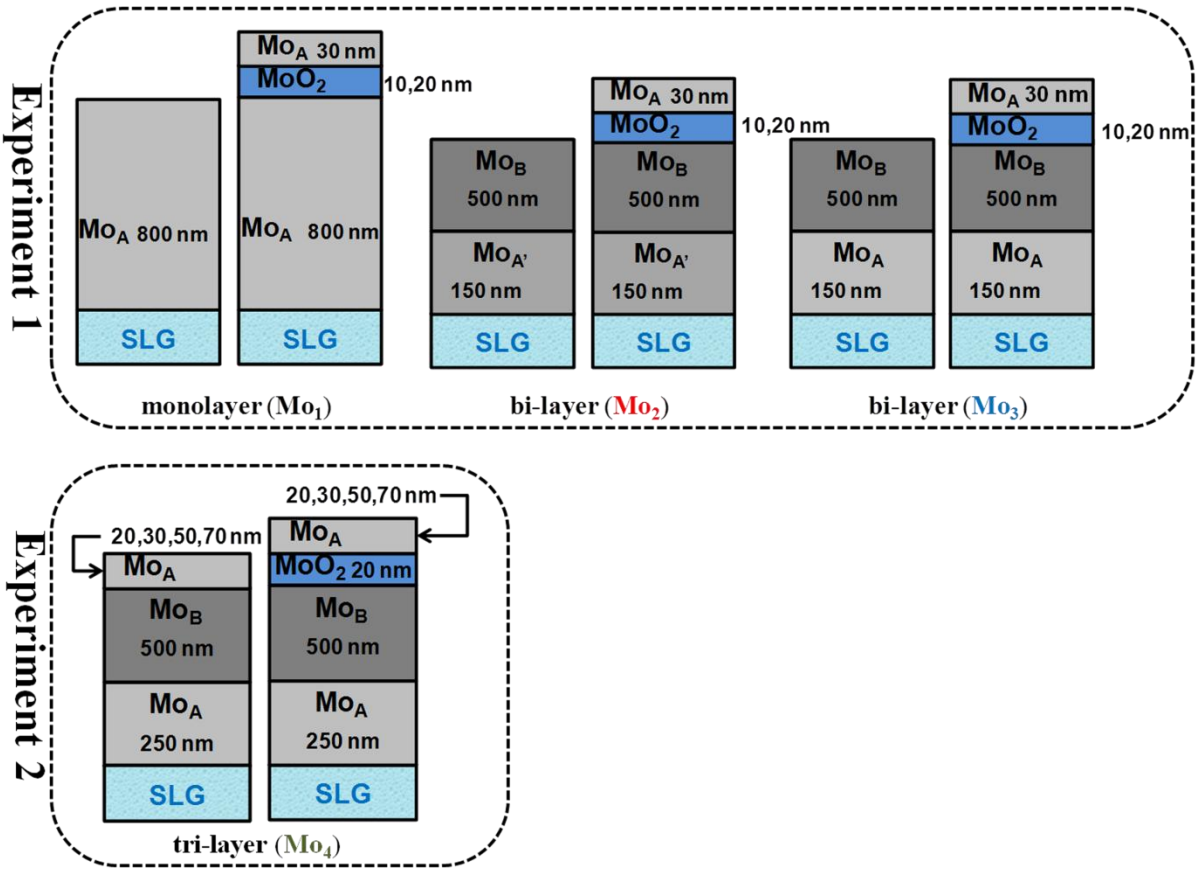

Figure 33. Graphical summary of the different back contact designs for experiment 1 and 2. Experiment 1: Comparison between Mo monolayer (Mo_1) and Mo bi-layers (Mo_2, Mo_3) and influence of an intermediate MoO_2 layer (10, 20 nm). Experiment 2: Influence of the thickness of a Mo_A cap layer in a tri-layer configuration and impact of the introduction of a 20 nm MoO_2 layer in this configuration.

Experiment 1: comparison between Mo mono- and bi-layer and impact of the thickness of intermediate MoO_2 layer in back contact selenization and CZTSe solar cells

As previously stated, one of the major drawbacks that CZTS(e) technology suffers from is the degradation of the Mo back contact usually coupled with the formation of a thick $MoS(e)_2$ layer and the presence of many voids at this interface. Our previous works on CZTSe were based on Mo monolayers sputtered with high kinetic energy conditions (Mo_A), which can be checked in Table 2 [115, 149]. The effects of the back contact degradation after selenization can be clearly observed in Figure 20 of section 2.3.1.

In order to cope with this problem at the back interface, multilayer configurations were designed. Such complex layered structures have been frequently reported in the literature. Their use as previously stated is linked with the widely accepted fact that properties such as good adhesion and low resistivity can be hard to obtain at the same time [135-137]. In that manner, high pressure deposited Mo layers are usually used as bottom layers, whereas lower pressure deposited Mo layers are on top. This is due to the fact that

porous layers obtained in higher sputtering pressures regimes are more adherent than compact layers obtained at lower pressure regimes. Nevertheless, the latter are much more conductive than the former [135-137].

In our particular case when using low pressure conditions and high power density for the Mo deposition, our films showed good electrical features, sheet resistance ~ 0.2-0.3 Ω/sq for 800 nm of Mo_A, but no poor adhesion properties in contrast with the literature [136, 137]. Nevertheless, as shown in Figure 20, a severe problem of overselenization usually took place. Therefore, we decided to invert the typical stack order of bi-layers configuration in terms of pressure that is commonly reported in the literature: bottom/high pressure and top/low pressure, in order to deal with this problem. The main reason to do so, is that an increase in the sputtering pressure can lead to a higher incorporation of O_2 from the background sputtering environment reducing the formation of $MoSe_2$ [138]. This can be due to a more porous structure with more inter-granular space where impurities can be adsorbed and/or diffuse [135, 139].

In order to understand the impact of the sputtering conditions onto the Mo structure XRD measurements of Mo_1, Mo_2 and Mo_3 have been carried out. See Figure A2-1 of the appendices section (A.S.) A2.

All the differences easily observed, i.e. wider and more asymmetric peaks for bi-layers (Mo_2 and Mo_3) compared with the monolayer (Mo_1) can be linked to the contribution of Mo_B in the bi-layers configuration. This type of Mo is obtained at higher Ar pressure than Mo_A, leading to a slightly less compact layer with commonly lower macroscopic stress but with higher microstrains and smaller crystallites [135, 223, 224].

The differences in the morphology between Mo_A and Mo_B type layers can be checked via SEM images shown in Figure A2-2 in A.S. A2.

Likewise, the impact on the electrical properties can be observed in Table 3 by looking at the sheet resistance obtained by the four point probe method. The monolayer has higher electrical conductivity than Mo_3 and Mo_2, in this order, being again directly linked to the sputtering deposition conditions. Furthermore, when the MoO_2 layer is introduced as part of the back contact designs no significant changes can be measured in the sheet resistance, at least up to 20 nm of MoO_2, because of its metallic electrical conductivity features [225].

To test the resilience against selenization of the different back contacts of Experiment 1, a selenization following the steps reported in the experimental section was carried out with all the back contact structures. Table 4 shows the XRF estimated values for the $MoSe_2$ layer thickness formed after the annealing and the thickness for the non selenized underlaying Mo layer (Note that all the Mo configurations with MoO_2 intermediate layers have a 30 nm Mo_A sacrificial top layer).

Table 4. XRF estimated values for the thickness of a $MoSe_2$ layer formed after the selenization of different Mo configurations, and Mo layer thickness remaining after the same annealing process. Note all the Mo configurations with MoO_2 have a 30 nm sacrificial Mo_A top layer.

Sample name	$MoSe_2$ (nm)	Remaining Mo (nm)
Mo_1	688	542
Mo_1-10MoO_2	255	622
Mo_1-20MoO_2	240	649
Mo_2	84	560
Mo_2-10MoO_2	174	571
Mo_2-20MoO_2	140	589
Mo_3	75	560
Mo_3-10MoO_2	155	596
Mo_3-20MoO_2	174	567

At a first glance it is obvious that Mo_1 is overselenized compared with Mo_2 and Mo_3, which barely have formed $MoSe_2$ (688 nm of $MoSe_2$ against 84/75 nm respectively). Additionally, SEM and EDX analyses were performed in a cross section configuration of samples Mo_1, Mo_1-10MoO_2 and Mo_1-20MoO_2 in Figure 34. The effects of the introduction of 10 and 20 nm of MoO_2 as intermediate layer, deposited on top of Mo_1 with a sacrificial 30 nm cap layer of Mo_A (easily selenized as it has been shown) after the selenization process can be seen in that image.

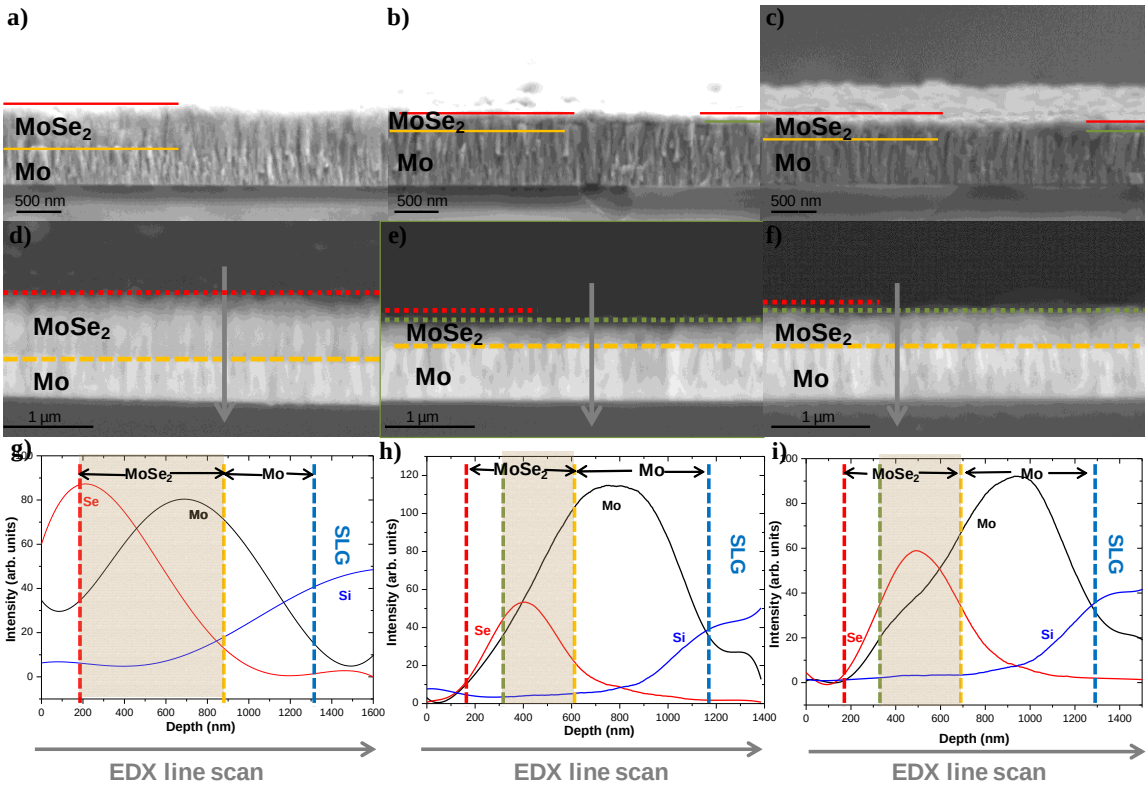

Figure 34. Cross sectional SEM and elemental depth profiles from EDX line scan images of samples Mo_1, Mo_1-10MoO_2 and Mo_1-20MoO_2 after selenization; a), b) and c): Secondary electrons detector images for selenized Mo_1, Mo_1-10MoO_2 and Mo_1-20MoO_2 respectively; d), e) and f): back scattered electrons detector images for selenized Mo_1, Mo_1-10MoO_2 and Mo_1-20MoO_2; g), h) and i): EDX line scan elemental depth profile of selenized Mo_1, Mo_1-10MoO_2 and Mo_1-20MoO_2 respectively.

Figures 34a and d show a SEM cross sectional image of Mo_1 obtained with both secondary and back scattered electron detectors respectively. It seems clear that a large $MoSe_2$ layer arises after selenization, visualized between the red and the orange lines. When the MoO_2 layer is introduced the formation of $MoSe_2$ is clearly reduced already with a thickness of 10 nm (Figure 34b and e) if we compare the layer between the red and the orange lines with the reference case. Surprisingly, Figures 34c and f show slightly larger $MoSe_2$ formation when a 20 nm MoO_2 layer is introduced. This could be explained by possible local differences in the homogeneity of the evaporated layer, since the results from XRF (integrated over a much larger area than the SEM and EDX cross sectional analyses) point to similar or even lower formation of $MoSe_2$ and likewise for the remaining Mo after the thermal process (see Table 4). Further confirmation of the $MoSe_2$ reduction can be noticed by comparing the colored areas of the EDX elemental depth line scans of Figures g, h and i belonging to Mo_1, Mo_1-10MoO_2 and Mo_1-20MoO_2 respectively. The area marked corresponds to the thickness of the $MoSe_2$ layer.

By focusing again on Table 4, it is interesting to see how the bi-layers, Mo_2 and Mo_3, act as natural barriers against selenization (cases Mo_2 and Mo_3). Nevertheless, when introducing the MoO_2 layer, 10

and 20 nm, the selenization is further reduced since despite having a larger value of $MoSe_2$ thickness compared with the reference cases, we should take into account that a sacrificial 30 nm Mo_A cap layer was also introduced. Therefore, we should leave out the thickness of the $MoSe_2$ layer intentionally grown on top of the MoO_2 layer, which in a rough estimation could be about 100 nm. In any case if we look at the value of the remaining Mo (non selenized) for the selenized bi-layers with 10 and 20 nm MoO_2, the value is larger than for the reference cases, Mo_2 and Mo_3, confirming the effectiveness of this oxide layer as Se barrier.

To understand the impact of the selenization on the structure of the different back contact configurations, XRD analysis of the selenized back contacts of Experiment 1 were performed (All the peaks have been indexed with the card JCPDS-3-65-3481). Nevertheless, before addressing this point a brief hint on the $MoSe_2$ structural properties and their implications on solar cell performance are revised. $MoSe_2$ is a p-type semiconductor and layered compound with an indirect bandgap of 1.4 eV. It has a hexagonal structure based on sandwiched Se-Mo-Se sheets [130, 226-228]. It is important to note that this compound can be present in the solar cells with two main crystalline orientations, with the c-axis either parallel or perpendicular to the substrate [229, 230]. These two different orientations differ in adhesion and electrical properties, due to the different alignment of the $MoSe_2$ multilayered structure with respect to the substrate [231]. When the c-axis is perpendicular to the substrate, then the $MoSe_2$ sheets are parallel to the same, creating a natural barrier for selenization but weakening its bonding strength to the Mo and reducing its electrical conductivity. If the c-axis is parallel, then the $MoSe_2$ layers are oriented perpendicular to the Mo substrate increasing the adhesion and the electrical conductivity, but also the degree of Mo selenization [232, 233].

Figure A2-3 of the A.S. shows the difference between the monolayer Mo_1 and the bi-layers Mo_2 and Mo_3 when undergoing our standard selenization process. As it was confirmed by XRF an important reduction of the $MoSe_2$ formation can be noticed since the 100 and 110 diffraction peaks, typical for the $MoSe_2$ with the c-axis parallel to the substrate, are dramatically reduced when comparing Mo_1 with Mo_2 and Mo_3. Moreover, the contribution of different crystalline orientations of the $MoSe_2$ can be observed, due to the change in the c-axis orientation. The (002) diffraction plane belongs to the c-axis being perpendicular to the substrate, the 100 and the 110 diffraction peaks belong to the c-axis oriented parallel to the substrate and the 103 has been assigned to a mixture of both orientations [229, 233].

The role of 10 and 20 nm intermediate MoO_2 layer combined with a 30 nm Mo_A cap layer on the $MoSe_2$ structure and formation is presented in Figure 35a and b, for the case of a Mo_1 monolayer and a Mo_3 bi-layer respectively (note that the behavior of Mo_2 is similar to Mo_3).

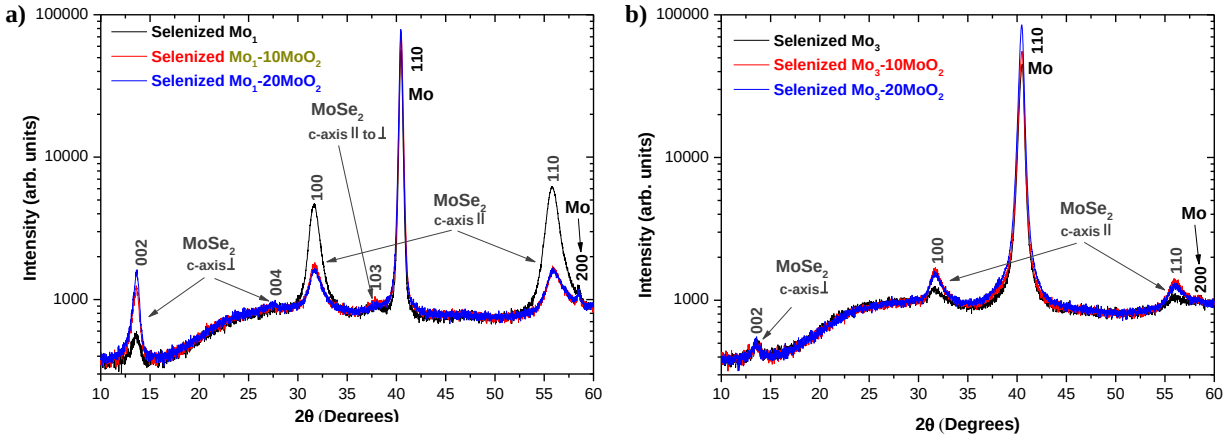

Figure 35. XRD patterns of different back contact configurations; a) Mo_1, Mo_1-10MoO_2 and Mo_1-20MoO_2; b) Mo_3, Mo_3-10MoO_2 and Mo_3-20MoO_2. Different crystalline orientations can be noticed for $MoSe_2$ due to changes in the c-axis orientation. Note that the MoO_2 layer was combined with a sacrificial 30 nm Mo_A cap layer.

In the case of Mo_1 intense diffraction 100 and 110 peaks confirm the overselenization of this type of back contact. These peaks correspond to typical orientations for $MoSe_2$ with the Se-Mo-Se sheets oriented perpendicular to the substrate, i.e. c-axis parallel to the same. In contrast, when adding either 10 or 20 nm of MoO_2 the intensity of these peaks is strongly reduced, despite having 30 nm of a sacrificial Mo_A layer, which will be easily selenized. Interestingly, when looking at lower diffraction angles, a remarkable change in texture of the $MoSe_2$ formed can be observed when introducing the MoO_2 layer. This is due to the contribution of the (001) orientation, mainly driven by 002 but also 004 diffraction peaks. In this case, Se-Mo-Se sheets oriented parallel to the substrate, i.e. with c-axis being perpendicular to the same, seem to be growing due to the presence of the MoO_2 layer. Furthermore, a correlation with the thickness of the MoO_2 layer and the intensity of the $MoSe_2$ 002 diffraction peak can be drawn. Finally, an additional diffraction peak, 103, emerging from the background can be assigned to the mixture of the two main $MoSe_2$ crystalline orientations, as it has been reported in the literature [233]. Structural surface sensitive analyses were also performed in this set of samples using Raman spectroscopy. The results are shown in Figure A2-4 of the A.S.; it can be clearly observed again a change in texture when comparing the samples with and without MoO_2 layer, due to the difference in the relative intensity between the most intense Raman modes.

In the case of the bi-layers, the XRD analyses are very similar, so that only the case of Mo_3 is shown in Figure 35b. It can be easily noticeable, as already confirmed by XRF, that the formation of $MoSe_2$ is reduced when using this type of complex Mo structure. The most intense and typical diffraction peaks for $MoSe_2$, 100 and 110, are relatively small (see black line of figure 35b). When introducing the MoO_2 layer (red and blue lines) the intensity of those peaks is bigger, but this is due to the contribution of the $MoSe_2$ coming from the additional 30 nm Mo_A cap layer. Therefore, the MoO_2 layer for this case seems to be not

necessary to avoid overselenization of the Mo back contact. Additionally, the 002 diffraction peak typical for $MoSe_2$ with c-axis perpendicular to the Mo surface remain unchanged in contrast with the monolayer case.

Up to now, it seems clear that MoO_2 is reducing the selenization of the Mo and induces changes in the orientation of the $MoSe_2$ when growing in contact with this layer, at least for the case of Mo_1. A reasonable question to make at this stage was whether this oxide is selenized, partially selenized or not? According to the literature, the selenization reaction for this oxide is thermodynamically much more demanding in energy than the reaction between Mo and Se, and thereby it can be inferred that the oxide cannot be selenized (See A.S. A2 for the specifics of the selenization reactions mentioned before) [142]. In order to go further on the structural changes induced by this layer, selenization tests using similar configurations to the ones presented in figure 33 when using MoO_2, but with no additional Mo_A cap layer were performed. In this way, more light could be shed for instance on the specific location of the $MoSe_2$ layer with the c-axis growing perpendicular to the Mo surface, which usually is reported to be at the $MoSe_2$/absorber interface [233]. Specifically, 10, 20 and 30 nm of MoO_2 layers were grown on top of both monolayers and bi-layers to look at the $MoSe_2$ structural changes induced by this oxide. The results are shown in the A2 part of the A.S, in Figure A2-5. Two main findings can be drawn from that figure. The first one is a direct correlation between the amount of $MoSe_2$ growing with the c-axis perpendicular to the substrate and the thickness of the MoO_2 layer. The second one is the confirmation of the integrity (at least to some extent) of the MoO_2 layer after the selenization process, since the main peaks of its monoclinic structure have been indexed for the 30 nm MoO_2 case, even when using a θ-2θ Bragg-Brentano XRD configuration.

It should be noted that so far the orientation of $MoSe_2$ grains has been linked with temperature processing, Se partial pressure, absorber composition, Mo orientation and Na content [130, 131, 226, 229-231, 233]. We report for the first time the induction of the growth of $MoSe_2$ grains with the c-axis perpendicular to the Mo substrate, i.e. acting as a natural Se barrier, when depositing a thin MoO_2 layer on the Mo back contact before selenization. The possibility of controlling the amount of $MoSe_2$ sheets growing parallel to the Mo substrate can be directly linked to the thickness of the MoO_2 layer, and thereby its beneficial properties could be maximized, avoiding its detrimental characteristics, i.e. poor electrical features and delamination issues.

Moreover, Raman spectroscopy was also performed in this set of samples and the spectra are shown in Figure A2-6.

All the back contact configurations presented in Experiment 1 were implemented as part of CZTSe solar cells. First, a comparison of cells performance based on plain monolayers (Mo_1) and bi-layers (Mo_2 and Mo_3) is shown in Figure 36 via illuminated J-V curves along with a summary of the main optoelectronic parameters, and cross sectional SEM images of completed solar cells.

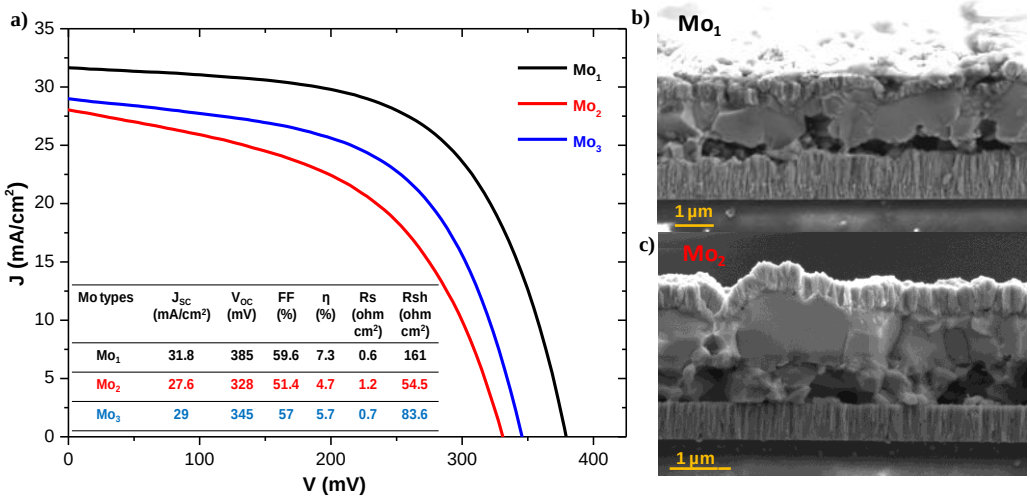

Figure 36. a) J-V illuminated curves of CZTSe with Mo_1, Mo_2 and Mo_3 back contacts; b) SEM cross sectional image of full CZTSe solar cells based on Mo_1 and Mo_2 back contacts (Note that the CZTSe cell based on Mo_3 has similar features than the Mo_2 one).

At a first glance, by looking at Figure 36a it seems obvious that CZTSe cells based on monolayer back contact perform better than the Mo_2 and Mo_3 bi–layer based cells, 7.3% versus 4.7% and 5.7% respectively. An important degradation in V_{OC} and/or FF seemed to take place. Interestingly, when looking at Figure 36b and c, it can be observed that the cell performing better is the one that presents larger back contact interface degradation along with a thicker $MoSe_2$ layer (See figure A2-7 of A.S. for better comparison of both back contact interface morphologies). As already mentioned, those features are usually reported as undesired in order to allow for high efficient devices [119, 222]. Nevertheless, it has been also reported that a $MoSe_2$ layer could act as buffer layer between the Mo and the absorber, promoting an ohmic contact, and thereby improving the electrical transport. By looking at the absorber/Mo back contact interface of images b and c, it seems reasonable to think that bi-layers might led to a too small $MoSe_2$ layer, insufficient to promote a good band alignment to avoid hole blocking transport and recombination of minority carriers at this interface [129-131]. The $MoSe_2$ layer can barely be seen by looking at the SEM images, which correlates also with the small values of $MoSe_2$ thickness obtained by XRF in Table 4. As a result, it can be concluded that an efficient tuning of the $MoSe_2$ thickness is of utmost importance in order to boost CZTSe devices performance. In consequence, we can conclude that bi-layers are suitable structures to cope with overselenization but they need to be combined with a sacrificial Mo_A cap layer in order to produce a $MoSe_2$ layer with the adequate thickness to avoid a high series resistance (R_S) and to promote a good band alignment of the back contact interface. This is the reason that led us to investigate the influence of the Mo_A cap layer as part of a tri-layer Mo configuration in Experiment 2. As an example, Figure A2-8 of the S.I. shows a cross sectional SEM image of a tri-layer (Mo_4 back contact type) with 30 nm Mo_A cap layer. A ~100 nm $MoSe_2$ in thickness has grown between the absorber and the Mo. It should be noted that recently another way to control overselenization and $MoSe_2$ thickness growth at the back contact of CZTSe solar cells has been reported by Li et al [222].

Nevertheless, this work relies in a prealloying step at low temperature to control the $MoSe_2$ thickness, and thereby it would be only interesting when synthesizing CZTSe from metallic precursors. In the present work, the Mo tri-layer that we have defined offers an easy and flexible way adaptable for all CZTSe precursors, since even when selenizing bare Mo-tri-layers the $MoSe_2$ that is formed is clearly determined by the Mo_A cap layer thickness as it will be shown further on.

Going back to Experiment 1, the impact of the intermediate MoO_2 layer as part of different Mo configurations, Mo_1 and Mo_3, on the optoelectronic properties of CZTSe solar cells can be seen in Figure 37. Figure 37a shows the J-V illuminated curves of a monolayer configuration (Mo_1) and its combination with a 10 or 20 nm MoO_2 layer grown with a 30 nm Mo_A cap layer (solid lines), and the same oxide combinations with a bi-layer configuration (Mo_3, dashed lines). Additionally, a table with a summary of the main optoelectronic parameters of the cell is included. It has to be noted that none of the solar cells produced in this experimental part showed any delamination issue, usually linked with the presence of $MoSe_2$ with the c-axis perpendicular to the substrate as mentioned before. Apparently, it is obvious that despite performing very different the CZTSe cells based on plain Mo cases, 7.3% Mo_1 and 5.7% Mo_3, after the introduction of the MoO_2 layer both cells exceed 8% when using 20 nm of MoO_2, 8.2% and 8.1% for Mo_1 and Mo_3 respectively (Mo_2 results are not shown, but they are similar to the ones based on Mo_3, going from 4.7% for the reference case to 8.1% for the 20 nm MoO_2 case). An important increase in V_{OC} and FF takes place, especially in the case of Mo_3 (about 80 mV more for V_{OC} and 7% absolute increase in FF), which is clearly responsible for the efficiency change. Moreover, the shunt resistance (R_{SH}) suffers a dramatic change as well, from 161 to 314 Ohm cm^2 for Mo_1 and from 83.6 to 611 Ohm cm^2 for Mo_3. It has to be noted that Figure 37a belongs to the best cells obtained from completed samples processed with every specific back contact type, but Figure A2-9 from the A.S. shows the statistical spread for all the cells processed in the experiment.

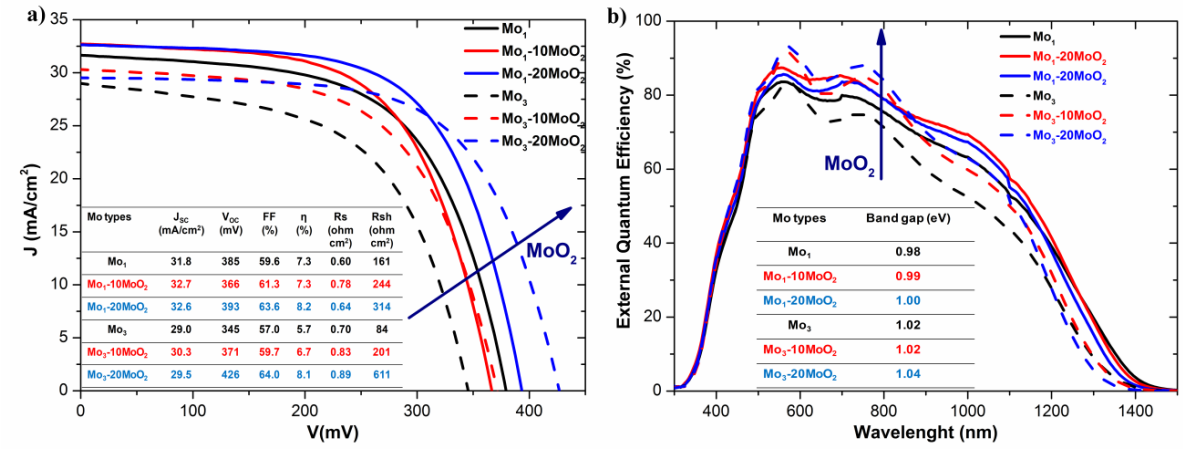

Figure 37. J-V illuminated curves and EQE of CZTSe solar cells with different back contact configurations with and without MoO_2. a) J-V illuminated curves of CZTSe with Mo_1, Mo_1-10MoO_2,

Mo_1-20MoO_2, Mo_3, Mo_3-10MoO_2 and Mo_3-20MoO_2 back contacts. b) EQE of CZTSe solar cells based on Mo_1 Mo_1-10MoO_2, Mo_1-20MoO_2, Mo_3, Mo_3-10MoO_2 and Mo_3-20MoO_2 back contacts. (Note that the results of the CZTSe cell based on Mo_2 are similar to the ones based on Mo_3).

Figure 37b shows the spectrally resolved photocurrent collection via EQE. An increase in the whole absorption range (from 500 to 1300 nm) with the addition of a MoO_2 layer takes place correlating with the values of J_{SC} from Figure 37a. This fact evidences that whichever phenomena occurring in the CZTSe cells after the MoO_2 introduction take place, cannot be only correlated with a pure back contact modification. If it was the case, the EQE will only presumably have a clear impact on electrons photogenerated deeper in the absorber (800 -1300 nm) and not on all the spectral absorption range. The band gap of the different CZTSe absorbers was extracted from the energy derivative of the EQE plots and a subsequent Gaussian fit. Interestingly, for both Mo_1 and Mo_3 cases, the band gap increased after the introduction of the MoO_2 layer, reaching a maximum value for the 20 nm MoO_2 case. This fact is directly reflected in the EQE plots via a faster decrease near the band gap edge. It is significant the difference between the EQE plots of Mo_1 and Mo_3, showing a better photocurrent collection in the whole absorption range for the overselenized monolayer compared with the almost non selenized bi-layer. This will point out again towards the necessity of controlling the thickness of $MoSe_2$ layer to avoid poor carrier collection at the CZTSe back and bulk regions.

At this stage, it seems clear that evidences arisen from the optoelectrical characterization point out towards a change in the full CZTSe absorber and not only at the back region. In order to gather more information, SEM images of full CZTSe cells based on different back contact designs were taken. Figure 38 shows cross sectional SEM images of CZTSe solar cells based on Mo_3, Mo_3-10nmMoO_2 and Mo_3-20nmMoO_2. Additionally, SEM top view images of the CZTSe absorbers are included as insets for every image. Figure 38a shows a CZTSe cell with a bi-layer Mo_3 back contact, the average grain size is less than 1 μm as evidenced by the SEM cross sectional view, not reaching the full absorber thickness (~1.6 μm). The SEM top view inset further reveals numerous grains of several hundreds of nanometers. When the MoO_2 oxide layer is introduced an important improvement in the grain size is achieved, obtaining grains as large as the absorber thickness for both 10 and 20 nm in thickness. In the case of 20 nm thickness the length of CZTSe grains reaches values up to several microns (3-4 μm), correlating with the highest performing devices. Therefore, the introduction of the MoO_2 layer has enhanced CZTSe grain growth assisting the sintering of the absorber. The bigger grain sizes also correlate with the increased values of R_{SH} after the oxide introduction, since bigger grain sizes will lead to less grain boundaries (GB) where there could be more possibilities for carrier recombination. Nevertheless, although GB have been proved to be positive for electronic transport in CIGS [194, 216, 234], a recent study based on a new alkali doping for CZTSSe seems to conclude the opposite [93]. Furthermore, Sardashti et al. observed this latter type of GB behavior for CZTSSe absorbers following and oxidation, oxygen removal and subsequent air post-annealing route, such as the one we have used in this work to produce CZTSe solar

cells [218], as reported by Neuschitzer et al [219]. In consequence, GB with an inverted potential (negatively charged) compared with what it was commonly observed for CIGS and more recently CZTS(e) (positively charged GB) [213, 216, 217], i.e. repelling minority carriers (electrons) and attracting holes would lead to a better device performance [93]. It is important to note that this would be the typical behavior that could be expected for a polycrystalline semiconductor, since GB contain numerous defects that enhance recombination and lower devices performance.

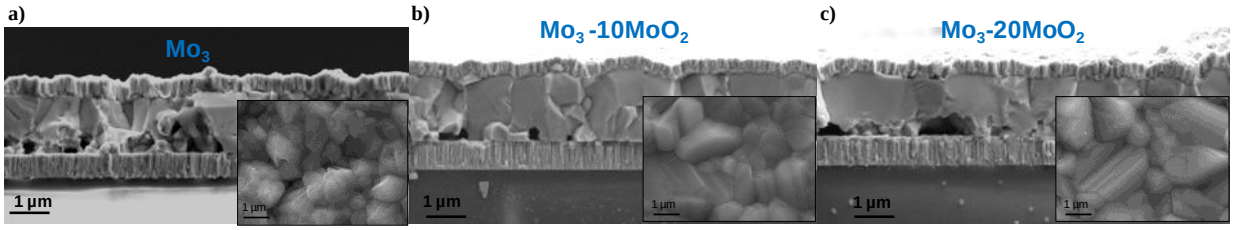

Figure 38. Cross sectional SEM images of CZTSe solar cells with different back contact configurations with and without MoO_2 (inset belongs to SEM top view of the absorber of each cell): a) Mo_3, b) Mo_3-10MoO_2 and c) Mo_3-20MoO_2 back contacts. (Note that CZTSe cells based on Mo_2 are similar to the ones based on Mo_3).

In addition to Figure 38, SEM top images of CZTSe absorbers grown on the rest of back contacts analyzed in Experiment 1 are included in Figure A2-10 of the A.S.

It is well known that the sintering of CZTS(e) is enhanced by alkali impurities, mainly Na [203, 207, 214]. Furthermore, the typical impact of alkali doping in CZTS(e) performance is related with a V_{OC} and FF increase [207, 208], i.e. similar to what we observed for our MoO_2 containing cells. Thus, it seems reasonable to speculate about Na diffusion modification coming from the Soda Lime Glass (no alkali barrier was used for this work) during the absorber sintering induced by the presence of the MoO_2 oxide intermediate layer. In order to confirm this hypothesis, TOF-SIMS compositional depth profiles of CZTSe full cells based on different back contacts with and without MoO_2 layers were obtained. The results are shown in Figure A2-11 from the A.S. No significant variations can be drawn from the Na depth compositional profiles. Nevertheless, if the final Na profile is not significantly modified, it seems reasonable to think about a possible change of the formation dynamics of the Na containing species during the sintering. In this way, the formation of different either in chemical type or in amount Na species (Na polyselenides, Na-Mo-O species, Na-Zn-Se species…) compared with the non MoO_2 reference cases might have occurred. In consequence, if these new species could act as higher temperature liquid or solid fluxes that could assist the sintering for a longer time, then the final grain size would be considerably affected. The relevance of sodium polyselenides for sintering improvement in CZTSSe absorbers has been reported by Sutter-Fella et al. It was suggested that the availability of Se to effectively form liquid Na_2Se_x phases on the samples surface is increased via NaF evaporation on the samples surface prior to Selenization [207]. A complex phase diagram for the Na-Mo-O system can be found in the

literature, evidencing the multiple possibilities in terms of compound formation [235]. In the literature there is also evidence of a higher Na content for CIGS with a more oxidized Mo surface [236]. Zellner et al. reported a reduction in the activation energy for Na diffusion by air annealing, supporting the idea of Na diffusion assisted by oxygen presence [237]. It has been also suggested that Mo-O species can enhance Na diffusion via solubility of Na, i.e. formation of Na containing oxides, such as Na_2MoO_4 [238, 239]. In consequence, we can speculate with a more homogeneous distribution of Na diffusion assisted by the MoO_2 layer towards the CZTSe absorber. It is important to keep in mind that the MoO_2 is evenly covering the whole back surface and is spatially located very close to the absorber. This fact would be in contrast with the Mo-O species naturally present in the Mo back contact after sputtering, since their presence might be randomly distributed across the Mo layer. Furthermore, it is well known that Na diffuses through the Mo grain boundaries via oxygen species [137, 139, 240]. Thus, if the MoO_2 is present in a more uniform way, i.e. covering the whole Mo surface through 10 or 20 nm thick MoO_2 layers, then the Na "diffusion path" towards the absorbed might be enhanced, since the diffusion channels will not only be at the GB, but at the whole Mo surface. Furthermore, if we take into account as it was confirmed by XRF, XRD and SEM measurements that MoO_2 acts as a selenium barrier, then the availability of Se at the bottom region of the absorber would be maximized in a similar way as it was reported by Sutter-Fella et al for the front absorber region. The formation of Na_2Se_x liquid phases will be promoted at the interface between the MoO_2 and the $Mo_A/MoSe_2$ upper layer and close to the back of the precursor/absorber, since Na will be preferentially adsorbed/located to/in this layer, acting as a Na reservoir for the sintering process. It has to be noted that the sticky coefficient for Na_2Se_x is higher than for Se, significantly increasing the Se availability for the absorber growth process [196]. It is interesting to see that in the work of Scofield et al. despite having similar Na levels for CIS absorbers (confirmed by SIMS) grown on different Mo types, the grains of the absorber were different [241]. This would be in agreement with our observations and could confirm that even when the final Na profiles in CZTSe absorbers grown on different Mo configurations are similar, the thermodynamic processes leading to these profiles seem to be more important than the final Na level themselves. We propose the MoO_2 intermediate layer as a relevant agent capable of modifying the Na diffusion thermodynamics during the absorber sintering.

To further understand the CZTSe structural changes induced by the back contact modification we decided to perform Raman spectroscopy analyses of CZTSe absorbers as part of full solar cells. The upper layers (TCO and CdS buffer) of the cells were etched away in diluted aqueous HCl solution. The spectra obtained with a green excitation laser source (532.5 nm) are shown in Figure 39. It should be noted that the Raman spectra obtained belong to the first 20-50 nm of the analyzed absorbers, since Raman is a powerful surface sensitive structural characterization technique. Additionally, a summary with parameters extracted from the spectra to assess the CZTSe crystal quality and the impact of the MoO_2 layer in the absorber surface structure is included in Table A2-1 of the A.S.

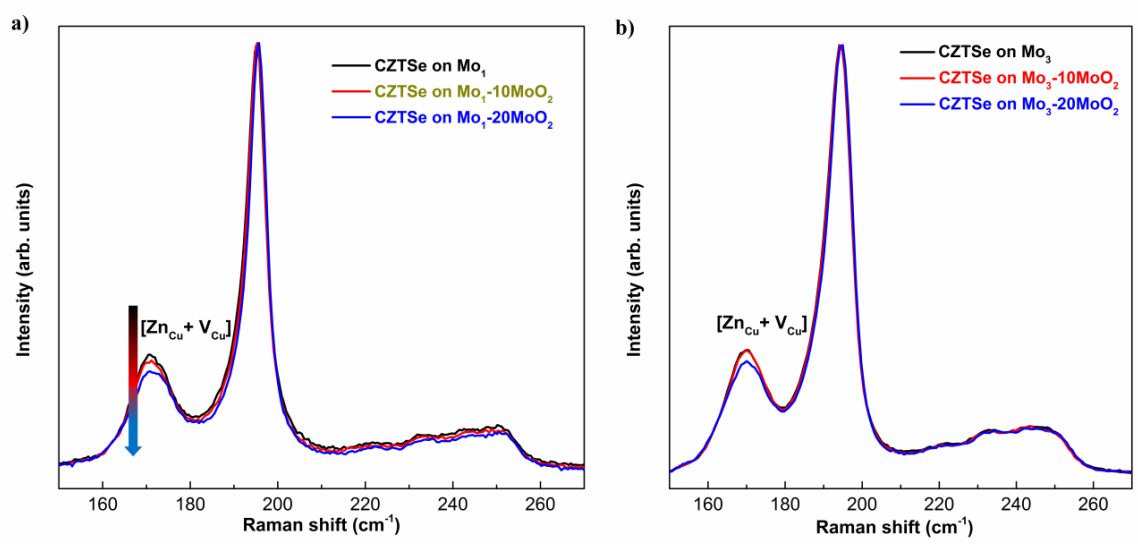

Figure 39. Raman spectra of CZTSe samples grown on different back contact configurations: a) Mo_1, Mo_1-10MoO_2 and Mo_1-20MoO_2 and b) Mo_3, Mo_3-10MoO_2 and Mo_3-20MoO_2. All Raman spectra are measured with 532 nm excitation wavelength. The arrow indicates changes in the intensity of B modes correlating with the back contact modification.

It can be clearly observed that the introduction of the MoO_2 has induced structural changes in the CZTSe absorbers. In particular, when focusing in Figure 39a the narrowing of the main peak confirms the increase in grain size after the introduction of the MoO_2 (see table A2-1 from A.S. for FWHM). Furthermore, the decrease in the relative intensity of peaks around the spectral region of 170 cm^{-1} when the oxide is applied, has been experimentally linked with an increase in concentration of [Zn_{Cu} + V_{Cu}] defect clusters [242]. In the case of the work of Dimitrievska et al, the changes in the Raman spectra were induced by compositional variations in the CZTSe absorbers, but in our particular case the compositional ranges are very similar (See table A2-2 of A.S.), leaving the back contact modification via MoO_2 addition as the main cause to explain the structural changes observed in CZTSe. It has to be noted that the samples were cooled down following the same temperature regime, i.e. naturally cool down to room temperature, and thereby order/disorder effects in the cation sublattice can be discarded [62, 68, 69]. In conclusion, the introduction of the MoO_2 layer induces relevant structural changes in the CZTSe absorbers confirmed by SEM and Raman spectroscopy, leading to a more depleted Cu surface since a decrease in Cu/Zn and Cu/Sn vibration units is corroborated by the Raman technique. A correlation with high performing devices and a Copper depleted surface has been already reported in the literature [218, 219]. Before moving to the second experimental part of this work, a question that could be still pending from the results already presented would be whether the MoO_2 itself on top of the different Mo configurations without any Mo_A sacrificial cap layer could give better or similar results to the ones already shown. The answer is no, since a general degrading in all optoelectronic parameters takes place when the oxide is applied alone. Thus, the relevance of the $MoSe_2$ layer as a buffer between the CZTSe absorber and the Mo back contact is again clearly revealed as crucial for the technology. Finally, a table summarizing these

results (table A2-3), based on Mo_1 and Mo_3 configurations with different thickness of MoO_2 layers but no Mo_A cap layer (analogue to the cases analyzed by XRD in Figure A2-5 of the A.S.) is included in the A2 section of the A.S.

Experiment 2: Influence of Mo cap layer thickness from Mo tri-layer configuration and impact of a 20 nm MoO_2 layer in CZTSe solar cells

With the aim of improving further the properties of the back contact interface of our CZTSe cells, a tri-layer configuration as it was prior stated was used. The top sacrificial layer, Mo_A will allow for a fine tuning of the $MoSe_2$ layer growing between the Mo back contact and the CZTSe absorber, which we have proved to be very important to achieve high performing devices, in agreement with the literature [119, 222]. The objective of Experiment 2, as shown in Figure 33, is to study the effect of the thickness of the top layer in a tri-layer configuration and its combination with a 20 nm intermediate MoO_2 layer on CZTSe cells based on these back contacts. The role of a Mo_A layer ranging from 20 to 70 nm with and without a 20 nm underlying MoO_2 layer was investigated. Figure 40 shows J-V illuminated curves for CZTSe cells based on a tri-layer configuration (Mo_4) with and without the influence of an intermediate MoO_2 layer. Again, none of the solar cells studied in this experimental part showed delamination problems.

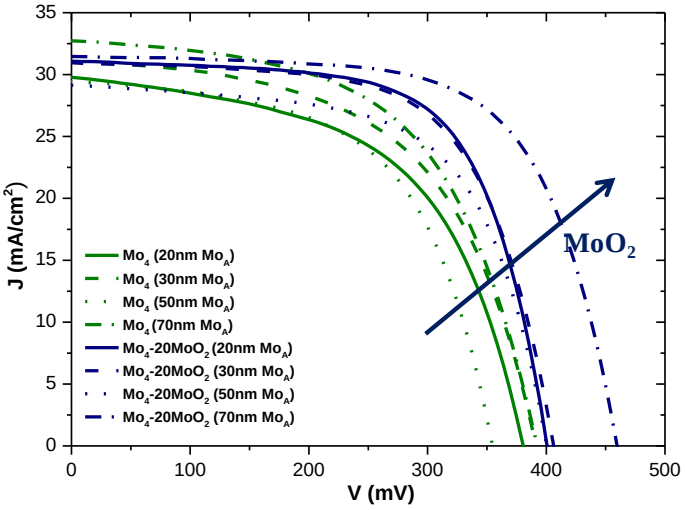

Figure 40. J-V illuminated curves of CZTSe cells based on Mo_4 tri-layers with different thickness of cap layer (20, 30, 50 and 70 nm) with and without a 20 nm underlying MoO_2 layer.

It can be easily concluded from Figure 40 by focusing on the green lines (tri-layer back contact configurations with different Mo_A cap layers) that the thickness of the cap layer is clearly affecting the devices performance, changing all the optoelectronic parameters. Table 5 summarizes those parameters, and an increase in efficiency from 6.2% to 7.2% was obtained when changing the cap layer from 20 to 70 nm. The photocurrent (J_{SC}) also experienced a remarkable increase from 29.8 to 32.7 mA/cm^2 and finally V_{OC} and FF moderately increased as well. It is interesting to note how besides the sample with 50 nm all

the parameters seem to increase in parallel with the Mo_A cap layer thickness increase, and thereby we believe some processing damage could lower the performance of this particular sample. As proved before, the cap layer thickness can control the $MoSe_2$ layer thickness and therefore affect the final performance of CZTSe devices. Table A2-4 of A.S. shows the $MoSe_2$ thickness values of back contacts analogue to those belonging to the CZTSe cells in green from Figure 40 after selenization, obtained by XRF. The $MoSe_2$ thickness increases progressively from about 80 nm to 120 nm for 20 nm to 70 nm of Mo_A respectively. Nevertheless, this data should only be taken as a qualitative way to compare the amount of $MoSe_2$ formed since SEM cross sectional images of selenized cells and back contacts usually give larger values when estimating the $MoSe_2$ thicknesses.

Focusing now on the blue lines, which belong to the same set of samples analyzed before but with an underlying 20 nm MoO_2 layer, a significant performance increase for all the cases (different Mo_A thickness) compared with the green lines is achieved. A major increase in V_{OC} and FF has boosted the efficiency up to a maximum of 9.5%. The V_{OC} achieved a maximum value of 459 mV, which we believe is currently one of the highest reported for the pure selenide kesterite compound, largely exceeding the CZTSe world record device (423 mV) [85]. An absolute increase in the efficiency values of more than 2% has been possible just with the insertion of a thin MoO_2 intermediate layer. Again a dramatic change in R_{SH} occurs after the introduction of MoO_2 layer going from 149 to 758 ohm cm^2 for the case of 70 nm Mo_A cap layer. The statistical spread of the main optoelectronic parameters for all the cells, besides the case based on 50 nm (due to a possible experimental damage), is shown in Figure A2-12 of A.S.

It should be noted that in contrast with the results from Figure 37a, where the value of J_{SC} was slightly improved in all cases when introducing the MoO_2, in this case the photocurrent was slightly reduced in most of the cases. Figure A2-13a from A.S. shows the EQE plots for the cases where 30 and 70 nm Mo_A cap layer was used along with their MoO_2 based counterparts. It should be noted that other plots are not shown for reasons of simplicity. Figure A2-13b compares the J_{SC} values obtained from J-V curves and from the integration of the EQE signal over the full absorption range. The values obtained from EQE are systematically several mA/cm^2 much larger than the ones obtained from J-V for the MoO_2 containing samples. Therefore, it could be possible that when introducing the MoO_2 some light induced defects are activated under strong illumination conditions, i.e. the light from the AM1.5G standard conditions of our solar simulator. As a result, the current collection is reduced under these illumination conditions, being notably increased when illuminating via monochromatic light from EQE. Therefore, if we take into account the value of J_{SC} obtained from the EQE spectrum the efficiency of the best solar cell would be 10.4% (total area).

New results

Although the best results have been obtained using a Mo multilayered structure combined with MoO_2, it is important to take into consideration that the Mo tri-layer configuration (Mo_4) that we have defined

offers a wide range in terms of optimization/usage. Recent results using this type of back contact layout but changing the thickness of the Mo_A and Mo_B constituent layers allowed us to increase the efficiency from 7.2 to 8.9% as it can be observed in Figure A2-14 of the A.S [243]. In addition, a similar experimental procedure to the one performed in experiment 2 was done with the new optimized tri-layer configuration, in this case changing the thickness of the Mo_A cap layer from 30 to 120 nm. An efficiency increase from 8.3% to 9.2% was obtained for the thickest Mo_A upper layer, as it can be seen in Figure A2-15 in the A.S. In addition V_{OC} values in the range of 450-490 mV were systematically obtained [243]. We believe by further tuning of this tri-layer configuration and with MoO_2, higher CZTSe devices performance could be achieved.

SUMMARY

We have developed a Mo multilayer configuration capable of dealing with one of the most relevant issues of CZTS(e) technology, overselenization of the back region with the subsequent absorber decomposition and reduction of devices performance. A tri-layer configuration has been designed in order to deal with this problem, but also to efficiently tune the thickness of the $MoSe_2$ directly in contact with the CZTSe absorber. The thickness of a top sacrificial Mo_A cap layer is the parameter which allows for $MoSe_2$ thickness control. By modifying its thickness, optoelectronic parameters such as FF and V_{OC} can be increased.

Additionally, we introduced for the first time a nanometric intermediate MoO_2 layer as part of several Mo configurations in CZTS(e) technology. This layer acts as an efficient barrier against selenization. Moreover, it causes a texture change in the $MoSe_2$ layer growing in contact, inducing its growth with the c-axis perpendicular to the substrate. A correlation of the amount of $MoSe_2$ with the Se-Mo-Se sheets growing parallel to the Mo substrate and the MoO_2 layer thickness was confirmed with this work. In this thesis we report for the first time the induction of a specific orientation of $MoSe_2$ via an intermediate layer. Therefore, its beneficial properties such as Se diffusion blocking can be exploited without suffering adverse phenomena such as delamination and/or poor conductivity arising from an uncontrolled layer thickness growth. In addition, the use of MoO_2 intermediate layers results in a significant increase in CZTSe grain size probably due to a Na dynamics modification via O presence in the MoO_2 layer. There are numerous literature reports linking O presence with an enhanced Na diffusion [236-239]. Furthermore, a remarkable improvement in the efficiency of the devices regardless the type of Mo configuration chosen was also obtained, when using 20 nm of MoO_2. The increase was mainly in R_{SH}, FF and V_{OC}. One of the largest V_{OC} of the technology, 459 mV was finally achieved.

Currently, after further tuning of Mo tri-layer configurations, values for V_{OC} around 490 mV have been obtained which are by far the largest of the CZTSe technology [243]. In summary, the use of back contact modifications and intermediate MoO_2 layers developed in this thesis could set a viable route to be

explored in CZTS(e) technology in order to deal with the severe voltage deficit that currently is hindering its progress.

5.2. Removing ZnSe by a sequential oxidizing/passivating chemical etching

In this section the removal of ZnSe, the most common secondary phase for CZTSe absorbers, is studied and different oxidizing etchings are compared in terms of phase removal and solar cell performance. $KMnO_4$, $K_2Cr_2O_7$ and H_2O_2 in H_2SO_4 acidic medium, were investigated. After the use of these etchants, elemental Se^0 was detected in the surface of CZTSe absorbers, evidenced by its characteristic red color. Therefore, a Na_2S aqueous solution was succesfully used to remove this layer. Besides removing Se remains in the surface of CZTSe absorbers, Na_2S had a passivating role since different oxides were removed after its use, as confirmed by XPS measurements. A rough estimation of the Urbach Energy (E_U) also supported the passivation character of this alkaline solution, reducing the density of surface states and improving the characteristics of the p-n junction. An efficiency increase from 3.6% to 5% was achieved when using $KMnO_4/H_2SO_4$ + Na_2S aqueous solutions due to an increase in all the main optoelectronic parameters.

Efficiencies as high as 8.2% were obtained by our group using this etching combined with an air post-annealing of the full devices [244]. Currently, the efficiency has exceeded the 10% value by using the same oxidative step combined with a new passivating solution, $(NH4)_2S$ developed by Xie at al [105, 120]. This new etching combination was explored and established for our baseline processing in the course of this thesis as well.

The insights of this oxidizing/passivating etching can be found in the second article used for the completion of the requirements for the Doctor of Philosophy in Electronic Engineering of the Universitat Politècnica de Catalunya, published in *Chemistry A European Journal*, entitled "ZnSe Etching of Zn-Rich $Cu_2ZnSnSe_4$: An Oxidation Route for Improved Solar-Cell Efficiency" (DOI: 10.1002/chem.201302589). The article is attached in the A.S. A3.

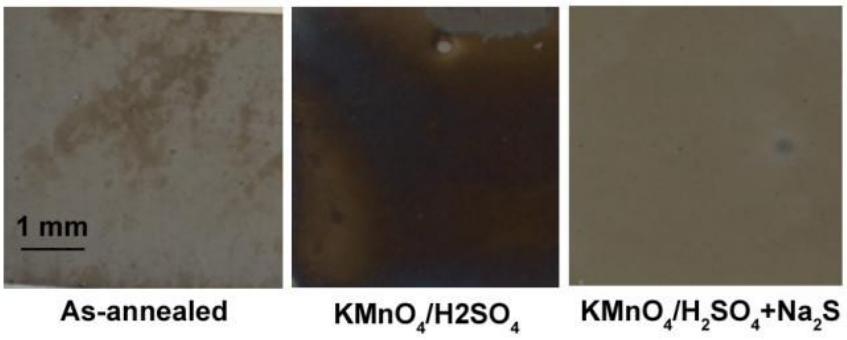

Figure 41. Optical images of films as-annealed (unetched), as-etched with $KMnO_4/H_2SO_4$ and as-etched with $KMnO_4/H_2SO_4$ + Na_2S. Note the presence of the ZnSe phase in the as-annealed absorber, accordingly a red elemental Se^0 layer is formed after the $KMnO_4/H_2SO_4$ etching and when the Na_2S solution is used a clean surface is obtained.

5.3. Flexible CZTSe solar cells

Kesterite has definitely emerged in the last decade as a potential replacement for its already commercialized chalcopyrite counterpart CIGS. The earth-abundant and relatively low toxic kesterite components are certainly appealing for an ambitioned marketability in the TW production level. Nevertheless, the PV market is extremely competitive and unstable especially for technologies other than the more mature crystalline Si based ones, as it was noticed in the last five years [5, 8]. Currently, specific market niches more oriented to portable consumer electronics and BIPV seem to capture the attention of investors and project developers. In order to produce PV modules suitable for these market niches is necessary to use alternative substrates to SLG, and thereby flexible and light-weight substrates opposite to the conventional and rigid glass ones are very interesting. In consequence, the development of kesterite in flexible and light-weight substrates is industrially strategic due to its enormous market potential.

The last part of this thesis is devoted to preliminary experiments to implement CZTSe devices in flexible and light-weight 50 μm SS substrates. Many challenges need to be addressed when working with this type of substrates, such as impurities diffusion from the SS during the CZTSe annealing, i.e. Fe, Cr, Mn…etc, and the lack of alkali elements typical for flexible substrates which is paramount for high efficient devices.

Herein, a Cr diffusion barrier and back contact optimization was performed in order to deal with the undesired impurities diffusion. Additionally, different doping methods with Na and/or K were compared in flexible CZTSe devices.

This section is divided into two different subsections. The first one focuses on the preliminary experiments to develop the first CZTSe flexible devices on SS reported in the literature. Likewise, the second one deals with the optimization of doping strategies based on Na and/or K to increase the devices

efficiency. Furthermore, the diffusion barrier and back contact layouts are examined in terms of devices performance as well.

5.3.1. Proof of concept. First flexible thin film CZTSe solar cell

This subsection includes the first experiments carried out by our research group synthesizing CZTSe absorbers on 50 µm austhenitic SS (AISI SS340). The use of a Cr barrier as suitable way to impede SS impurities such as Fe was first demonstrated for CZTSe technology in this work. This barrier is commonly used in the same field in CIGS technology [173]. Two different annealing temperatures, 450 ºC and 550 ºC, were used to produce CZTSe absorbers. An efficiency of 3.5% was obtained when annealing at the lowest temperature and without any extrinsic alkali supply. A low photocurrent and a steep decrease of the EQE plot from 600 nm evidenced a strong contribution of non radiative recombination at the space charge region and at the bulk. In addition, a very low V_{OC} further pointed towards the need for an intensive processing optimization. Nonetheless, this was the first flexible thin film CZTSe device reported in the literature.

These results can be found in the A.S. A4 in the third article included in this thesis to comply with the requirements for the Doctor of Philosophy in Electronic Engineering of the Universitat Politècnica de Catalunya. The title is "Earth-abundant absorber based solar cells onto low weight stainless steel substrates", and was published in *Solar Energy Materials and Solar Cells* (DOI: 10.1016/j.solmat.2014.07.030)

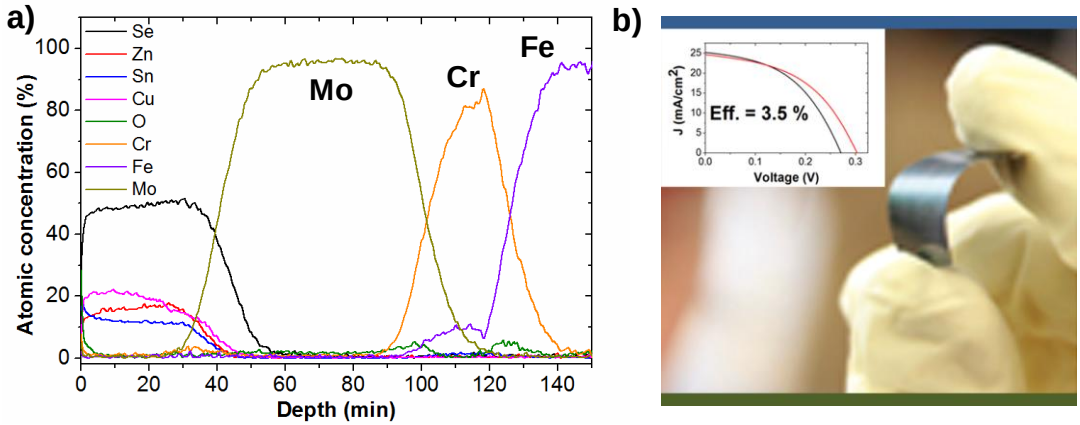

Figure 42: a) Auger depth compositional profile of a flexible CZTSe device on SS substrate. The effectiveness of a 200 nm Cr barrier against Fe diffusion can be noticed. b) Flexible CZTSe solar cells on SS with maximum conversion efficiency of 3.5% with no Na content. Images from ref [180].

The necessity of an extrinsic alkali supply was evident after the first laboratory tests, and thereby the experiments of the next subsection were carried out.

5.3.2. Alkali doping strategies for flexible CZTSe solar cells

The importance of Na alkali doping in CIGS films was already reported in 1993 by Hedstrom et al [245]. Since then, many papers and scientific approaches to explain the beneficial effects of this alkali element have been published [186, 187, 189, 190, 246-248]. For some aspects, the information already published is even contradictory, and thereby it is easy to conclude that alkali doping is still an object for discussion that captures the interest of the thin-film chalcogenide research community.

As it was already stated in section 2.5, K has recently emerged as a paramount alkali element to allow for the latest advances and efficiency increases in CIGS technology, even making possible the world record 20.4% efficient thin film flexible device [161, 199, 200, 202, 249].

In consequence, in the last part of this thesis different alkali strategies were implemented in flexible and light weight CZTSe solar cells developed in 50 μm ferritic SS substrates (AISI SS403). Na doped Mo targets (MoNa), SLG pieces placed underneath the SS substrates during the annealing, NaF and KF pre-absorber synthesis evaporation (PAS) and post deposition evaporation (PDT) were compared in terms of CZTSe absorber microstructure and morphology and devices performance.

Additionally, a detailed Cr barrier and back contact optimization was performed with the aim of improving the efficiency of the non-doped reference devices, which easily suffer from low performance due to Fe and Cr impurities in-diffusion towards the absorber during the annealing step.

Record flexible CZTSe devices of 5.6% and 6.1% efficiency were obtained when doping with KF-PAS and MoNa with a new surface Ge doping respectively [105].

To the best of our knowledge this is the first work which clearly reports on the beneficial effects of K in CZTS(e) technology. Moreover, a full optimization for the use of MoNa layers was also presented for the first time in the field.

The results described in this last experimental section are detailed in the last article within this thesis to comply with the requirements for the Doctor of Philosophy in Electronic Engineering of the Universitat Politècnica de Catalunya. The title is "Alkali doping strategies for flexible and light-weight $Cu_2ZnSnSe_4$ solar cells", and was published in *Journal of Materials Chemistry A*, DOI: 10.1039/C5TA09640E.

The article has been attached in the A.S. A5.

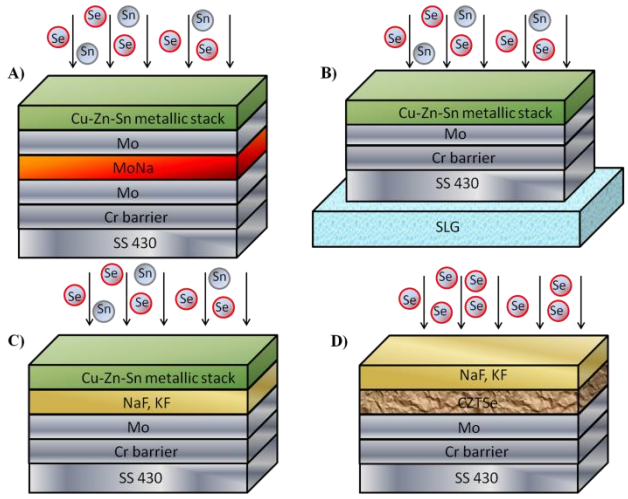

Figure 43: Visual scheme of different alkali doping strategies used in this thesis: A) Na doped Mo targets (MoNa), B) SLG piece underneath the flexible substrates, C) NaF, KF pre-absorber synthesis (PAS) Evaporation and D) NaF, KF post deposition evaporation (PDT).

6. CONCLUSIONS

The aim of this thesis is to develop customized processing solutions for CZTS(e) based solar cells in order to minimize or avoid specific problems of this technology, which are systematically reported in the literature. Currently the maximum device efficiency obtained is 12.6%, and is still very far from the 15-18% desired value for commercialization. Therefore, implementing tailored processes focusing on the technology issues is necessary to increase its market viability. Additionally, the development of CZTSe absorbers on flexible and light-weight SS substrates was also a major goal of this thesis. It should be noted that the use of flexible and light-weight substrates combined with CZTS(e) increases its already high industrial potential due to a more diverse market niche that could ease to a great extent its ambitioned future commercialization. Consequently, the thesis is structured into two different parts. Nonetheless, both parts are interrelated since all the new processing steps developed in the first part of this thesis using conventional and rigid SLG substrates are compatible with the use of flexible and light ones.

In the first part, two paramount working areas are identified as interesting fields to developed new processing approaches. The first one is the back contact interface, in which a decomposition reaction between CZTSe and the common Mo back contact takes place. As a result, presence of voids due to the volatility of part of the decomposition reaction products, such as $Sn(S,Se)_y$ and S(e) gaseous species is very common even in the best devices reported in the literature. Additionally, an excessive $MoSe_2$ layer is also a product generated from the uncontrolled decomposition of the CZTSe absorber at the back region. The presence of this layer, even if necessary due to its accepted properties as buffer layer between the absorber and the Mo to improve the ohmicity of the back interface for the hole transport, is also identified as negative for the electronic transport when present in an uncontrolled manner. In this thesis, two new processing strategies have been developed to minimize all the detrimental effects at the back contact interface previously mentioned.

The first one is based on the introduction of an intermediate 10 nm i-ZnO layer between the Mo back contact and the metallic precursors before the annealing. In this way, the CZTSe absorber and the Mo are no longer in direct contact during the absorber growth process, which results in a significant reduction of the voids at the back CZTSe/Mo interface. An improvement in the devices efficiency from 2.5% to 6% was obtained when using a 10 nm i-ZnO layer. It has to be noted that this layer is already included in the common CZTSe solar cell processing (TCO), in contrast with other intermediate layers reported in the literature which rely on materials not common or necessary for CZTSe processing.

The second one is related to the excessive generation of $MoSe_2$, usually known as overselenization. Different Mo configurations were studied and introduced in CZTSe solar cells. Monolayers, bi-layers and tri-layers were investigated. It was concluded that a tri-layer structure relying in a highly compact layer at the bottom, a more porous one in the middle, and again a cap compact layer grown on top was the

optimum configuration. The bottom layer controls the electrical properties of the multilayer structure, whereas the medium one avoids overselenization, and the cap layer is easily selenized and thereby it can effectively allow for $MoSe_2$ thickness control. Efficiencies in the range of 9%-10% can be obtained when using this configuration and are susceptible of further improvement. Besides using this configuration, an additional innovative approach for the back interface was implemented combined with these multilayer Mo designs. The introduction of a thin MoO_2 layer thermally evaporated from the pure oxide powder resulted in an efficient barrier for selenization but also in an innovative way to efficiently assist the absorber sintering. Large grains correlating with a large efficiency increase due to V_{OC}, FF and R_{SH} were obtained. A 9.5% efficient device with one of the largest Voc for the technology was produced, 459 mV. It has to be noted that this work was the first one introducing MoO_2 in CZTSe technology, opening a new research path for the kesterite community to deal with one of the main current issues of the technology, the V_{OC} deficit. Furthermore, despite the MoO_2 layer was thermally evaporated, it can be deposited in-line with the Mo layer via an Oxygen supply source in the sputtering chamber, and thereby easily integrated in the common CZTS(e) processing line.

The second paramount working area was the CZTSe surface. It is well known that the best devices are obtained for off stoichiometric Cu-poor Zn-rich conditions. In consequence, different secondary phases can be present when synthesizing the absorbers, but the most probable one is ZnSe. Its presence was judged to be highly detrimental when present in the surface of the devices, limiting J_{SC} and affecting the p-n junction properties. In this thesis an innovative and customized approach to remove ZnSe from the CZTSe surface was developed. Different conventional, cheap and relatively low toxic oxidizing agents such as $KMnO_4$, $K_2Cr_2O_7$ and H_2O_2 in H_2SO_4 acidic medium were studied. These etchants were able to oxidize Se^{-2} from the ZnSe to Se^0, but the presence of this compound on the CZTSe surface was detrimental for device performance. Thus, an additional etching step relying in aqueous Na_2S solutions was introduced. An efficiency increase from 3.6% to 5% was achieved when using $KMnO_4/H_2SO_4$ + Na_2S aqueous solutions due to an increase in all the main optoelectronic parameters. The increase of J_{SC} correlated with the ZnSe removal but the increase in V_{OC} and R_{SH} was correlated with an improvement of the p-n junction properties due to a passivation of surface states giving rise to a reduction in those parameters. Using this oxidizing etching combined with a post annealing treatment of the full cells has led to a 10.6% CZTSe device with the highest V_{OC} for the pure selenide compound of the literature.

The second part of this thesis deals with the implementation of CZTSe technology in flexible and light weight SS substrates. Many issues arising from the use of these substrates needed to be addressed, such as Fe and Cr impurities diffusion from the SS and the lack of alkali dopants necessary for high efficient devices. Preliminary experiments introducing Cr diffusion barriers to avoid impurities diffusion led to 3.5% efficient devices, with no alkali presence. These were the first flexible thin film CZTSe devices reported in the literature. Since it was evident the need for alkali sources to further increase the efficiency of the devices, different strategies were studied and used in flexible CZTSe solar cells. Na doped Mo

targets (MoNa), SLG pieces placed underneath the SS substrates during the annealing, NaF and KF pre-absorber synthesis evaporation (PAS) and post deposition evaporation (PDT) were the methods compared in terms of absorber structural and morphological features and devices performance. Likewise, a detailed and comprehensive Cr barrier and back contact optimization was performed in parallel to increase the efficiency of the non-doped reference cells, since their performance was hindered by undesired impurities in-diffusion from the SS substrates. Finally, 5.6% and 6.1% efficient flexible CZTSe solar cells were obtained when doping with KF-PAS and MoNa combined with a new surface Ge doping respectively. The beneficial effects of K in CZTS(e) devices performance were reported in this thesis for the first time in the technology.

In summary, relevant processing approaches specifically designed for CZTSe absorbers have been developed in this thesis. A significant increase in devices efficiency during the course of this PhD was obtained using processes developed in this thesis, from 4.8% to 10.6% efficient CZTSe SLG based devices. In the case of flexible substrates, the most relevant aspects of the processing were fully developed in this thesis, achieving one of the highest efficiencies for flexible CZTSe devices. Nevertheless, a long way is still ahead of kesterite technology to further improve its efficiency, creating exciting challenges for researchers willing to explore interesting but highly complex materials, as kesterites undoubtedly are.

ACKNOWLEDGEMENTS

I would like to thank first my advisors Edgardo Saucedo and Marcel Placidi for the assistance during the course of this thesis, being the source of many ideas that are now an active part of this manuscript. I am grateful for the opportunity received to become a member of the solar energy materials and systems group of IREC, so that I need to thank Edgardo again but also Alejandro Pérez-Rodríguez, head of the group. They made the opportunity to become real, and every day they work to create a working atmosphere that I believe greatly contributes to increase scientific production and to feel at home when working in the group lab and facilities. What can I say? It was very fun and rather easy to work in the group and to fit in! I also need to thank Prof. Ramón Alcubilla, my thesis tutor, for giving me the chance to enroll the electronic engineering department of the UPC and make possible to complete my PhD in his group after many tribulations.

I am extremely thankful for the nice colleagues with whom I shared many hours in the lab and without whom this PhD just would not have been possible, both scientifically and personally speaking. Moisés, Yudania, Haibing, Markus, Andrew, Mira, Xavi, Diouldé, Sergio, Nacho, Florian, Mónica, Laura, Rokas, Paul, Max, Víctor and Juan thanks for being part of this journey!

I would like to thank to my family and friends (outside of the lab) for making the intense moments that I believe every PhD thesis should have more bearable. I want to thank my grandmother Chefa for some character traits that I think I have inherited from her and they are beneficial when coping with a PhD thesis, this is resilience, patience and stubbornness. Although I am sure she could not understand very well what I was doing I have the comfort to know that she knew that at least I was happy and enjoying what I was doing. Her memories have been very present especially at the end of this thesis.

I would like to thank my parents, but specially my mother, since she also has my grandma's genes, but additionally she is a very empathic person and has a very acute sense to evaluate everyday life issues but being very pragmatic. I believe some of these realistic visions were applied by me when designing experiments and analyzing data during this thesis.

I would also like to thank my brothers, Juan and Lucas since they share a lot of things with me although we are really different, but on top of everything we all are very curious, we like and enjoy learning new things. We certainly like to discuss, maybe too much! But again, what would it be this PhD without inner and outer discussions…

I want to thank my friends here in Barcelona, since I believe we are a family outside our beloved region, Galicia. Runis, Sechix, Mariano and Irene (fake Galician but it will do) we will be back one day, that is for sure! I want to say thanks too to the Barcelona gang, full of other expats inside Catalonia. What a nice

team we are! In addition, I cannot forget my friends from Galicia: Vic, Patty, Angie, Calbert and Lucia for hosting me during my holiday trips and of course for your unconditional support.

Last but not least, I would like to thank to all of these people that at some point has crossed my life or IREC's life which I believe has almost be the same in the last four years. Thanks to Maruzzi, Rakala, Mamalus, Momix, La Chica, Cocolus and Monas since without you everything would have been much more boring!

Since this is my space I would like to add that I believe I have worked very hard during this PhD, of course with all the support from my research group, but I have also tried to make more fun our work place. I hope I managed to do so, at least to some extent. As scientists we need to spend a lot of hours in the lab, but is not much better to build up an enjoyable entourage while doing it?

REFERENCES

1. European Photovoltaic Industry Association and Geenpeace, *Solar Generation 6. Solar Photovoltaic Electricity Empowering the World,* 2011, p. 3,6,10,14.

2. B. Parida, S. Iniyan and R. Goic, *A review of solar photovoltaic technologies,* Renewable and Sustainable Energy Reviews, 2011, 1625-1636.

3. European Photovoltaic Technology Platform, *A Strategic Research Agenda for Photovoltaic Solar Energy Technology,* 2011, p. 4,6,11,16.

4. SolarPower Europe, *Global market outlook for Solar Power 2015-2019,* 2015, p. 6.

5. International Energy Agency, IEA-PVPS report , *Trends 2014 in photovoltaic applications,* 2014, p. 5,6,43,46.

6. European Photovoltaic Industry Association, *Global market outlook for Photovoltaics until 2016,* 2012, p. 5, 39.

7. International Renewable Energy Agency, *Renewable energy and jobs. Annual review 2015*, 2015, p. 4.

8. International Energy Agency, IEA-PVPS report, *Annual report 2014,* 2015: p. 94.

9. M. Hoogwijk, PhD thesis, Universiteit Utrecht, 2004, p. 150.

10. P.A. Illes, *Evolution of space solar cells,* Solar Energy Materials & Solar Cells, 2001, **68**, 1-13.

11. A.A. Bayod, *Células y módulos fotovoltaicos,* in *Sistemas fotovoltaicos*, Prensas Universitarias de Zaragoza, Zaragoza, 2009, p. 36-40.

12. J.L. Gray, *The Physics of the Solar Cell*, in *Handbook of Photovoltaic Science and Engineering*, John Wiley & Sons, Ltd, 2005, p. 61-112.

13. M.A. Green, *Solar cells : operating principles, technology, and system applications*, Prentice-Hall. Englewood Cliffs, N.J, 1982, p. 85-102.

14. P. Purnomo Sidi, S. Didik, P. Wahyudi, S. Harry, and H. Djoko, *Electric Energy Management and Engineering in Solar Cell System,* in Solar Cells - Research and Application Perspectives, Open Access under CC BY 3.0 license, 2013, p. 330.

15. T. Kirchartz and U. Rau, *Introduction to Thin-Film Photovoltaics*, in *Advanced Characterization Techniques for Thin Film Solar Cells*, Wiley-VCH Verlag GmbH & Co. KGaA, 2011, p. 1-32.

16. J.E. Phillips, R.W. Birkmire, B.E. McCandless, P.V. Meyers, and W.N. Shafarman, *Polycrystalline heterojunction solar cells: A device perspective*, physica status solidi (b), 1996, **194**, 31-39.

17. U. Rau and H.W. Schock, *Electronic properties of Cu(In,Ga)Se_2 heterojunction solar cells-recent achievements, current understanding, and future challenges*, Applied Physics A, 1999, **69**, 131-147.

18. A. Chirila, S. Buecheler, F. Pianezzi, P. Bloesch, C. Gretener, A.R. Uhl, C. Fella, L. Kranz, J. Perrenoud, S. Seyrling, R. Verma, S. Nishiwaki, Y.E. Romanyuk, G. Bilger, and A.N. Tiwari, *Highly efficient Cu(In,Ga)Se_2 solar cells grown on flexible polymer films*, Nature Materials, 2011, **10**, 857-861.

19. S.S. Hegedus and W.N. Shafarman, *Thin-film solar cells: device measurements and analysis*, Progress in Photovoltaics: Research and Applications, 2004, **12**, 155-176.

20. T.J. Huang, X. Yin, G. Qi, and H. Gong, *CZTS-based materials and interfaces and their effects on the performance of thin film solar cells*, physica status solidi (RRL) – Rapid Research Letters, 2014, **08**, 735-762.

21. Fraunhofer Institute for Solar Energy Systems, ISE, *Photovoltaics report*, 2015, p. 29,31,32.

22. K. Masuko, M. Shigematsu, T. Hashiguchi, D. Fujishima, M. Kai, N. Yoshimura, T. Yamaguchi, Y. Ichihashi, T. Mishima, N. Matsubara, T. Yamanishi, T. Takahama, M. Taguchi, E. Maruyama, and S. Okamoto, *Achievement of More Than 25% Conversion Efficiency With Crystalline Silicon Heterojunction Solar Cell*, Photovoltaics, IEEE Journal of, 2014, **4**, 1433-1435.

23. Panasonic corporation, *Panasonic HIT Solar Cell Achieves World's Highest Energy Conversion Efficiency of 25.6% at Research Level*, 10 April 2014, http://eu-solar.panasonic.net/developer/fileadmin/user_upload/News_PDFs/140410_Panasonic_HIT_E.pdf . Accessed: October 2015.

24. M.A. Green, K. Emery, Y. Hishikawa, W. Warta, and E.D. Dunlop, *Solar cell efficiency tables (version 46)*, Progress in Photovoltaics: Research and Applications, 2015, **23**, 805-812.

25. V. Steckenreiter, J. Hensen, A. Knorr, E. Garralaga Rojas, S. Kajari-Schröder, and R. Brendel, *Reconditioning of silicon substrates for manifold re-use in the layer transfer process with porous*

silicon, in *The 22nd International Photovoltaic Science and Engineering Conference*, 2012, Hangzhou, China.

26. European Photovoltaic Technology Platform, *Europe Industry Initiative team. PV implementation plan 2013-2015*, 2013, p. 7, 8.27.

28. A.G. Alberle, *Thin-film solar cells.* Thin Solid Films, 2009, **517**, 4706-4710.

29. First Solar Inc., *First Solar Achieves Efficiency, Durability Milestones, 5 February 2015*, http://files.shareholder.com/downloads/FSLR/910320849x0x807660/D0F909F7-514B-4EE4-A92E-109785D7939E/FSLR_News_2015_2_5_English.pdf. Accessed: October 2015.

30. ZSW, *New best mark in thin-film solar performance with 21.7 percent efficiency*, 22 September 2014, http://www.zsw-bw.de/uploads/media/pr12-2014-ZSW-WorldrecordCIGS.pdf. Accessed: October 2015.

31. European Photovoltaic Industry Association, *Global Market outlook for photovoltaics 2013-2017*, 2013, p. 5, 41, 54.

32. L. El Chaar, L.A. lamont, and N. El Zein, *Review of photovoltaic technologies*, Renewable and Sustainable Energy Reviews, 2011, **15**, 2165-2175.

33. Fraunhofer Institute for Solar Energy Systems, ISE, *New world record for solar cell efficiency at 46%*, 1 December 2014, https://www.ise.fraunhofer.de/en/press-and-media/pdfs-zu-presseinfos-englisch/2014/press-release-new-world-record-for-solar-cell-efficiency-at-46-percent.pdf. Accessed: October 2015.

34. International Energy Agency, *Technology Road Map.Solar Photovoltaic Energy*, 2010, p. 7, 24-26.

35. M.K. Nazeeruddin, E. Baranoff, and M. Grätzel, *Dye-sensitized solar cells: A brief overview.* Solar Energy, 2011, **85**, 1172-1178.

36. M.A. Green, *Crystalline and thin-film silicon solar cells: state of the art and future potential*, Solar Energy, 2003, **74**, 181-192.

37. S. Emin, S. P. Singh, L. Han, N. Satoh, and A. Islam, *Colloidal quantum dot solar cells*, Solar Energy, 2011, **85**, 1264-1282.

38. D. Mocatta, G. Cohen, J. Schattner, O. Millo, E. Rabani, and U. Banin, *Heavily Doped Semiconductor Nanocrystal Quantum Dots*, Science, 2011, **332**, 77-81.

39. N. López, L.A. Reichertz, K.M. Yu, K. Campman, and W. Walukiewicz, *Engineering the Electronic Band Structure for Multiband Solar Cells*, Physical Review Letters, 2011, **106**, 1-4.

40. S. Baluschev, T. Miteva, V. Yakutkin, G. Nelles, A. Yasuda, and G. Wegner, *Up-Conversion Fluorescence: Noncoherent Excitation by Sunlight*, Physical Review Letters, 2006, **93**, 1-3.

41. E. Pedrueza, J.L. Valdés, V. Chirvony, R. Abargues, J. Hernández-Saz , M. Herrera, S.I. Molina, and J.P. Martínez-Pastor, *Novel Method of Preparation of Gold-Nanoparticle-Doped TiO_2 and SiO_2 Plasmonic Thin Films: Optical Characterization and Comparison with Maxwell–Garnett Modeling*, Advanced Functional Materials, 2011, **21**, 3502-3507.

42. J.-L. Wu, F.-C. Chen, Y.-S. Hsiao, F.-C. Chien, P. Chen, C.-H. Kuo, M.H. Huang, and C.-S. Hsu, *Surface Plasmonic Effects of Metallic Nanoparticles on the Performance of Polymer Bulk Heterojunction Solar Cells*, ACS Nano, 2011, **5**, 959-967.

43. R.W. Miles, *Inorganic Photovoltaic Solar Cells*. Materials today, 2007, **10**, 20-27.

44. F. Meillaud, M. Boccard, G. Bugnon, M. Despeisse, S. Hänni, F.J. Haug, J. Persoz, J.W. Schüttauf, M. Stuckelberger, and C. Ballif, *Recent advances and remaining challenges in thin-film silicon photovoltaic technology*, Materials today, 2015, **18**, 378-384.

45. R.W. Miles, K.H. Haynes, and I. Forbes, *Photovoltaic solar cells: An overview of state-of-art cell development and evirinmental issues*. Progress in Crystal Growth and characterisation of Materials, 2005. **51**: p. 1-42.

46. First Solar Inc., *First Solar Achieves 5GW Photovoltaic Production Milestone*, 17 November 2011, http://investor.firstsolar.com/releases.cfm?ReleasesType=&Year=2011. Accessed: October 2015.

47. First Solar Inc., *Annual report 2014*, 2015, http://files.shareholder.com/downloads/FSLR/910320849x0x819571/AD02242D-C0E5-4C49-AE46-A8265164AD5F/First_Solar_2014_Annual_Report_Bookmark_-_Final.pdf, p. 4,10. Accessed: October 2015.

48. Greentech media, *First Solar Is Sold Out of Module Capacity for 2015 and Most of 2016, 4 August 2015*, *http://www.greentechmedia.com/articles/read/First-Solar-is-Sold-Out-of-Module-Capacity-for-2015-and-Most-of-2016*. Accessed: October 2015.

49. Kazmerski L.L., *Solar photovoltaics R&D at the tipping point: A 2005 technology overview*, Journal of Electron Spectroscopy and Related Phenomena, 2006, **150**, 105-135.

50. V.M. Fthenakis, *Life cycle impact analysis of cadmium in CdTe PV production*, Renewable and Sustainable Energy Reviews, 2004, **8**, 303-334.

51. V.M. Fthenakis and H.C. Kim, *Photovoltaics: Life-cycle analyses*, Solar Energy, 2011, **85**, 1609-1628.

52. European Commission, *Report on Critical Raw Materials for the EU, May* 2014, p. 3,31.

53. U.S. Department of Energy, Critical materials strategy, December 2011, p. 115-118.

54. V. Fthenakis, *Sustainability of photovoltaics: The case for thin-film solar cells*, Renewable and Sustainable Energy Reviews, 2009, **13**, 2746-2750.

55. H. Wang, *Progress in Thin Film Solar Cells Based on Cu_2ZnSnS_4*, International Journal of Photoenergy, 2011, **2011**, 10.

56. W. Wang, M.T. Winkler, O. Gunawan, T. Gokmen, T.K. Todorov, Y. Zhu, and D.B. Mitzi, *Device Characteristics of CZTSSe Thin-Film Solar Cells with 12.6% Efficiency*, Advanced Energy Materials, 2013, **4**, 1301465.

57. S.R. Hall, J.T. Szymanski, and J.M. Stewart, *Kesterite and stannite, structurally similar but distinct minerals*, Canadian Mineralogist, 1978, **16**, 131-137.

58. B.R. Pamplin, *Super-Cell Structure of Semiconductors*, Nature, 1960, **188**, 136-137.

59. S. Chen, X.G. Gong, A. Walsh, and S.-Y. Wei, *Crystal and electronic band structure of Cu_2ZnSnX_4 (X = S and Se) photovoltaic absorbers: First-principles insights*, Applied Physics Letters, 2009, **94**, 041903-1, 3.

60. A. Walsh, S. Chen, S.-H. Wei, and X.-G. Gong, *Kesterite Thin-Film Solar Cells: Advances in Materials Modelling of Cu_2ZnSnS_4*, Advanced Energy Materials, 2012, **2**, 400-409.

61. S. Chen, X.G. Gong, A. Walsh, and S.-H. Wei, *Electronic structure and stability of quaternary chalcogenide semiconductors derived from cation cross-substitution of II-VI and I-III-VI_2 compounds*, Physical Review B, 2009, **79**, 165211.

62. S. Schorr, *The crystal structure of kesterite type compounds: A neutron and X-ray diffraction study*, Solar Energy Materials and Solar Cells, 2011, **95**, 1482-1488.

63. S. Schorr, H.-J. Hoebler, and M. ovar, *A neutron diffraction study of the stannite-kesterite solid solution series*, European Journal of Mineralogy, 2007, **19**, 65-73.

64. X. Fontané, V. Izquierdo-Roca, E. Saucedo, S. Schorr, V.O. Yukhymchuk, M.Y. Valakh, A. Pérez-Rodríguez, and J.R. Morante, *Vibrational properties of stannite and kesterite type compounds: Raman scattering analysis of $Cu_2(Fe,Zn)SnS_4$*, Journal of Alloys and Compounds, 2012, **539**, 190-194.

65. S. Chen, A. Walsh, Y. Luo, J.-H. Yang, X.G. Gong, and S.-H. Wei, *Wurtzite-derived polytypes of kesterite and stannite quaternary chalcogenide semiconductors*, Physical Review B, 2010, **82**, 195203.

66. X. Lin, J. Kavalakkatt, K. Kornhuber, D. Abou-Ras, S. Schorr, M.C. Lux-Steiner, and A. Ennaoui, *Synthesis of $Cu_2Zn_xSn_ySe_{1+x+2y}$ nanocrystals with wurtzite-derived structure*, RSC Advances, 2012, **2**, 9894-9898.

67. M. Grossberg, J. Krustok, J. Raudoja, and T. Raadik, *The role of structural properties on deep defect states in Cu_2ZnSnS_4 studied by photoluminescence spectroscopy*, Applied Physics Letters, 2012, **101**, 102102.

68. G. Rey, A. Redinger, J. Sendler, T.P. Weiss, M. Thevenin, M. Guennou, B. El Adib, and S. Siebentritt, *The band gap of $Cu_2ZnSnSe_4$: Effect of order-disorder*, Applied Physics Letters, 2014, **105**, 112106.

69. J.J.S. Scragg, L. Choubrac, A. Lafond, T. Ericson, and C. Platzer-Björkman, *A low-temperature order-disorder transition in Cu_2ZnSnS_4 thin films*, Applied Physics Letters, 2014, **104**, 041911.

70. K. Ito and T. Nakazawa, *Electrical and Optical Properties of Stannite-Type Quaternary Semiconductor Thin Films*, Japanese Journal of Applied Physics, 1988, **27**, 2094-2097.

71. K. Jimbo, R. Kimura, T. Kamimura, S. Yamada, W.S. Maw, H. Araki, K. Oishi, and H. Katagiri, *Cu2ZnSnS4-type thin film solar cells using abundant materials*, Thin Solid Films, 2007, **515**, 5997-5999.

72. A.T. Magorian, *PhD Thesis*, University of Stuttgart, 2001.

73. S. Ahn, S. Jung, J. Gwak, A. Cho, K. Shin, K. Yoon, D. Park, H. Cheong, and J.H. Yun, *Determination of band gap energy (E_g)of $Cu_2ZnSnSe_4$ thin films: On the discrepancies of reported band gap values*, Applied Physics Letters, 2010, **97**, 021905-3.

74. P.M.P. Salomé, P.A. Fernandes, A.F. da Cunha, J.P. Leitao, J. Malaquias, A. Weber, J.C. González, and M.I.N. da Silva, *Growth pressure dependence of $Cu_2ZnSnSe_4$ properties*, Solar Energy Materials and Solar Cells, 2010, **94**, 2176-2180.

75. Q. Shu, J.-H. Yang, S. Chen, B. Huang, H. Xiang, X.-G. Gong, and S.-H. Wei, *$Cu_2Zn(Sn,Ge)Se_4$ and $Cu_2Zn(Sn,Si)Se_4$ alloys as photovoltaic materials: Structural and electronic properties*, Physical Review B, 2013, **87,** 115208.

76. M. Pilvet, M. Kauk-Kuusik, M. Altosaar, M. Grossberg, M. Danilson, K. Timmo, A. Mere, and V. Mikli, *Compositionally tunable structure and optical properties of $Cu_{1.85}(Cd_xZn_{1-x})_{1.1}SnS_{4.1}$ ($0\leq x\leq 1$) monograin powders*, Thin Solid Films, 2015, **582**, 180-183.

77. Z. Su, J.M.R. Tan, X. Li, X. Zeng, S.K. Batabyal, and L.H. Wong, *Cation Substitution of Solution-Processed Cu_2ZnSnS_4 Thin Film Solar Cell with over 9% Efficiency*, Advanced Energy Materials, 2015, **5**, 1500682.

78. Z.-Y. Xiao, Y.-F. Li, B. Yao, R. Deng, Z.-H. Ding, T. Wu, G. Yang, C.-R. Li, Z.-Y. Dong, L. Liu, L.-G. Zhang, and H.-F. Zhao, *Bandgap engineering of $Cu_2Cd_xZn_{1-x}SnS_4$ alloy for photovoltaic applications: A complementary experimental and first-principles study*, Journal of Applied Physics, 2013, **114**, 183506.

79. X. Wu, W. Liu, S. Cheng, Y. Lai, and H. Jia, *Photoelectric properties of Cu_2ZnSnS_4 thin films deposited by thermal evaporation*, Journal of Semiconductors, 2012, **33**, 022002.

80. Q. Guo, H.W. Hillhouse, and R. Agrawal, *Synthesis of Cu_2ZnSnS_4 Nanocrystal Ink and Its Use for Solar Cells*, Journal of the American Chemical Society, 2009, **131,** 11672-11673.

81. R. Adhi Wibowo, E. Soo Lee, B. Munir, and K. Ho Kim, *Pulsed laser deposition of quaternary $Cu_2ZnSnSe_4$ thin films*, physica status solidi (a), 2007, **204**, 3373-3379.

82. A. Nagaoka, K. Yoshino, H. Taniguchi, T. Taniyama, and H. Miyake, *Preparation of Cu_2ZnSnS_4 single crystals from Sn solutions*, Journal of Crystal Growth, 2012, **341**, 38-41.

83. S. Adachi, *Physical Properties*, in *Copper Zinc Tin Sulfide-Based Thin-Film Solar Cells*, John Wiley & Sons Ltd., 2015, p. 149-179.

84. V. Chawla and B. Clemens, *Effect of composition on high efficiency CZTSSe devices fabricated using co-sputtering of compound targets*, in *Photovoltaic Specialists Conference (PVSC), 2012 38th IEEE*, 2012.

85. Y.S. Lee, T. Gershon, O. Gunawan, T.K. Todorov, T. Gokmen, Y. Virgus, and S. Guha, *$Cu_2ZnSnSe_4$ Thin-Film Solar Cells by Thermal Co-evaporation with 11.6% Efficiency and Improved Minority Carrier Diffusion Length*, Advanced Energy Materials, 2014. **5**, 1401372.

86. S. Chen, et al., *Defect physics of the kesterite thin-film solar cell absorber Cu_2ZnSnS_4,* Applied Physics Letters, 2010, **96**, 021902-1,3.

87. S. Chen, J.-H. Yang, X.G. Gong, A. Walsh, and S.-H. Wei, *Intrinsic point defects and complexes in the quaternary kesterite semiconductor Cu_2ZnSnS_4,* Physical Review B, 2010, **81**, 245204.

88. H. Katagiri, K. Jimbo, M. Tahara, H. Araki, and K. Oishi, *The Influence of the Composition Ratio on CZTS-based Thin Film Solar Cells*, MRS Online Proceedings Library, 2009, **1165**.

89. H. Katagiri, M. Nishimura, T. Onozawa, S. Maruyama, M. Fujita, T. Sega, and T. Watanabe, *Rare-metal free thin film solar cell*, in *Proceedings of the Power Conversion Conference*, 1997, Nagaoka, Japan, 1003-1006.

90. T. Kato, H. Hiroi, N. Sakai, S. Muraoka, and H. Sugimoto. *Characterization of Front and Back Interfaces on Cu_2ZnSnS_4 Thin-Film Solar Cells*, in *27th European Photovoltaic Solar Energy Conference and Exhibition*, 2012, Frankfurt, Germany.

91. L. Vauche, L. Risch, Y. Sánchez, M. Dimitrievska, M. Pasquinelli, T. Goislard de Monsabert, P.-P. Grand, S. Jaime-Ferrer, and E. Saucedo, *8.2% pure selenide kesterite thin-film solar cells from large-area electrodeposited precursors*, Progress in Photovoltaics: Research and Applications, 2015, **24**, 38-51.

92. G. Larramona, S. Levcenko, S. Bourdais, A. Jacob, C. Choné, B. Delatouche, C. Moisan, J. Just, T. Unold, and G.C. Dennler, *Fine-Tuning the Sn Content in CZTSSe Thin Films to Achieve 10.8% Solar Cell Efficiency from Spray-Deposited Water–Ethanol-Based Colloidal Inks.* Advanced Energy Materials, 2015, **5**, 1501404.

93. H. Xin, S.M. Vorpahl, A.D. Collord, I.L. Braly, A.R. Uhl, B.W. Krueger, D.S. Ginger, and H.W. Hillhouse, *Lithium-doping inverts the nanoscale electric field at the grain boundaries in $Cu_2ZnSn(S,Se)_4$ and increases photovoltaic efficiency*, Physical Chemistry Chemical Physics, 2015, **17**, 23859-23866.

94. T. Kato, N. Sakai, and H. Sugimoto, *Efficiency improvement of $Cu_2ZnSn(S,Se)_4$ submodule with graded bandgap and reduced backside ZnS segregation*,in *Photovoltaic Specialist Conference (PVSC), 2014 IEEE 40^{th}*, 2014.

95. G. Qijie, C. Yanyan, J.V. Caspar, W.E. Farneth, A.S. Ionkin, L.K. Johnson, L. Meijun, I. Malajovich, D. Radu, K.R. Choudhury, H.D. Rosenfeld, and W. Wei, *A simple solution-based route to high-efficiency CZTSSe thin-film solar cells*, in *Photovoltaic Specialists Conference (PVSC), 2012 38th IEEE*, 2012.

96. T. Fukano, S. Tajima, and T. Ito, *Enhancement of Conversion Efficiency of Cu_2ZnSnS_4 Thin Film Solar Cells by Improvement of Sulfurization Conditions*, Applied Physics Express, 2013, **6**, 062301.

97. Crystalsol, *Crystalsol sets European cell efficiency record for CZTS based photovoltaic cells*, May 2013, *http://www.crystalsol.com*. Accessed: October 2015.

98. R. Lechner, S. Jost, J. Palm, M. Gowtham, F. Sorin, B. Louis, H. Yoo, R.A. Wibowo, and R. Hock, *$Cu_2ZnSn(S,Se)_4$ solar cells processed by rapid thermal processing of stacked elemental layer precursors*,Thin Solid Films, 2013, **535**, 5-9.

99. B. Shin, O. Gunawan, Y. Zhu, N.A. Bojarczuk, S.J. Chey, and S. Guha, *Thin film solar cell with 8.4% power conversion efficiency using an earth-abundant Cu_2ZnSnS_4 absorber*, Progress in Photovoltaics: Research and Applications, 2013, **21**, 72–76

100. F. Jiang, S. Ikeda, T. Harada, and M.C. Matsumura, *Pure Sulfide Cu_2ZnSnS_4 Thin Film Solar Cells Fabricated by Preheating an Electrodeposited Metallic Stack*, Advanced Energy Materials, 2014, **4**, 1301381.

101. S. Giraldo, M. Neuschitzer, S. López-Marino, Y. Sánchez, M. Colina, M. Placidi, P. Pistor, A. Pérez-Rodríguez, and E. Saucedo, *10.1% Efficiency $Cu_2ZnSnSe_4$ Solar Cells through a Novel Absorber Engineering with Ge Optimizing the Open Circuit Voltage*, in *32nd EUPVSEC*, 2015, Hamburg (Germany).

102. S. Chen, A. Walsh, X.-G. Gong, and S.-H. Wei, *Classification of Lattice Defects in the Kesterite Cu_2ZnSnS_4 and $Cu_2ZnSnSe_4$ Earth-Abundant Solar Cell Absorbers*, Advanced Materials, 2013, **25,** 1522-1539.

103. S. Siebentritt, *Why are kesterite solar cells not 20% efficient?*, Thin Solid Films, 2013, **535**, 1-4.

104. T.K. Todorov, K.B. Reuter, and D.B. Mitzi, *High-Efficiency Solar Cell with Earth-Abundant Liquid-Processed Absorber*, Advanced Materials, 2010, **22**, E156-E159.

105. S. Giraldo, M. Neuschitzer, T. Thersleff, S. López-Marino, Y. Sánchez, H. Xie, M. Colina, M. Placidi, P. Pistor, V. Izquierdo-Roca, K. Leifer, A. Pérez-Rodríguez, and E. Saucedo, *Large*

Efficiency Improvement in $Cu_2ZnSnSe_4$ Solar Cells by Introducing a Superficial Ge Nanolayer, Advanced Energy Materials, 2015, 5, 1501070.

106. A. Polizzotti, I.L. Repins, R. Noufi, S.-H. Wei, and D.B. Mitzi, *The state and future prospects of kesterite photovoltaics*, Energy & Environmental Science, 2013, **6**, 3171-3182.

107. I.L. Repins, M.J. Romero, J.V. Li, W. Su-Huai, D. Kuciauskas, J. Chun-Sheng, C. Beall, C. DeHart, J. Mann, H. Wan-Ching, G. Teeter, A. Goodrich, and R. Noufi, *Kesterite Successes, Ongoing Work, and Challenges: A Perspective From Vacuum Deposition*, Photovoltaics, IEEE Journal of, 2012, **3**, 439-445.

108. I. Repins, N. Vora, C. Beall, S.-H. Wei, Y. Yan, M. Romero, G. Teeter, H. Du, B. To, M. Young, and R. Noufi, *Kesterites and Chalcopyrites: A Comparison of Close Cousins*, MRS Online Proceedings Library, 2011, **1324**.

109. S. Siebentritt and S. Schorr, *Kesterites—a challenging material for solar cells*, Progress in Photovoltaics: Research and Applications, 2012, **20**, 512-519.

110. T. Gershon, B. Shin, T. Gokmen, S. Lu, N. Bojarczuk, and S. Guha, *Relationship between Cu_2ZnSnS_4 quasi donor-acceptor pair density and solar cell efficiency*, Applied Physics Letters, 2013, **103**, 193903.

111. T. Gokmen, O. Gunawan, T.K. Todorov, and D.B. Mitzi, *Band tailing and efficiency limitation in kesterite solar cells*, Applied Physics Letters, 2013, **103**, 103506

112. J. Krustok, R. Josepson, T. Raadik, and M. Danilson, *Potential fluctuations in $Cu_2ZnSnSe_4$ solar cells studied by temperature dependence of quantum efficiency curves*, Physica B: Condensed Matter, 2010, **405**, 3186-3189.

113. S. Oueslati, G. Brammertz, M. Buffière, C. Köble, T. Oualid, M. Meuris, and J. Poortmans, *Photoluminescence study and observation of unusual optical transitions in $Cu_2ZnSnSe_4$/CdS/ZnO solar cells*, Solar Energy Materials and Solar Cells, 2015, **134**, 340-345.

114. A. Fairbrother, E. García-Hemme, V. Izquierdo-Roca, X. Fontané, F.A. Pulgarín-Agudelo, O. Vigil-Galán, A. Pérez-Rodríguez, and E. Saucedo, *Development of a Selective Chemical Etch To Improve the Conversion Efficiency of Zn-Rich Cu_2ZnSnS_4 Solar Cells*, Journal of the American Chemical Society, 2012, **134**, 8018-8021.

115. S. Lopez-Marino, M. Placidi, A. Perez-Tomas, J. Llobet, V. Izquierdo-Roca, X. Fontane, A. Fairbrother, M. Espindola-Rodriguez, D. Sylla, A. Perez-Rodriguez, and E. Saucedo, *Inhibiting*

the absorber/Mo-back contact decomposition reaction in $Cu_2ZnSnSe_4$ solar cells: the role of a ZnO intermediate nanolayer, Journal of Materials Chemistry A, 2013, **1**, 8338-8343.

116. S. López-Marino, Y. Sánchez, M. Placidi, A. Fairbrother, M. Espindola-Rodríguez, X. Fontané, V. Izquierdo-Roca, J. López-García, L. Calvo-Barrio, A. Pérez-Rodríguez, and E. Saucedo, *ZnSe Etching of Zn-Rich $Cu_2ZnSnSe_4$: An Oxidation Route for Improved Solar-Cell Efficiency*, Chemistry – A European Journal, 2013, **19**, 14814-14822.

117. M. Mousel, A. Redinger, R. Djemour, M. Arasimowicz, N. Valle, P. Dale, and S. Siebentritt, *HCl and Br_2-MeOH etching of $Cu_2ZnSnSe_4$ polycrystalline absorbers, T*hin Solid Films, 2013, **535**, 83-87.

118. S. Oueslati, G. Brammertz, M. Buffière, H. ElAnzeery, D. Mangin, O. ElDaif, O. Touayar, C. Köble, M. Meuris, and J. Poortmans, *Study of alternative back contacts for thin film $Cu_2ZnSnSe_4$ -based solar cells*, Journal of Physics D: Applied Physics, 2015, **48,** 035103.

119. B. Shin, Y. Zhu, N.A. Bojarczuk, S.J. Chey, and S. Guha, *Control of an interfacial $MoSe_2$ layer in $Cu_2ZnSnSe_4$ thin film solar cells: 8.9% power conversion efficiency with a TiN diffusion barrier*, Applied Physics Letters, 2012, **101**, 053903.

120. H. Xie, Y. SÁnchez, S. López-Marino, M. Espíndola-Rodríguez, M. Neuschitzer, D. Sylla, A. Fairbrother, V. Izquierdo-Roca, A. Pérez-Rodríguez, and E. Saucedo, *Impact of Sn(S,Se) Secondary Phases in $Cu_2ZnSn(S,Se)_4$ Solar Cells: a Chemical Route for Their Selective Removal and Absorber Surface Passivation*, ACS Applied Materials & Interfaces, 2014, **6**, 12744-12751.

121. I.V. Dudchak and L.V. Piskach, *Phase equilibria in the Cu_2SnSe_3-$SnSe_2$-ZnSe system*, Journal of Alloys and Compounds, 2003, **351**, 145-150.

122. I.D. Olekseyuk, I.V. Dudchak, and L.V. Piskach, *Phase equilibria in the Cu_2S-ZnS-SnS_2 system*, Journal of Alloys and Compounds, 2004, **368**, 135-143.

123. J.J. Scragg, P.J. Dale, D. Colombara, and L.M. Peter, *Thermodynamic Aspects of the Synthesis of Thin-Film Materials for Solar Cells*, ChemPhysChem, 2012, **13**, 3035-3046.

124. A. Weber, H. Krauth, S. Perlt, B. Schubert, I. Kötschau, S. Schorr, and H.W. Schock, *Multi-stage evaporation of Cu_2ZnSnS_4 thin films*, Thin Solid Films, 2009, **517**, 2524-2526.

125. A. Redinger, D.M. Berg, P.J. Dale, and S. Siebentritt, *The Consequences of Kesterite Equilibria for Efficient Solar Cells*, Journal of the American Chemical Society, 2011, **133**, 3320-3323.

126. F. Hergert and R. Hock, *Predicted formation reactions for the solid-state syntheses of the semiconductor materials Cu_2SnX_3 and Cu_2ZnSnX_4 (X= S, Se) starting from binary chalcogenides*, Thin Solid Films, 2007, **515**, 5953-5956.

127. J.J. Scragg, J.T. Wätjen, M. Edoff, T. Ericson, T. Kubart, and C. Platzer-Björkman, *A Detrimental Reaction at the Molybdenum Back Contact in $Cu_2ZnSn(S,Se)_4$ Thin-Film Solar Cells*, Journal of the American Chemical Society, 2012, **134**, 19330-19333.

128. M. Buffière, G. Brammertz, M. Batuk, C. Verbist, D. Mangin, C. Koble, J. Hadermann, M. Meuris, and J. Poortmans, *Microstructural analysis of 9.7% efficient $Cu_2ZnSnSe_4$ thin film solar cells*, Applied Physics Letters, 2014, **105**, 183903.

129. W.N. Shafarman and J.E. Phillips, *Direct current-voltage measurements of the Mo/$CuInSe_2$ contact on operating solar cells*, in *Photovoltaic Specialists Conference, 1996, Conference Record of the Twenty Fifth IEEE*, 1996.

130. W. Takahiro, K. Naoki, N. Takayuki, and N. Mikihiko, *Chemical and Structural Characterization of Cu(In,Ga)Se_2/Mo Interface in Cu(In,Ga)Se_2 Solar Cells*, Japanese Journal of Applied Physics, 1996, **35**, L1253.

131. T. Wada, N. Kohara, S. Nishiwaki, and T. Negami, *Characterization of the Cu(In,Ga)Se_2/Mo interface in CIGS solar cells*, Thin Solid Films, 2001, **387**, 118-122.

132. H. Cui, C.-Y. Lee, W. Li, X. Liu, X. Wen, and X. Hao, *Improving Efficiency of Evaporated Cu_2ZnSnS_4 Thin Film Solar Cells by a Thin Ag Intermediate Layer between Absorber and Back Contact*, International Journal of Photoenergy, 2015, **2015**, p. 9.

133. F. Liu, K. Sun, W. Li, C. Yan, H. Cui, L. Jiang, X. Hao, and M.A. Green, *Enhancing the Cu_2ZnSnS_4 solar cell efficiency by back contact modification: Inserting a thin TiB_2 intermediate layer at Cu_2ZnSnS_4/Mo interface*, Applied Physics Letters, 2014, **104**, 051105.

134. W. Li, J. Chen, H. Cui, F. Liu, and X. Hao, *Inhibiting MoS_2 formation by introducing a ZnO intermediate layer for Cu_2ZnSnS_4 solar cells*, Materials Letters, 2014, **130**, 87-90.

135. C. Roger, S. Noël, O. Sicardy, P. Faucherand, L. Grenet, N. Karst, H. Fournier, F. Roux, F. Ducroquet, A. Brioude, and S. Perraud, *Characteristics of molybdenum bilayer back contacts for Cu(In,Ga)Se_2 solar cells on Ti foils*, Thin Solid Films, 2013, **548**, 608–616.

136. P.M.P. Salomé, J. Malaquias, P.A. Fernandes, and A.F.d. Cunha, *Mo bilayer for thin film photovoltaics revisited*, Journal of Physics D: Applied Physics, 2010, **43**, 345501.

137. J.H. Scofield, A. Duda, D. Albin, B.L. Ballard, and P.K. Predecki, *Sputtered molybdenum bilayer back contact for copper indium diselenide-based polycrystalline thin-film solar cells,* Thin Solid Films, 1995, **260**, 26-31.

138. C. Leidholm, C. Hotz, A. Breeze, C. Sunderland, W. Ki, and D. Zehnder, *Final Report: Sintered CZTS Nano-particle Solar Cells on Metal Foil,* NREL Report No. NREL/SR-5200-56501 2012.

139. P. Blösch, S. Nishiwaki, L. Kranz, C.M. Fella, F. Pianezzi, T. Jäger, C. Adelhelm, E. Franzke, S. Buecheler, and A.N. Tiwari, *Sodium-doped molybdenum back contact designs for Cu(In,Ga)Se_2 solar cells,* Solar Energy Materials and Solar Cells, 2014, **124**, 10-16.

140. P.M.P. Salomé, V. Fjallstrom, A. Hultqvist, P. Szaniawski, U. Zimmermann, and M. Edoff, *The effect of Mo back contact ageing on Cu(In,Ga)Se_2 thin-film solar cells,* Progress in Photovoltaics: Research and Applications, 2014, **22**, 83-89.

141. K.-J. Yang, J.-H. Sim, B. Jeon, D.-H. Son, D.-H. Kim, S.-J. Sung, D.-K. Hwang, S. Song, D.B. Khadka, J. Kim, and J.-K. Kang, *Effects of Na and MoS_2 on Cu_2ZnSnS_4 thin-film solar cell,* Progress in Photovoltaics: Research and Applications, 2014, **23**, 862–873.

142. A. Duchatelet, G. Savidand, R.N. Vannier, and D. Lincot, *Optimization of $MoSe_2$ formation for Cu(In,Ga)Se_2-based solar cells by using thin superficial molybdenum oxide barrier layers,* Thin Solid Films, 2013, **545**, 94-99.

143. S. Kasap, P. Capper, J. Wang, and M. Isshiki, *Wide-Bandgap II-VI Semiconductors: Growth and Properties,* in *Springer Handbook of Electronic and Photonic Materials,* Springer US, 2007, p. 325-342.

144. J. Just, D. Lutzenkirchen-Hecht, R. Frahm, S. Schorr, and T. Unold, *Determination of secondary phases in kesterite Cu_2ZnSnS_4 thin films by x-ray absorption near edge structure analysis.* Applied Physics Letters, 2011, **99**, 262105-3.

145. J.T. Wätjen, J. Engman, M. Edoff, and C. Platzer-Bjorkman, *Direct evidence of current blocking by ZnSe in $Cu_2ZnSnSe_4$ solar cells,* Applied Physics Letters, 2012, **100**, 173510-3.

146. W.-C. Hsu, I. Repins, C. Beall, C. DeHart, G. Teeter, B. To, Y. Yang, and R. Noufi, *The effect of Zn excess on kesterite solar cells,* Solar Energy Materials and Solar Cells, 2013, **113**, 160-164.

147. N. Vora, J. Blackburn, I. Repins, C. Beall, B. To, J. Pankow, G. Teeter, M. Young, and R. Noufi, *Phase identification and control of thin films deposited by co-evaporation of elemental Cu, Zn,*

Sn, and Se, Journal of Vacuum Science & Technology A: Vacuum, Surfaces, and Films, 2012, **30**, 051201-7.

148. P.A. Fernandes, P.M.P. Salomé, and A.F. da Cunha, *Study of polycrystalline Cu_2ZnSnS_4 films by Raman scattering,* Journal of Alloys and Compounds, 2011, **509**, 7600-7606.

149. A. Fairbrother, X. Fontané, V. Izquierdo-Roca, M. Placidi, D. Sylla, M. Espindola-Rodriguez, S. López-Mariño, F.A. Pulgarín, O. Vigil-Galán, A. Pérez-Rodríguez, and E. Saucedo, *Secondary phase formation in Zn-rich $Cu_2ZnSnSe_4$-based solar cells annealed in low pressure and temperature conditions,* Progress in Photovoltaics: Research and Applications, 2014, **22**, 479-487.

150. X. Fontané, L. Calvo-Barrio, V. Izquierdo-Roca, E. Saucedo, A. Pérez-Rodriguez, J.R. Morante, D.M. Berg, P.J. Dale, and S. Siebentritt, *In-depth resolved Raman scattering analysis for the identification of secondary phases: Characterization of $Cu_2ZnSnSe_4$ layers for solar cell applications,* Applied Physics Letters, 2011, **98**, 181905-3.

151. A. Redinger, K. Hones, X. Fontané, V. Izquierdo-Roca, E. Saucedo, N. Valle, A. Perez-Rodriguez, and S. Siebentritt, *Detection of a ZnSe secondary phase in coevaporated $Cu_2ZnSnSe_4$ thin films,* Applied Physics Letters, 2011, **98**, 101907-3.

152. M. Bär, B.A. Schubert, B. Marsen, S. Krause, S. Pookpanratana, T. Unold, L. Weinhardt, C. Heske, and H.W. Schock, *Impact of KCN etching on the chemical and electronic surface structure of Cu_2ZnSnS_4 thin-film solar cell absorbers,* Applied Physics Letters, 2011, **99**, 152111.

153. S. Niki, P.J. Fons, A. Yamada, Y. Lacroix, H. Shibata, H. Oyanagi, M. Nishitani, T. Negami, and T. Wada, *Effects of the surface $Cu_{2-x}Se$ phase on the growth and properties of $CuInSe_2$ films,* Applied Physics Letters, 1999, **74**, 1630-1632.

154. B.-A. Schubert, B. Marsen, S. Cinque, T. Unold, R. Klenk, S. Schorr, and H.-W. Schock, *Cu_2ZnSnS_4 thin film solar cells by fast coevaporation,* Progress in Photovoltaics: Research and Applications, 2011, **19**, 93-96.

155. L. Weinhardt, O. Fuchs, D. GroÃŸ, E. Umbach, C. Heske, N.G. Dhere, A.A. Kadam, and S.S. Kulkarni, *Surface modifications of $Cu(In,Ga)S_2$ thin film solar cell absorbers by KCN and H_2O_2 / H_2SO_4 treatments,* Journal of Applied Physics, 2006, **100**, 024907.

156. H. Katagiri, et al., *Enhanced Conversion Efficiencies of Cu_2ZnSnS_4-Based Thin Film Solar Cells by Using Preferential Etching Technique,* Applied Physics Express, 2008, **1**, 041201-1, 2.

157. K. Furuta, N. Sakai, T. Kato, H. Sugimoto, Y. Kurokawa, and A. Yamada, *Improvement of $Cu_2ZnSn(S,Se)_4$ solar cell efficiency by surface treatment*, physica status solidi (c), 2015, **12**, 704-707.

158. M. Kauk-Kuusik, K. Timmo, M. Danilson, M. Altosaar, M. Grossberg, and K. Ernits, *p-n junction improvements of Cu_2ZnSnS_4/CdS monograin layer solar cells*, Applied Surface Science, 2015, **357, Part A**, 795-798.

159. K. Timmo, M. Altosaar, J. Raudoja, M. Grossberg, M. Danilson, O. Volobujeva, and E. Mellikov. *Chemical etching of $Cu_2ZnSn(S,Se)_4$ monograin powder*, in *Photovoltaic Specialists Conference (PVSC), 2010 35th IEEE*, 2010.

160. P. Reinhard, A. Chirila, P. Blosch, F. Pianezzi, S. Nishiwaki, S. Buechelers, and A.N. Tiwari. *Review of progress toward 20% efficiency flexible CIGS solar cells and manufacturing issues of solar modules*, in *Photovoltaic Specialists Conference (PVSC), Volume 2, 2012 IEEE 38th*, 2012.

161. A. Chirila, P. Reinhard, F. Pianezzi, P. Bloesch, A.R. Uhl, C. Fella, L. Kranz, D. Keller, C. Gretener, H. Hagendorfer, D. Jaeger, R. Erni, S. Nishiwaki, S. Buecheler, and A.N. Tiwari, *Potassium-induced surface modification of $Cu(In,Ga)Se_2$ thin films for high-efficiency solar cells*, Nature Materials, 2014, **12**, 1107-1111.

162. Miasolé, *MiaSolé Achieves 15.7% Efficiency with Commercial-Scale CIGS Thin Film Solar Modules*, 2 December 2010, http://www.miasole.com/sites/default/files/MiaSole_release_Dec_02_2010.pdf. Accessed: October 2015.

163. P. Blösch, S. Nishiwaki, A. Chirila, L. Kranz, C. Fella, F. Pianezzi, C. Adelhelm, E. Franzke, S. Buecheler, and A.N. Tiwari, *Sodium-doped molybdenum back contacts for flexible $Cu(In,Ga)Se_2$ solar cells*, Thin Solid Films, 2013, **535**, 214-219.

164. Y. Takeshi and N. Tokio, *Cd-Free Flexible $Cu(In,Ga)Se_2$ Thin Film Solar Cells with ZnS(O,OH) Buffer Layers on Ti Foils*, Applied Physics Express, 2009, **2**, 072201.

165. A. Chirilă, P. Bloesch, P. Pianezzi, S. Seyrling, A.R. Uhl, S. Buecheler, S. Nishiwaki, and A.N. Tiwari, *Development of high efficiency flexible CIGS solar cells on different substrates*, in *The 21st International Photovoltaic Science and Engineering Conference*, Fukuoka, Japan, 2011.

166. Nanosolar, *Nanosolar Achieves 17.1% Aperture Efficiency Through Printed CIGS Process*, 6 October 2011, http://www.semiconductor-today.com/news_items/2011/OCT/NANOSOLAR_061011.html. Accessed: May 2014.

167. F. Pianezzi, A. Chirilă, P. Blösch, S. Seyrling, S. Buecheler, L. Kranz, C. Fella, and A.N. Tiwari, *Electronic properties of Cu(In,Ga)Se_2 solar cells on stainless steel foils without diffusion barrier*, Progress in Photovoltaics: Research and Applications, 2012, **20**, 253-259.

168. S. Ishizuka, A. Yamada, K. Matsubara, P. Fons, K. Sakurai, and S. Niki, *Development of high-efficiency flexible Cu(In,Ga)Se_2 solar cells: A study of alkali doping effects on CIS, CIGS, and CGS using alkali-silicate glass thin layers*, Current Applied Physics, 2010, **10**, S154-S156.

169. K. Moriwaki, M. Nomoto, S. Yuuya, N. Murakami, T. Ohgoh, K. Yamane, S. Ishizuka, and S. Niki, *Monolithically integrated flexible Cu(In,Ga)Se_2 solar cells and submodules using newly developed structure metal foil substrate with a dielectric layer*, Solar Energy Materials and Solar Cells, 2013, **112**, 106-111.

170. T. Satoh, Y. Hashimoto, S.-i. Shimakawa, S. Hayashi, and T. Negami, *Cu(In,Ga)Se_2 solar cells on stainless steel substrates covered with insulating layers*, Solar Energy Materials and Solar Cells, 2003, **75**, 65-71.

171. R. Wuerz, A. Eicke, M. Frankenfeld, F. Kessler, M. Powalla, P. Rogin, and O. Yazdani-Assl, *CIGS thin-film solar cells on steel substrates*, Thin Solid Films, 2009, **517**, 2415-2418.

172. C.Y. Shi, Y. Sun, Q. He, F.Y. Li, and J.C. Zhao, *Cu(In,Ga)Se_2 solar cells on stainless-steel substrates covered with ZnO diffusion barriers*, Solar Energy Materials and Solar Cells, 2009, **93**, 654-656.

173. C. Platzer-Björkman, S. Jani, J. Westlinder, M.K. Linnarsson, J. Scragg, and M. Edoff, *Diffusion of Fe and Na in co-evaporated Cu(In,Ga)Se_2 devices on steel substrates*, Thin Solid Films, 2013, **535**, 188-192.

174. F. Kessler and D. Rudmann, *Technological aspects of flexible CIGS solar cells and modules*, Solar Energy, 2004, **77**, 685-695.

175. Z. Zhou, Y. Wang, D. Xu, and Y. Zhang, *Fabrication of Cu_2ZnSnS_4 screen printed layers for solar cells*, Solar Energy Materials and Solar Cells, 2010, **94**, 2042-2045.

176. Q. Tian, X. Xu, L. Han, M. Tang, R. Zou, Z. Chen, M. Yu, J. Yang, and J. Hu, *Hydrophilic Cu_2ZnSnS_4 nanocrystals for printing flexible, low-cost and environmentally friendly solar cells*, CrystEngComm, 2012, **14**, 3847-3850.

177. F. Liu, *Flexible Cu_2ZnSnS_4 Solar Cells Fabricated Based on Successive Ionic Layer Adsorption and Reaction Method*, in *International Photonics and Optoelectronics Meetings (POEM)*, Wuhan, China, 2013.

178. C.-Y. Peng, T.P. Dhakal, S. Garner, P. Cimo, S. Lu, and C.R. Westgate, *Fabrication of Cu_2ZnSnS_4 solar cell on a flexible glass substrate*, Thin Solid Films, 2014, **562**, 574-577.

179. P. Bras, J. Sterner, and C. Platzer-Björkman, *Influence of hydrogen sulfide annealing on copper-zing-tin-sulfide solar cells sputtered from a quaternary compound target*, Thin Solid Films, 2014, **582**, 233-238.

180. S. Lopez-Marino, M. Neuschitzer, Y. Sánchez, A. Fairbrother, M. Espindola-Rodriguez, J. Lopez-García, M. Placidi, L. Calvo-Barrio, A. Perez-Rodriguez, and E. Saucedo, *Earth-abundant absorber based solar cells onto low weight stainless steel substrate*, Solar Energy Materials and Solar Cells, 2014, **130**, 347-353.

181. R. Caballero, C.A. Kaufmann, T. Eisenbarth, T. Unold, R. Klenk, and H.-W. Schock, *High efficiency low temperature grown $Cu(In,Ga)Se_2$ thin film solar cells on flexible substrates using NaF precursor layers*, Progress in Photovoltaics: Research and Applications, 2011, **19**, 547-551.

182. P.M.P. Salomé, H. Rodriguez-Alvarez, and S. Sadewasser, *Incorporation of alkali metals in chalcogenide solar cells*, Solar Energy Materials and Solar Cells, 2015, **143**, 9-20.

183. R. Caballero, C.A. Kaufmann, T. Eisenbarth, A. Grimm, I. Lauermann, T. Unold, R. Klenk, and H.W. Schock, *Influence of Na on $Cu(In,Ga)Se_2$ solar cells grown on polyimide substrates at low temperature: Impact on the $Cu(In,Ga)Se^2$/Mo interface*, Applied Physics Letters, 2010, **96**, 092104.

184. M. Ruckh, D. Schmid, M. Kaiser, R. Schäffler, T. Walter, and H.W. Schock, *Influence of substrates on the electrical properties of $Cu(In,Ga)Se_2$ thin films*, Solar Energy Materials and Solar Cells, 1996, **41-42**, 335-343.

185. P.M.P. Salome, A. Hultqvist, V. Fjallstrom, M. Edoff, B. Aitken, K. Vaidyanathan, K. Zhang, K. Fuller, and C. Kosik Williams, *$Cu(In,Ga)Se_2$ Solar Cells With Varying Na Content Prepared on Nominally Alkali-Free Glass Substrates*, Photovoltaics, IEEE Journal of, 2013, **3**, 852-858.

186. M.A. Contreras, B. Egaas, P. Dippo, J. Webb, J. Granata, K. Ramanathan, S. Asher, A. Swartzlander, and R. Noufi. *On the role of Na and modifications to $Cu(In,Ga)Se_2$ absorber materials using thin-MF (M=Na, K, Cs) precursor layers [solar cells]*, in *Photovoltaic Specialists Conference, 1997, Conference Record of the Twenty-Sixth IEEE*, 1997.

187. T. Nakada, H. Ohbo, M. Fukuda, and A. Kunioka, *Improved compositional flexibility of Cu(In,Ga)Se_2-based thin film solar cells by sodium control technique,* Solar Energy Materials and Solar Cells, 1997, **49**, 261-267.

188. D.J. Schroeder and A.A. Rockett, *Electronic effects of sodium in epitaxial $CuIn_{1-x}Ga_xSe_2$,* Journal of Applied Physics, 1997, **82**, 4982-4985.

189. M. Bodegärd, K. Granath, and L. Stolt, *Growth of Cu(In,Ga)Se_2 thin films by coevaporation using alkaline precursors,* Thin Solid Films, 2000, **361-362,** 9-16.

190. M. Bodegard, L. Stolt, and J. Hedstrom. *The influence of sodium on the grain structure of $CuInSe_2$ films for photovoltaic applications*, in *12th European Photovoltaic Solar Energy Conference,* 1994.

191. D. Rudmann, D. Brémaud, A.F. da Cunha, G. Bilger, A. Strohm, M. Kaelin, H. Zogg, and A.N. Tiwari, *Sodium incorporation strategies for CIGS growth at different temperatures,* Thin Solid Films, 2005. **480-481**, 55-60.

192. D. Cahen and R. Noufi, *Defect chemical explanation for the effect of air anneal on CdS/$CuInSe_2$ solar cell performance,* Applied Physics Letters, 1989, **54**, 558-560.

193. L. Kronik, D. Cahen, and H.W. Schock, *Effects of Sodium on Polycrystalline Cu(In,Ga)Se_2 and Its Solar Cell Performance*, Advanced Materials, 1998, **10**, 31-36.

194. S. Siebentritt, M. Igalson, C. Persson, and S. Lany, *The electronic structure of chalcopyrites—bands, point defects and grain boundaries,* Progress in Photovoltaics: Research and Applications, 2010, **18**, 390-410.

195. D.W. Niles, K. Ramanathan, F. Hasoon, R. Noufi, B.J. Tielsch, and J.E. Fulghum, *Na impurity chemistry in photovoltaic CIGS thin films: Investigation with x-ray photoelectron spectroscopy,* Journal of Vacuum Science & Technology A, 1997, **15**, 3044-3049.

196. D. Braunger, D. Hariskos, G. Bilger, U. Rau, and H.W. Schock, *Influence of sodium on the growth of polycrystalline Cu(In,Ga)Se_2 thin films,* Thin Solid Films, 2000, **361-362**, 161-166.

197. J.E. Granata, J.R. Sites, S. Asher, and R.J. Matson. *Quantitative incorporation of sodium in $CuInSe_2$ and Cu(In,Ga)Se_2 photovoltaic devices*, in *Photovoltaic Specialists Conference, 1997, Conference Record of the Twenty-Sixth IEEE,* 1997.

198. A. Rockett, J.S. Britt, T. Gillespie, C. Marshall, M.M. Al Jassim, F. Hasoon, R. Matson, and B. Basol, *Na in selenized Cu(In,Ga)Se_2 on Na-containing and Na-free glasses: distribution, grain structure, and device performances,* Thin Solid Films, 2000, **372,** 212-217.

199. P. Jackson, D. Hariskos, R. Wuerz, W. Wischmann, and M. Powalla, *Compositional investigation of potassium doped Cu(In,Ga)Se_2 solar cells with efficiencies up to 20.8%,* physica status solidi (RRL) – Rapid Research Letters, 2014, **8**, 219-222.

200. A. Laemmle, R. Wuerz, and M. Powalla, *Efficiency enhancement of Cu(In,Ga)Se_2 thin-film solar cells by a post-deposition treatment with potassium fluoride,* physica status solidi (RRL) – Rapid Research Letters, 2013, **7**, 631-634.

201. A. Laemmle, R. Wuerz, and M. Powalla, *Investigation of the effect of potassium on Cu(In,Ga)Se_2 layers and solar cells,* Thin Solid Films, 2014, **582**, 27-30.

202. F. Pianezzi, P. Reinhard, A. Chirila, B. Bissig, S. Nishiwaki, S. Buecheler, and A.N. Tiwari, *Unveiling the effects of post-deposition treatment with different alkaline elements on the electronic properties of CIGS thin film solar cells,* Physical Chemistry Chemical Physics, 2014, **16**, 8843-8851.

203. W.M. Hlaing Oo, J.L. Johnson, A. Bhatia, E.A. Lund, M.M. Nowell, and M.A. Scarpulla, *Grain Size and Texture of Cu_2ZnSnS_4 Thin Films Synthesized by Cosputtering Binary Sulfides and Annealing: Effects of Processing Conditions and Sodium,* Journal of Electronic Materials, 2011, **40**, 2214-2221.

204. M. Johnson, S.V. Baryshev, E. Thimsen, M. Manno, X. Zhang, I.V. Veryovkin, C. Leighton, and E.S. Aydil, *Alkali-metal-enhanced grain growth in Cu_2ZnSnS_4 thin films,* Energy & Environmental Science, 2014, **7**, 1931-1938.

205. Y. Li, Q. Han, T. Kim, and W. Shi, *The optical influence of Na on $Cu_2ZnSnSe_4$ films deposited with Na-containing sol-gel precursor,* Journal of Sol-Gel Science and Technology, 2014, **69**, 260-265.

206. T. Prabhakar and N. Jampana, *Effect of sodium diffusion on the structural and electrical properties of Cu_2ZnSnS_4 thin films,* Solar Energy Materials and Solar Cells, 2011, **95**, 1004.

207. C.M. Sutter-Fella, J.A. Stückelberger, H. Hagendorfer, F. La Mattina, L. Kranz, S. Nishiwaki, A.R. Uhl, Y.E. Romanyuk, and A.N. Tiwari, *Sodium Assisted Sintering of Chalcogenides and Its Application to Solution Processed $Cu_2ZnSn(S,Se)_4$ Thin Film Solar Cells,* Chemistry of Materials, 2014, **26**, 1420-1425.

208. J.V. Li, D. Kuciauskas, M.R. Young, and I.L. Repins, *Effects of sodium incorporation in Co-evaporated $Cu_2ZnSnSe_4$ thin-film solar cells*, Applied Physics Letters, 2013, **102**, 163905.

209. G. Altamura, C. Roger, L. Grenet, J.l. Bleuse, H.l.n. Fournier, S. Perraud, and H. Mariette, *Influence of sodium-containing substrates on Kesterite CZTSSe thin films based solar cells*, MRS Online Proceedings Library, 2013, **1538**, 103-106.

210. A.D. Collord, H. Xin, and H.W. Hillhouse, *Combinatorial Exploration of the Effects of Intrinsic and Extrinsic Defects in $Cu_2ZnSn(S,Se)_4$*, Photovoltaics, IEEE Journal of, 2014, **5**, 288-298.

211. Y.-R. Lin, V. Tunuguntla, S.-Y. Wei, W.-C. Chen, D. Wong, C.-H. Lai, L.-K. Liu, L.-C. Chen, and K.-H. Chen, *Bifacial sodium-incorporated treatments: Tailoring deep traps and enhancing carrier transport properties in Cu_2ZnSnS_4 solar cells*, Nano Energy, 2015, **16**, 438-445.

212. H. Zhou, T.-B. Song, W.-C. Hsu, S. Luo, S. Ye, H.-S. Duan, C.-J. Hsu, W. Yang, and Y. Yang, *Rational Defect Passivation of $Cu_2ZnSn(S,Se)_4$ Photovoltaics with Solution-Processed Cu_2ZnSnS_4:Na Nanocrystals*, Journal of the American Chemical Society, 2013, **135**, 15998-16001.

213. J.B. Li, V. Chawla, and B.M. Clemens, *Investigating the Role of Grain Boundaries in CZTS and CZTSSe Thin Film Solar Cells with Scanning Probe Microscopy*, Advanced Materials, 2012, **24**, 720-723.

214. T. Gershon, B. Shin, N. Bojarczuk, M. Hopstaken, D.B. Mitzi, and S. Guha, *The Role of Sodium as a Surfactant and Suppressor of Non-Radiative Recombination at Internal Surfaces in Cu_2ZnSnS_4*, Advanced Energy Materials, 2014, **5**, 1400849.

215. K.-J. Yang, J.-H. Sim, B. Jeon, D.-H. Son, D.-H. Kim, S.-J. Sung, D.-K. Hwang, S. Song, D.B. Khadka, J. Kim, and J.-K. Kang, *Effects of Na and MoS_2 on Cu_2ZnSnS_4 thin-film solar cell*, Progress in Photovoltaics: Research and Applications, 2014, **23**, 862-863.

216. C.S. Jiang, R. Noufi, K. Ramanathan, J.A. AbuShama, H.R. Moutinho, and M.M. Al-Jassim, *Does the local built-in potential on grain boundaries of $Cu(In,Ga)Se_2$ thin films benefit photovoltaic performance of the device?*, Applied Physics Letters, 2004, **85**, 2625-2627.

217. C.S. Jiang, I.L. Repins, C. Beall, H.R. Moutinho, K. Ramanathan, and M.M. Al-Jassim, *Investigation of micro-electrical properties of $Cu_2ZnSnSe_4$ thin films using scanning probe microscopy*, Solar Energy Materials and Solar Cells, 2015, **132**, 342-347.

218. K. Sardashti, R. Haight, T. Gokmen, W. Wang, L.-Y. Chang, D.B. Mitzi, and A.C. Kummel, *Impact of Nanoscale Elemental Distribution in High-Performance Kesterite Solar Cells,* Advanced Energy Materials, 2015, **5**, 1402180.

219. M. Neuschitzer, Y. Sanchez, T. Olar, T. Thersleff, S. Lopez-Marino, F. Oliva, M. Espindola-Rodriguez, H. Xie, M. Placidi, V. Izquierdo-Roca, I. Lauermann, K. Leifer, A. Pérez-Rodríguez, and E. Saucedo, *Complex Surface Chemistry of Kesterites: Cu/Zn Reordering after Low Temperature Postdeposition Annealing and Its Role in High Performance Devices,* Chemistry of Materials, 2015, **27**, 5279-5287.

220. H.-S. Duan, W. Yang, B. Bob, C.-J. Hsu, B. Lei, and Y. Yang, *The Role of Sulfur in Solution-Processed $Cu_2ZnSn(S,Se)_4$ and its Effect on Defect Properties,* Advanced Functional Materials, 2012, **23**, 1466-1471.

221. O. Gunawan, T. Gokmen, C.W. Warren, J.D. Cohen, T.K. Todorov, D.A.R. Barkhouse, S. Bag, J. Tang, B. Shin, and D.B. Mitzi, *Electronic properties of the $Cu_2ZnSn(Se,S)_4$ absorber layer in solar cells as revealed by admittance spectroscopy and related methods,* Applied Physics Letters, 2012, **100**, 253905.

222. J. Li, Y. Zhang, W. Zhao, D. Nam, H. Cheong, L. Wu, Z. Zhou, and Y. Sun, *A Temporary Barrier Effect of the Alloy Layer During Selenization: Tailoring the Thickness of $MoSe_2$ for Efficient $Cu_2ZnSnSe_4$ Solar Cells,* Advanced Energy Materials, 2015. **5**, 1402178.

223. K.-H. Müller, *Stress and microstructure of sputterdeposited thin films: Molecular dynamics investigations.* Journal of Applied Physics, 1987, **62**, 1796-1799.

224. T.J. Vink, M.A.J. Somers, J.L.C. Daams, and A.G. Dirks, *Stress, strain, and microstructure of sputterdeposited Mo thin films,* Journal of Applied Physics, 1991, **70**, 4301-4308.

225. W.H. McCarroll and K.V. Ramanujachary, *Oxides: Solid-State Chemistry*, in *Encyclopedia of Inorganic Chemistry*, John Wiley & Sons, Ltd., 2006. P. 26-28.

226. D. Abou-Ras, G. Kostorz, D. Bremaud, M. Kälin, F.V. Kurdesau, A.N. Tiwari, and M. Döbeli, *Formation and characterisation of $MoSe_2$ for $Cu(In,Ga)Se_2$ based solar cells,* Thin Solid Films, 2005, **480-481**, 433-438.

227. M.K. Agarwal and L.T. Talele, *Growth conditions and structural characterization of molybdenum sulphoselenide single crystals: (MoS_xSe_{2-x}, $0 \leq x \leq 2$),* Materials Research Bulletin, 1985, **20**, 329-336.

228. A. Jäger-Waldau, M.C. Lux-Steiner, E. Bucher, L. Scandella, A. Schumacher, and R. Prins, *MoS_2 thin films prepared by sulphurization*, Applied Surface Science, 1993, **65-66**, 465-472.

229. D. Abou-Ras, D. Mukherji, G. Kostorz, D. Brémaud, M. Kälin, D. Rudmann, M. Döbeli, and A.N. Tiwari, *Dependence of the $MoSe_2$ Formation on the Mo Orientation and the Na Concentration for Cu(In,Ga)Se_2 Thin-Film Solar Cells*, MRS Online Proceedings Library, 2005, **865**, F8.1

230. S. Nishiwaki, N. Kohara, T. Negami, and T. Wada, *$MoSe_2$ layer formation at Cu(In,Ga)Se_2 /Mo Interfaces in High Efficiency Cu(In_{1-x} Ga_x)Se_2 Solar Cells*, Japanese Journal of Applied Physics, 1998, **37**, L71.

231. J.-H. Yoon, J.-H. Kim, W.M. Kim, J.-K. Park, Y.-J. Baik, T.-Y. Seong, and J.-h. Jeong, *Electrical properties of CIGS/Mo junctions as a function of $MoSe_2$ orientation and Na doping*, Progress in Photovoltaics: Research and Applications, 2013, **22**, 90-96.

232. J.A. Wilson and A.D. Yoffe, *The transition metal dichalcogenides discussion and interpretation of the observed optical, electrical and structural properties*, Advances in Physics, 1969, **18**, 193-335.

233. R. Würz, D. Fuertes Marrón, A. Meeder, A. Rumberg, S.M. Babu, T. Schedel-Niedrig, U. Bloeck, P. Schubert-Bischoff, and M.C. Lux-Steiner, *Formation of an interfacial $MoSe_2$ layer in CVD grown $CuGaSe_2$ based thin film solar cells*, Thin Solid Films, 2003, **431-432**, 398-402.

234. C.S. Jiang, M.A. Contreras, I. Repins, H.R. Moutinho, Y. Yan, M.J. Romero, L.M. Mansfield, R. Noufi, and M.M. Al-Jassim, *How grain boundaries in Cu(In,Ga)Se_2 thin films are charged: Revisit*, Applied Physics Letters, 2012, **101**, 033903.

235. T. Gnanasekaran, K.H. Mahendran, K.V.G. Kutty, and C.K. Mathews, *Phase diagram studies on the Na-Mo-O system*, Journal of Nuclear Materials, 1989, **165**, 210-216.

236. J.-H. Yoon, T.-Y. Seong, and J.-h. Jeong, *Effect of a Mo back contact on Na diffusion in CIGS thin film solar cells*, Progress in Photovoltaics: Research and Applications, 2013, **21**, 58-63.

237. M.B. Zellner, R.W. Birkmire, E. Eser, W.N. Shafarman, and J.G. Chen, *Determination of activation barriers for the diffusion of sodium through CIGS thin-film solar cells*, Progress in Photovoltaics: Research and Applications, 2003, **11**, 543-548.

238. B.M. Basol, V.K. Kapur, C.R. Leidholm, A. Minnick, and A. Halani. *Studies on substrates and contacts for CIS films and devices*, in *Photovoltaic Energy Conversion, 1994, Conference Record*

of the Twenty Fourth. IEEE Photovoltaic Specialists Conference - 1994, 1994 IEEE First World Conference on, 1994.

239. M. Ruckh, D. Schmid, M. Kaiser, R. Schaffler, T. Walter, and H.W. Schock. *Influence of substrates on the electrical properties of Cu(In,Ga)Se_2 thin films*, in *Photovoltaic Energy Conversion, 1994, Conference Record of the Twenty Fourth. IEEE Photovoltaic Specialists Conference - 1994, 1994 IEEE First World Conference on*, 1994.

240. M. Bodegard, K. Granath, L. Stolt, and A. Rockett, *The behaviour of Na implanted into Mo thin films during annealing*, Solar Energy Materials and Solar Cells, 1999, **58**, 199-208.

241. J.H. Scofield, S. Asher, D. Albin, J. Tuttle, M. Contreras, D. Niles, R. Reedy, A. Tennant, and R. Noufi. *Sodium diffusion, selenization, and microstructural effects associated with various molybdenum back contact layers for CIS-based solar cells*, in *Photovoltaic Energy Conversion, 1994, Conference Record of the Twenty Fourth. IEEE Photovoltaic Specialists Conference - 1994, 1994 IEEE First World Conference on*, 1994.

242. M. Dimitrievska, A. Fairbrother, E. Saucedo, A. Pérez-Rodríguez, and V. Izquierdo-Roca, *Influence of compositionally induced defects on the vibrational properties of device grade $Cu_2ZnSnSe_4$ absorbers for kesterite based solar cells*, Applied Physics Letters, 2015. **106**, 073903.

243. S. Lopez-Marino, M. Espíndola-Rodríguez, Y. Sánchez, X. Alcobé, H. Xie, M. Neuschitzer, S. Giraldo, F. Oliva, M. Placidi, V. Izquierdo-Roca, A. Pérez-Rodríguez, and E. Saucedo, *Back contact modifications in high efficiency $Cu_2ZnSnSe_4$ solar cells. Role of MoO_x thin layers*, in *6th Euroepan Kesterite Workshop*, Newcastle, UK, 2015.

244. M. Neuschitzer, Y. Sanchez, S. López-Marino, H. Xie, A. Fairbrother, M. Placidi, S. Haass, V. Izquierdo-Roca, A. Perez-Rodriguez, and E. Saucedo, *Optimization of CdS buffer layer for high-performance $Cu_2ZnSnSe_4$ solar cells and the effects of light soaking: elimination of crossover and red kink.* Progress in Photovoltaics: Research and Applications, 2015, **23**, 660–1667

245. J. Hedstrom, H. Ohlsen, M. Bodegard, A. Kylner, L. Stolt, D. Hariskos, M. Ruckh, and H. Schock. *ZnO/CdS/Cu(In,Ga)Se_2 thin film solar cells with improved performance*, in *Photovoltaic Specialists Conference, 1993, Conference Record of the Twenty Third IEEE*, 1993.

246. D.J. Schroeder and A.A. Rockett, *Electronic effects of sodium in epitaxial $CuIn_{1-x}GaxSe_2$*, Journal of Applied Physics, 1997, **82**, 4982-4985.

247. D. Braunger, D. Hariskos, G. Bilger, U. Rau, and H.W. Schock, *Influence of sodium on the growth of polycrystalline Cu(In,Ga)Se_2 thin films*, Thin Solid Films, 2000, **361-362**, 161-166.

248. D. Rudmann, D. Brémaud, A.F. da Cunha, G. Bilger, A. Strohm, M. Kaelin, H. Zogg, and A.N. Tiwari, *Sodium incorporation strategies for CIGS growth at different temperatures*, Thin Solid Films, 2005, **480-481**, 55-60.

249. A. Laemmle, R. Wuerz, and M. Powalla, *Investigation of the effect of potassium on Cu(In,Ga)Se_2 layers and solar cells*, Thin Solid Films, 2015, **582**, 27-30.

APPENDICES

All the articles referenced in previous chapters are included in this section. Additionally, the supporting information of a manuscript with status "under review" in a high impact scientific journal at the time of this thesis submission is also included. In consequence, this section has been divided into the following subsections.

A1. Chapter 5.1.1. Minimizing decomposition at CZTSe/Mo interface

"Inhibiting the absorber/Mo-back contact decomposition reaction in $Cu_2ZnSnSe_4$ solar cells: the role of a ZnO intermediate nanolayer". Journal of Materials Chemistry A, 1, 2013, 19, 8338-8343.

A2. Chapter 5.1.2. Mo multilayer configurations. Role of MoO_x thin layers

Supplementary information of: *"The Importance of Back Contact Modification in High Efficiency $Cu_2ZnSnSe_4$ Solar Cells: the Role of a nanometric MoO_2 Layer"*. Nano Energy, 2016 (under review)

[Volume 26, August 2016, Pages 708–721 10.1016/j.nanoen.2016.06.034]

A3. Chapter 5.2. Removing ZnSe by a sequential oxidizing/passivating chemical etch.

"ZnSe Etching of Zn-Rich $Cu_2ZnSnSe_4$: An Oxidation Route for Improved Solar-Cell Efficiency". Chemistry – A European Journal, 2013, 19, 14814-14822.

A4. Chapter 5.3.1. Proof of concept. First flexible thin film CZTSe solar cell.

"Earth-abundant absorber based solar cells onto low weight stainless steel substrate". Solar Energy Materials and Solar Cells, 2014, 130, 347-353.

A5. Chapter 5.3.2. Alkali doping strategies for flexible CZTSe solar cells.

"Alkali doping strategies for flexible and light-weight $Cu_2ZnSnSe_4$ solar cells". Journal of Materials Chemistry A, 2016, 4, 1895-1907.

ATTENTION ¡

Pages 122 to 197 of the dissertation, containing the texts mentioned above, should be consulted on the web pages of the respective publishers.